VASCULAR ENDOTHELIAL GROWTH FACTOR B AND ITS ACTION IN THE DIABETIC HEART

by

Nathaniel Lal

A THESIS SUBMITTED IN PARTIAL FULFILLMENT OF
THE REQUIREMENTS FOR THE DEGREE OF

Doctor of Philosophy
in
THE FACULTY OF GRADUATE AND POSTDOCTORAL STUDIES
(Pharmaceutical Sciences)

THE UNIVERSITY OF BRITISH COLUMBIA
(Vancouver)

July 2020

The following individuals certify that they have read, and recommend to the Faculty of Graduate and Postdoctoral Studies for acceptance, the dissertation entitled:

Vascular endothelial growth factor b and its action in the diabetic heart

---

submitted by Nathaniel Lal in partial fulfillment of the requirements for

the degree of Doctor of Philosophy

in Pharmaceutical Sciences

Examining Committee:

Dr. Brian Rodrigues, Pharmaceutical Sciences
Supervisor

Dr. Judy Wong, Pharmaceutical Sciences
Supervisory Committee Member

Dr. Colin Ross, Pharmaceutical Sciences
University Examiner

Dr. Pascal Bernatchez, Medicine
University Examiner

Additional Supervisory Committee Members:

Dr. Angela Devlin, Medicine
Supervisory Committee Member

Dr. Susanne Clee, Medicine
Supervisory Committee Member

ABSTRACT

Fatty acid (FA) provision to the heart is from cardiomyocyte and adipose depots, plus lipoprotein lipase (LPL) action. Changes in cardiac metabolism (reduced glucose, greater FA utilization) is a major contributor towards diabetic cardiomyopathy. Vascular endothelial growth factor B (VEGFB) can regulate coronary angiogenesis and influence energy metabolism. Multiple models of heart failure have indicated a significant drop in VEGFB. In this thesis we hypothesized that there is a role for VEGFB in diabetic cardiomyopathy. The objectives of this thesis were to: Determine the changes in cardiac metabolism following diabetes with its effect on VEGFB production. Investigate the mechanisms behind VEGFB action in the heart subsequent to diabetes. Identify the potential benefits of VEGFB following chronic diabetes. With increasing severity of diabetes and dramatic loss of insulin, the heart is unable to control its own FA supply using LPL and undergoes dramatic reprogramming that is linked to handling of excess FA that arise from adipose tissue. This transition results in a cardiac metabolic signature that exhibits mitochondrial FA overload, oxidative stress, triglyceride storage and cell death. Under these conditions VEGFB production is impaired. Mechanistically, the immediate response to high glucose and the secretion of endothelial heparanase is the release of cardiomyocyte surface bound VEGFB, which triggers signaling pathways and gene expression to influence cardiomyocyte (autocrine action) and endothelial cell (paracrine effects) survival. Defects in numerous VEGFB pathways were associated with an increased cell death signature in our models of diabetes. Overexpression of VEGFB in the heart can regulate coronary angiogenesis and influence energy metabolism and we tested whether these effects can overcome the detrimental consequences of diabetes. VEGFB overexpression induced an angiogenic response that resulted in greater delivery of insulin,

amplifying its action in the TG (transgenic) heart. Additional mechanisms contributing towards enhancing insulin sensitivity included less delivery of lipoprotein lipase-derived FA, reduced accumulation of diacylglycerols and LysoPC and lower FA metabolism. The augmented effects on insulin action were preserved following diabetes. Our data suggest that using VEGFB as a cardio protective therapy against diabetic cardiomyopathy may be an intriguing and previously unappreciated approach.

LAY SUMMARY

During diabetes, the heart has limited capacity to use sugar and must adapt to largely using fats to generate energy. While necessary for the heart to manage its energy demands, this switch leads to many dire consequences. When using fats, the heart requires more oxygen, which is in short supply due to blood vessel defects in the heart. This leads to fat accumulation in the heart with associated cellular damage. VEGFB has emerged as a potentially efficacious agent against diabetic heart disease. VEGFB has the capability of a) enhancing blood vessel formation in the heart to help provide the necessary oxygen to use fat, b) shifting energy production back to using sugar and c) preventing cell death to delay heart failure. Using animal models (where the heart overproduces VEGFB), isolated cells from the heart and models of high glucose, this thesis will investigate VEGFB as a cardio protective therapy in diabetes.

PREFACE

All of the work presented in chapters 1, 2, 3 and 4 were conducted in the Faculty of Pharmaceutical Sciences at the University of British Columbia. Some chapters have been published in the following manuscripts and review article. This investigation adheres to the Guide for the Care and Use of Laboratory Animals published by the U.S. National Institutes of Health and the University of British Columbia, and was approved by Animal Care Committee at the University of British Columbia (Certificates A17-0072, A18-0023).

1. **Lal, N,** A. P. Chiu, F. Wang, D. Zhang, J. Jia, A. Wan, I. Vlodavsky, B. Hussein and B. Rodrigues. Loss of Vegfb and Its Signaling in the Diabetic Heart Is Associated with Increased Cell Death Signaling. **Am J Physiol Heart Circ Physiol 312, no. 6 (2017): H1163-H1175.** I am the first author responsible for conceiving the idea, designed the experiments, and generated most of the data. My supervisor Dr. B. Rodrigues, and I designed the experiments. Dr. B. Rodrigues and I wrote the manuscript. Dr. I. Vlodavsky provided materials for research and assist with valuable suggestions. Dr. A.P. Chiu (Figure 18), Dr. F. Wang (Figure 18), Dr. D. Zhang (Figure 19), J. Jia (Figure 20), B. Hussein (Figure 22) and Dr. A. Wan (Figure 23) helped collect proteins samples for Western Blots in the respective figures and provided editorial feedback to help revise the manuscript.

2. **Lal, N,** K. Puri and B. Rodrigues. Vascular Endothelial Growth Factor B and Its Signaling. **Front Cardiovasc Med 5, (2018): 39.** I performed the literature search to collect the informatiion for the review. Dr. B. Rodrigues and I wrote the manuscript, designed the figures and K. Puri created the figures.

3. Puri, K, **N. Lal**, R. Shang, S. Ghosh, S. Flibotte, R. Dyer, B. Hussein and B. Rodrigues. Diabetes Mellitus Severity and a Switch from Using Lipoprotein Lipase to Adipose-Derived Fatty Acid Results in a Cardiac Metabolic Signature That Embraces Cell Death. **J Am Heart Assoc 8, no. 21 (2019): e014022.** As the second author I worked with K. Puri and Dr. B. Rodrigues to design and perform experiments. I collected the data while K. Puri and Dr. B. Rodrigues analyzed the data and wrote the manuscript. Dr. S. Ghosh helped with metabolomic analysis, S. Flibotte analyzed the RNA Seq data, R. Dyer performed lipid and metabolomic analysis, R. Shang (Figure 10) used string db to view protein-protein interactions, B. Hussein (Figure 12) performed the mitochondrial stress test and all authors provided editorial feedback to help revise the manuscript.

4. Shang. R *, **N. Lal***, CS. Lee, V. Mai, Y. Zhai, S. Flibotte, I. Vlodavsky, I. Sultan, M. Räsänen, K. Alitalo, B. Hussein and B. Rodrigues. Cardiomyocyte-specific overexpression

of VEGFB isoforms and their distinct secretion patterns are linked to an expanded coronary vasculature that amplifies the cardiovascular action of insulin. **(Submitted). (2020).**
* Contributed equally to the manuscript. As the co-first author R. Shang and I conceived the idea, designed the experiments, and generated most of the data. Dr. B. Rodrigues, R. Shang and I wrote the manuscript. I was primarily responsible for the figures in this manuscript that are presented in this thesis. Dr. I. Vlodavsky provided materials for research and assist with valuable suggestions. Dr. K. Alitalo graciously provided the VEGFB transgenic rats. Dr. I. Sultan and Dr. M. Räsänen provided valuable insight regarding the VEGFB transgenic animals. S. Flibotte analyzed the RNA Seq data. CS. Lee (Figure 33) helped to generate the heat map, Y. Zhai (Figure 32) isolated RNA for qPCR analysis, V. Mai (Figure 31) helped collect proteins samples for Western Blots and B. Hussein (Figure 34) helped collect heart tissue for metabolomics analysis. All authors provided editorial feedback to help revise the manuscript.

TABLE OF CONTENTS

LIST OF TABLES

LIST OF FIGURES

LIST OF ABBREVIATIONS

AAV	adeno-associated virus
AMPK	AMP-activated protein kinase
ATGL	adipose triglyceride lipase
DAG	diacylglyceride
EC	endothelial cell
FA	fatty acid
FAO	fatty acid oxidation
GLUT	glucose transporter
HG	high glucose
HS	heparan sulfate
HSL	hormone sensitive lipase
HSPG	heparan sulfate proteoglycan
LPL	lipoprotein lipase
LysoPC	lysophosphatidylcholine
NRP1	neuropilin 1
NRP2	neuropilin 2
OCR	oxygen consumption rate
PDGFB	platelet derived growth factor subunit B
PDGFRβ	platelet derived growth factor receptor beta
PDH	pyruvate dehydrogenase
PDK	PIP3-dependent kinase
PDK1	pyruvate dehydrogenase kinase 1
PDK4	pyruvate dehydrogenase kinase 4
PLGF	placental growth factor
RHMEC	rat heart micro vessel endothelial cell
ROS	reactive oxygen species
SMC	smooth muscle cell
STZ	streptozotocin

T1D	type 1 diabetes
T2D	type 2 diabetes
TG	transgenic
VEGF	vascular endothelial growth factor
VEGFA	vascular endothelial growth factor A
VEGFB	vascular endothelial growth factor B
VEGFC	vascular endothelial growth factor C
VEGFD	vascular endothelial growth factor D
VEGFE	vascular endothelial growth factor E
VEGFR1	vascular endothelial growth factor receptor 1
VEGFR2	vascular endothelial growth factor receptor 2
VEGFR3	vascular endothelial growth factor receptor 3

ACKNOWLEDGEMENTS

My sincerest and deepest gratitude goes to my supervisor Dr. Brian Rodrigues. Dr. Rodrigues is an amazing mentor that is always engrossed in all of his students' success. The most succinct way to describe his mentorship is that he treats all of his students like members of a family. The training he has provided on how to not only be successful but to be a class act along the way are invaluable. I know even when I move on to the next stage of my career he will continue to be there for support and direction.

Outside of guiding me through my PhD career, Dr. Rodrigues has also had a significant impact on my personal life. Dr. Rodrigues is a strong advocate and follower of living a healthy lifestyle through diet and exercise. His example has been a significant influence on how I have changed my lifestyle and was able to lose a significant amount of weight. This change has vastly improved my life and I will be forever grateful for Dr. Rodrigues' encouragement and support.

I would like to thank my committee members Dr. Angela Devlin, Dr. Susanne Clee, Dr. Kathleen MacLeod, my chair Dr. Nislow and a special thank you to Dr. Judy Wong for agreeing to join my committee on short notice due to the retirement of Dr. MacLeod. All of your insight has greatly helped broadened my knowledge and passion for research.

I have been blessed to work with amazing group of colleagues during my time in the lab. Dr. Ying Wang, Dr. Amy Chiu and Dr. Dahai Zhang were great mentors to follow and provided me the support and encouragement in getting started. Bahira Hussein has been an irreplaceable source of support and friendship who has been there my entire time in the lab. Being able to mentor Karn Puri and watch him and his career evolve has been extremely rewarding, good luck in your career. Having Rui Shang join the lab has been a wonderful experience. She has brought

such a positive energy to not only the lab but really helped me push through the final stages of my PhD, thank you very much. To the newer members Jason Lee and Sophia Zhai, thank you as well for your support and I wish you the best of luck for your careers.

Finally, I would like to thank my family and friends (D.V, D.T and H.K) for all your love, support and encouragement.

DEDICATION

For my parents Aruna and Vimal Lal

CHAPTER 1: INTRODUCTION

1.1 Heart metabolism

The heart is an organ which requires a substantial amount of energy and displays substrate diversity utilizing fatty acids (FA), carbohydrates and ketones to generate the ATP needed for its continued function (1). Under normal physiological conditions almost 70% of ATP generation is produced from FA oxidation, with the remaining 30% produced from the breakdown of glucose and lactate (1). Even though the heart requires a substantial amount of FA, it has a limited ability for FA synthesis and instead relies upon delivery of FA from exogenous sources. These sources of FA include: breakdown of adipose tissue triglycerides; release from endogenous heart triglyceride stores and lipolysis of circulating triglyceride rich lipoproteins (chylomicrons and VLDL), which is catalyzed by lipoprotein lipase (LPL), located at the endothelial cell (EC) surface of the coronary vascular lumen (2, 3). LPL derived FA are considered the preferred source of FA for cardiomyocyte metabolism (4).

1.2 Lipoprotein Lipase

LPL is robustly expressed in the heart, and LPL-mediated lipolysis of circulating triglyceride -lipoproteins is considered a key source of FA for cardiac use (2). LPL activity is rapidly responsive to physiological conditions, in fasting, LPL activity increases in the heart (5). Accordingly, FA generated from circulating triglycerides are diverted away from storage and towards meeting the metabolic demands of cardiomyocytes. Consequently, LPL fulfills a "gate-keeping" role by regulating the supply of FA to meet tissue requirements. Interestingly, even though LPL is utilized at the EC surface to hydrolyze circulating triglycerides, ECs have very little expression of LPL (6). It is the underlying cardiomyocyte that is responsible for the synthesis and

processing of this enzyme (7). The cardiomyocyte initially makes LPL as an inactive monomer and through the use of chaperones in the endoplasmic reticulum, two LPL monomers are non-covalently linked into a mature and active LPL dimer. Upon dimerization LPL exits the ER and is then packaged into vesicles in the Golgi. Exocytosis of the LPL vesicle is controlled by protein kinase D and the cellular energy sensor AMP-activated protein kinase (AMPK), which enable a signaling cascade resulting in actin cytoskeleton polymerization to transport LPL to the plasma membrane and onto cardiomyocyte heparan sulfate proteoglycans (HSPG) (7, 8).

1.3 Heparanase

HSPG are ubiquitously present in every cellular compartment, particularly the extracellular matrix, cell surface, intracellular granules and nucleus (9). Made up of a core protein with numerous heparan sulfate (HS) side chains covalently attached, HSPG can act as not only a structural protein but can also sequester coagulation factors, chemokines, enzymes and growth factors (10). Attachment of these bioactive proteins is a clever arrangement, providing the cell with a rapidly accessible reservoir, precluding the need for de novo synthesis when the requirement for a protein is increased. Heparanase secreted from endothelial cells can quickly liberate myocyte cell surface bound proteins that modulate heart function in an autocrine and paracrine manner.

Heparanase is synthesized as a latent (Hep-L) 65 kDa enzyme that undergoes cellular secretion followed by HSPG-facilitated reuptake (11, 12). After undergoing proteolytic cleavage in lysosomes, a 50 kDa polypeptide is formed that is ~100-fold more active (Hep-A) than Hep-L (13, 14). In the presence of high glucose (HG), the EC responds with increased secretion of both Hep-L and Hep-A into the medium. In normal physiology, heparanase has a function in embryonic morphogenesis, wound healing and hair growth (15). Heparanase also has a unique responsibility in cardiac metabolism, by releasing myocyte HSPG bound proteins to enhance the diabetic heart's

ability to utilize FA (16). In this regard its release of lipoprotein lipase (LPL) for onward movement to the vascular lumen facilitates lipoprotein triglyceride breakdown and FA supply to the cardiomyocyte. In the diabetic heart, unregulated FA utilization is undesirable, leading to cardiac cell death. In addition to LPL release by Hep-A, Hep-L has a greater competence for releasing myocyte surface growth factors, such as members of the vascular endothelial growth factor (VEGF) family (17). The simultaneous release of LPL and VEGF growth factors can prime the cardiomyocyte to efficiently consume FA and also protect against lipotoxicity by regulating cardiomyocyte survival (18).

1.4 Diabetic cardiomyopathy

Cardiovascular disease is the leading cause of diabetes-related death and could be an outcome of atherosclerotic coronary artery disease or a consequence of an intrinsic malfunction of the heart muscle (labeled diabetic cardiomyopathy [DCM]) (18). Evidence of cardiomyopathy has also been reported in animal models of T1D and T2D (19). Cardiomyopathy is a complicated disorder and several factors have been associated with its development. These include an accumulation of connective tissue and insoluble collagen, impaired sensitivity to various ligands (e.g., β-agonists), and protein abnormalities that regulate intracellular calcium (20, 21). The view that diabetic cardiomyopathy could occur as a consequence of early alterations in cardiac metabolism has also been put forward (18) and embraces reduced glucose consumption, with a switch to predominant FA utilization. Unlike glucose, the oxidation of FAs requires proportionally greater oxygen to produce a similar amount of ATP (1). Regrettably, augmented FA oxidation increases the generation of reactive oxygen species (ROS) which have been implicated in apoptotic cell death (3).

1.5 Heart metabolism in diabetes

Glucose metabolism in the adult heart is reliant on glucose uptake via sarcolemmal transporters (22, 23). The predominant glucose transporter (GLUT) in the heart is encoded by the SLC2A4 gene, commonly known as GLUT4, and its mobilization to the plasma membrane to facilitate glucose uptake is dependent on the hormone insulin (22, 24, 25). Increased glucose in the blood particularly after a meal is sensed by the pancreas and stimulates pancreatic beta cells to secrete insulin. This circulating insulin traverses the blood stream and interacts with a number of organs such as adipose tissue, skeletal muscle, liver and the heart (26). Insulin binds to the insulin receptor which is a receptor tyrosine kinase and undergoes auto phosphorylation (27). Phosphorylated insulin receptor directs a phosphorylation cascade leading to phosphorylation of insulin receptor substrate 1 (IRS-1), to recruit PI3 kinase via SH2 domains on the p85 subunit. PI3 kinase catalyzes the phosphorylation of phosphatidylinositol bisphosphate (PIP_2) at the plasma membrane to PIP_3, which then recruits PIP3-dependent kinase (PDK) and Akt, allowing PDK to phosphorylate and activate Akt (27). Activated Akt allows for trafficking of GLUT4 storage vesicles to the plasma membrane and surface expression of GLUT4 (28). Reduced or ineffective insulin action resulting in inadequate glucose clearance from the bloodstream is a hallmark characteristic of the two major forms of diabetes, type 1 (T1D) and type 2 (T2D) diabetes. T1D is characterized by autoimmune destruction of pancreatic beta cells and deficient insulin production. Those with T1D require administration of insulin to regulate the levels of glucose in their blood. T2D is mainly a result of insulin resistance with a gradual loss of pancreatic beta cells. T2D is much more prevalent than T1D and is challenging to diagnose because the symptoms are not obvious until complications have already arisen. A number of factors contribute to the causes of T2D. Obesity, physical inactivity, unhealthy diets coupled with ethnicity and family history all play a role in the pathology

of T2D (29). During all forms of diabetes, glucose utilization is impaired and thus the heart is compelled to switch to predominantly FA to generate ATP (1). This metabolic switch requires an increase in FA delivery and utilization. This necessitates: a) augmented FA release from adipose tissue (30); b) enhanced FA uptake by cardiomyocyte-FA transporters; c) greater breakdown of endogenous triglycerides (31); d) increased LPL-mediated hydrolysis of lipoproteins (32), and e) enhanced expression of genes involved in FA oxidation (33, 34). As the concentration of FA in triglyceride-lipoproteins is markedly higher than albumin bound FA in in the circulation, LPL-mediated FA delivery is key to maintain heart ATP demands (21).

1.6 Heart LPL in diabetes

To examine LPL activity in the vascular lumen, negatively charged heparin can be used to displace LPL. However, using this approach in humans is inappropriate as an IV heparin injection will release LPL from a number of tissues such as adipose tissue and skeletal muscle and cannot be used to identify how diabetes influences cardiac LPL (35, 36). Similarly, tissue homogenate analysis of heart LPL fails to consider that only LPL at the vascular lumen is functional. Therefore, animal models of diabetes are required to study changes in LPL activity at the vascular lumen. As such, our lab has developed a robust model of T1D in rats using the beta cell toxin Streptozotocin (STZ) (37, 38). STZ is selectively taken up by the pancreatic beta cells leading to cell death and decreased insulin production, modeling T1D. The severity of diabetes in this model can be manipulated by the dose of STZ and changes in LPL activity are reflected in the different severities. We utilized two doses of STZ, 55 mg/kg (D55) to model moderate T1D with insufficient glycemic management and 100 mg/kg (D100) to model poorly controlled severe T1D. D55 animals can be used to study acute (4 days post STZ injection) and chronic (6-12 weeks) changes in LPL (39, 40). Both acute and chronic D55 animals display hypoinsulinemia and hyperglycemia with an increase

in LPL activity, however, there is an increase in plasma FA and triglyceride in chronic D55 that is not seen in acute D55 animals (39). The initial increase in LPL activity in the acute D55 model allows for regulated FA delivery, critical to maintain the energy need of the heart (38). Unfortunately, the prolonged increase in LPL for the chronic D55 model overwhelms the hearts FA oxidation (FAO) capacity leading to a buildup of FA metabolites, cardiac triglyceride storage and cell death (3). In D100 animals there is such a dramatic reduction of insulin that these animals can only be kept for at most 7 days without exogenous insulin supplementation. Within 4 days, D100 rats display severe hypoinsulinemia, hyperglycemia, decrease LPL activity, and increased plasma FFA/triglyceride (38). We believe this is a consequence of enhanced adipose tissue lipolysis and unregulated FA delivery to the heart and the heart responds by decreasing LPL activity in an attempt to limit the amount of FA it is receiving. This hyperlipidemia quickly saturates FAO in the heart with a severe mismatch in FA delivery and oxygen required to metabolize the FA. The resultant lipotoxicity quickly leads to an increase in cell death. Therefore, in the diabetic heart it would be useful to have arrangements to a) promote angiogenesis (to ensure a steady supply of oxygen to metabolize this excess of FA), and b) prevent cell demise (associated with increased FA oxidation).

1.7 VEGF family

The VEGF family consists of 6 growth factors; VEGFA, VEGFB, VEGFC, VEGFD, VEGFE and placental growth factor (PLGF) (41). These growth factors are able to bind and activate tyrosine kinase receptors called vascular endothelial growth factor receptors, of which there are three major types (VEGFR1-3) (Figure 1). VEGFA is able to bind VEGFR1 and VEGFR2, VEGFB and PLGF can only bind VEGFR1, VEGFC and VEGFD bind to both VEGFR2 and VEGFR3 while VEGFE only binds to VEGFR2. In addition to VEGFRs, there are two co-

receptors, Neuropilin-1 (NRP1) and Neuropilin-2 (NRP2) (Figure 1). These co-receptors can bind to VEGFRs to potentiate the latter's action; some VEGFs can also bind independently to NRPs (42).

1.7.1 VEGFA

The most extensively studied member of the VEGF family, VEGFA, was first isolated and cloned in 1989 (43). The VEGFA gene is located on chromosome 6p21.1 in humans, contains 8 exons, and alternative splicing through exons 6 and 7 leads to a number of isoforms named after the number of amino acids left after cleavage of the signal peptide (44). $VEGFA_{121}$ lacks both exons 6 and 7, which encode highly basic heparin binding domains, making this isoform acidic and freely soluble once secreted. $VEGFA_{186,}$ which lacks exon 6B, and the full length $VEGFA_{206}$ contain multiple heparin binding domains allowing for almost complete sequestration once secreted, due to their high heparin affinity. The most abundant and biologically relevant isoform, $VEGFA_{165}$ (henceforth referred to as VEGFA), lacks exon 6 but contains the heparin binding domain encoded in exon 7, allowing it to be sequestered onto the cell surface or extra cellular matrix once secreted. VEGFA is considered a key regulator of angiogenesis, promoting endothelial cell (EC) migration and proliferation (45) (Figure 1). This important role was illustrated in genetic studies where manipulation of this growth factor revealed severe defects in angiogenesis, with $VEGFA^{+/-}$ mice dying in utero (46). VEGFA also exhibits a number of additional functions; through the regulation of endothelial nitric oxide synthase (eNOS), it can increase vascular permeability and vasodilation (47), whereas increased Akt signaling gives VEGFA a role in cell survival (48). It has also been implicated in monocyte chemotaxis (49) and colony formation (50). The functions of VEGFA are mediated primarily through binding and activation of VEGFR2. Interestingly, VEFGA also binds to VEGFR1 and that too, with a 10-fold higher affinity (51).

Paradoxically, binding of VEGFA to VEGFR1 has limited receptor activation, suggestive of VEGFR1 being a negative regulator of VEGFA action (52) (Figure 1). In this regard, VEGFR1 knockout is embryonically lethal as in the absence of this receptor, VEGFA only binds to VEGFR2 leading to hyper vascularization (53).

1.7.2 Other VEGFs

VEGFC and VEGFD play a prominent role in lymphoangiogenesis (54, 55). Both of these growth factors are secreted as pro-proteins with long C and N terminals that require cleaving for them to become fully active and bind to VEGFR2 and VEGFR3 (Figure 1). Deletion of VEGFD does not produce any obvious phenotype (56), while experiments with recombinant VEGFD promote lymphatic EC angiogenesis. Deletion of VEGFC is embryonically lethal due to lack of lymphatic vessel development (57) while overexpression of VEGFC results in selective induction of lymphatic EC proliferation (58). VEGFE was discovered in the genome of the Orf virus which can occasionally infect humans through contact with goats and sheep, and leads to highly vascularized skin lesions (59). VEGFE acts in a similar fashion as $VEGFA_{165}$ but only binds VEGFR2 (Figure 1) and is structurally similar to $VEGFA_{121}$ with no heparin binding capabilities. PLGF is structurally similar to VEGFA, containing four isoforms (PLGF1-4) (60). PLGF1 and PLGF3 are freely diffusible lacking a heparin binding domain, while PLGF2 and PLGF4 contain an additional 21 basic amino acids enabling these isoforms to be sequestered. PLGF can only bind VEGFR1 but unlike VEGFA, PLGF is pro-angiogenic on binding to this receptor (Figure 1). PLGF null mice are healthy indicating PLGF as being redundant for vascular development. However, knockout of PLGF shows impaired angiogenesis in pathological conditions such as ischemia (61).

1.7.3 VEGFB

The VEGFB gene is located on chromosome 11q13.1 and alternative splicing leads to two isoforms. $VEGFB_{167}$ encompasses over 80% of transcripts (62) and contains a highly basic C-terminal heparin binding domain allowing it to be sequestered onto the cell surface, much like $VEGFA_{165}$. The other isoform, $VEGFB_{186}$ has a hydrophobic C-terminal and no heparin binding domain making it freely soluble (63) (Figure 2). Tissue expression analysis of VEGFB observed this growth factor to be highly expressed in the heart and skeletal muscle, with limited expression in most other tissues (64). The genetic expression of VEGFB is fairly stable and is not regulated by growth factors, hypoxia or hormones (65). Genetic knockout of VEGFB demonstrated that this growth factor is not relevant for normal health (66), as VEGFB null mice developed only a mild phenotype with no effect on mortality. VEGFB shares 47% of its amino acid sequence with VEGFA and contains the hallmark PXCVXXX-RCXGCC VEGF family motif (64), which lead to the initial studies focused on a role for VEGFB in angiogenesis. Unlike the other members of the VEGF family, VEGFB uncharacteristically does not promote angiogenesis (67-69). For example, although it was suggested that VEGFB is able to induce EC growth, this was ultimately attributed to VEGFA/VEGFB heterodimer formation that has only been see *in vitro*, and not a direct function of VEGFB (70). Through the use of adenoviral vectors to promote overexpression in muscle or peri-adventital tissue, VEGFB was unable to stimulate vessel growth (71). In mice transgenically overexpressing VEGFB in the skin, there was limited effect on blood vessel density although an increase in capillary diameter was observed (72). Finally, ischemic limb studies provided additional evidence against VEGFB being an angiogenic growth factor as it was ineffective in aiding vascular growth (73). Due to an absence of a role in angiogenesis, the novelty of this growth factor diminished after its discovery. More recently, the importance of VEGFB has been described

in cell survival (69) (Figure 3), a function that is especially relevant under pathological conditions (74).

1.7.3.1 Receptor binding

The action of VEGFB is coordinated by its binding to VEGFR1. The VEGFR1 gene is located on chromosome 13q12.3 and encodes a tyrosine kinase receptor comprised of an extracellular ligand binding domain, a transmembrane domain, intracellular tyrosine kinase domain and a carboxy-terminal region (51). Alternative splicing also generates a soluble form of VEGFR1 (sVEGFR1) that only contains the extra cellular ligand binding domain. Three members of the VEGF family, VEGFA, VEGFB and PLGF can bind VEGFR1, each with distinct functions. VEGFB binding leads to activation of a number of downstream activators similar to most tyrosine kinase receptors, including p38 MAPK, ERK/MAPK, PKB/AKT and PI3K (75). VEGFA binding to VEGFR1 does not produce significant receptor activation (75) (Figure 1), indicating that VEGFR1 could act as a negative regulator of VEGFA action. In this regard, deletion of the VEGFR1 gene is embryonically lethal (76), likely due to enhanced VEGFA action on VEGFR2, promoting uncontrolled angiogenesis. Interestingly, deletion of only the tyrosine kinase domain results in normal healthy mice (77), suggesting that the ligand binding domain is necessary for VEGFR1 regulation of VEGFA. Further evidence for a role of this receptor in regulating proper angiogenesis is the expression of this receptor primarily in the blood vessels of numerous organs such as the heart, kidney, liver and brain (78). Soluble VEGFR1 is also a potent anti-angiogenic factor that can bind VEGFA in the plasma. PLGF will bind VEGFR1, but unlike VEGFB, can induce angiogenesis (79) (Figure 1). The effect of binding of PLGF to VEGFR1 to induce angiogenesis has been suggested to be a consequence of its interaction with the immunoglobulin

domains two and three of the receptor, an action that is not seen with VEGFB that only binds to Ig domain two (80).

1.7.3.2 Enhanced VEGFA induced angiogenesis through VEGFB action

Unlike the futile studies related to examining the function of VEGFB in angiogenesis, recent studies have recognized a prominent role of this growth factor in sensitizing cells to VEGFA induced angiogenesis (74, 81). This phenomenon can be explained through the specificity of VEGFA and VEGFB binding to VEGFR1 and VEGFR2. VEGFA can bind to both VEGFR1 and VEGFR2, but only by binding VEGFR2 does VEGFA activate downstream signaling. It should be noted that VEGFR1 has an order of magnitude greater affinity for VEGFA (51). Conversely, binding of VEGFB to VEGFR1 initiates downstream signals (Figure 1). Transgenic (TG) overexpression of VEGFB revealed an interesting mechanism in which excess VEGFB can occupy VEGFR1, allowing more VEGFA activation of VEGFR2 (Figure 4). In a cardiomyocyte specific overexpression of VEGFB, TG rat hearts displayed enhanced activation of multiple downstream signaling VEGFA targets (74). Moreover, VEGFA administration to VEGFB TG animals presented greater downstream signaling after 10 minutes compared to wildtype. Accordingly, VEGFB knockout animals demonstrated blunted VEGFA action compared to wildtype, likely a result of increased available VEGFR1 negatively regulating this growth factor. In a more recent study, whole body adeno-associated virus (AAV) VEGFB transduction in mice showed unanticipated vascular effects in adipose tissue (81). As quickly as two weeks post AAV administration, increased capillary density and vessel size was observed. This enhanced capillary network displayed a normal pattern compared to whole body AAV administration of VEGFA which revealed abnormal vasculature and increased infiltration of inflammatory cells. This study reasoned that the increased vasculature seen in VEGFB AAV animals was not due to a direct effect

of VEGFB but a result of increased physiological VEGFA action of VEGFR2 due to less available VEGFR1 (Figure 4).

1.7.3.3 Role in cell survival

In addition to the indirect effects of VEGFB in enhancing VEGFA action, recent studies have recognized a prominent role of this growth factor in cell survival, and a number of exciting areas of research have emerged. While whole body knockout of the VEGFB gene has limited consequences, employing this mouse model in various disease conditions has uncovered a protective role for VEGFB. In a cerebral ischemic injury model, $VEGFB^{-/-}$ mice displayed a 40% greater increase in infarct size as well as severity of brain dysfunction compared to wildtype animals (82). This study also examined cultured neurons exposed to hypoxia to induce cell death and determined that cells cultured with 100 ng/mL VEGFB had less demise, further reinforcing a neuroprotective role for VEGFB. Through the use of a mouse cornea pocket assay, which causes degradation of corneal blood vessels, VEGFB null mice displayed accelerated degeneration and after three weeks had fewer blood vessels (69). Furthermore, in an oxygen induced blood vessel regression model, VEGFB deficient mice had increased regression and treatment with a VEGFB neutralizing antibody further intensified this observation. Conversely, intravitreal VEGFB treatment inhibited blood vessel regression. This survival effect of VEGFB was also observed in cells other than vascular EC. Hence, when primary chordial EC, retinal EC, $CD133^{+}CD34^{+}$ stem cells and aortic smooth muscle cells (SMC) isolated from VEGFB null mice were cultured in serum free medium or under H_2O_2-induced stress, they exhibited increased apoptosis and VEGFB treatment of these cells reduced this effect. Culture of retinal EC, chordial EC, pericytes, and SMC immortalized cell lines from also show decrease serum starved cell death when treated with VEGFB (Figure 3). Finally, in a model of acute myocardial infarction, $VEGFB^{-/-}$ mice

demonstrated reduced revascularization of the ischemic border 7 days post MI as a consequence of fewer thrombomodulin positive capillaries and smooth muscle α-actin positive covered vessels in the infarct area compared to wildtype animals (73). As was seen in other studies and models, administration of VEGFB to these $VEGFB^{-/-}$ mice induced revascularization.

Unlike VEGFB knockout animals, overexpression of VEGFB (particularly in the heart) produced significant alterations that were cardio protective. Rats with the VEGFB gene complexed to the αMHC promoter generates a cardiomyocyte-specific overexpression of VEGFB. These animals displayed a robust increase in arteries of all sizes, especially vessels >150 μm, in which there was a five-fold increase. Additionally, these hearts had capillaries with larger diameters (74) (Figure 3). A unique feature of these TG hearts was that they exhibited cardiac hypertrophy, but this was not accompanied by functional changes. Even at 22-months of age, there were no differences in ejection fraction, fractional shortening or maximal exercise capability. Moreover, gene expression analysis identified no change in genes related to cardiac hypertrophy. Exposing these animals to experimental MI revealed marked differences between the groups. Rats with cardiomyocyte overexpression of VEGFB had less severe decrease in ejection fraction, fractional shortening and an increase in left ventricular systolic and diastolic diameters at both 1 and 4 weeks post MI. The TG hearts also demonstrated better perfusion in both the non-infarcted area as well as the infarcted and border areas. Analysis of the infarct size post-mortem confirmed a substantial decrease in infarct size in TG hearts from both male and female rats. Additionally, this study treated mice with angiotensin II for two weeks to model hypertrophy and found decreased VEGFB mRNA expression in the heart. Along similar lines, in human heart samples from subjects that underwent heart transplant, there was decreased VEGFB mRNA in removed hearts from those with ischemic heart disease or dilated cardiomyopathy compared to donor hearts that were not

used for transplant (74). In another study (290 subjects, average age 63 and over 75% male), that had an MI displayed increased plasma VEGFB compared to healthy controls (83). However, within this MI group, patients that exhibited increased left ventricular remodeling six months' post MI; a marker for potential left ventricular dysfunction and heart failure, had lower plasma VEGFB prior to discharge. As defined in the study, LV remodeling was the variation of LV end diastolic volumes between discharge and 6 months' follow-up. These studies have led to investigation of VEGFB gene therapy in a number of heart disease models. In one study, echocardiography of mice that underwent transversal aortic constriction had lower ejection fraction and fractional shortening, left ventricular hypertrophy and had decreased VEGFB mRNA four weeks after surgery compared to sham treated animals (84). Treatment via VEGFB viral vectors 2 weeks' post-surgery abolished the decreases in ejection fraction, fractional shortening and displayed less severe hypertrophy after echocardiography analysis. These effects were suggested to be due to an increase in cardiomyocyte proliferation (detected by Ki-67 immunostaining) and decreased apoptosis (seen via cleaved caspase 3 immunostaining).

In another study, dogs were exposed to 28 days of left ventricular pacing via an external pacemaker to induce a model of dilated cardiomyopathy (85). Intracoronary VEGFB was delivered either 2 days prior to pacing or 2 weeks after initiation of the pacing protocol (these animals were labeled delayed AAV-CMV-VEGFB). Paced animals that did not receive VEGFB transgene displayed typical signs of decompensated heart failure with increased left ventricular end-diastolic pressure, decreased left ventricular systolic pressure and decreased mean arterial pressure. Animals given VEGFB viral vectors prior to pacing showed no significant changes while the delayed VEGFB treated animals had significant changes after 2 weeks of pacing but no further changes once VEGFB treatment was initiated. Finally, the cardio-protective ability of VEGFB was

examined with respect to mitigating the cardio toxic effects of drugs like doxorubicin (86). Doxorubicin is a commonly used anti-cancer drug that is effective against a variety of cancers by inhibiting cell cycle progression and stopping proliferation of malignant cells (87). However, multiple doses of doxorubicin have been found to be cardio toxic, leading to left ventricular dysfunction and heart failure. Mice injected with AAV9-VEGFB seven days before initiation of a multiple doxorubicin dose protocol, saw no decrease in heart weight and cardiomyocyte size as seen in control mice (86). Moreover, VEGFB pretreatment prevented cardiac microvasculature damage. Additionally, a single high dose injection of doxorubicin induced DNA double-strand breaks which was reduced in VEGFB pretreated animals.

Furthermore, the use of recombinant VEGFB protein has also been employed to investigate the mechanisms of this growth factor in preventing cell death (Figure 3). Treatment of primary aortic SMC with human recombinant VEGFB downregulated many genes involved in apoptosis such as Bmf, TrP53inp1, and DCN (88). In cell lines treated with VEGFB, there was a substantial downregulation of many BH3-only protein genes such as Bad and Bid, and other genes related to cell death like Casp9, Bax and TNF-α. A rat ganglion cell line treated with VEGFB and exposed to hydrogen peroxide (H_2O_2) or serum starvation to induce cell death revealed that VEGFB was protective in both instances and promoted cell survival (88). This serum starved cell survival effect was not seen with other VEGFR1 ligands like PLGF, whereas VEGFA had a weaker effect. Additionally, in an optic nerve crush injury model, injection of VEGFB into the eye following injury resulted in an increase in the number of viable ganglion cells when measured 2 weeks post procedure. Similarly, inhibition of VEGFB with a neutralizing antibody decreased the number of viable cells in this model. VEGFB treatment was also able to reduce neuronal apoptosis following NMDA or ischemia induced apoptosis. In all of these models, real-time PCR revealed that VEGFB

treatment reduced the expression of apoptotic genes and VEGFR1 blockade using a neutralizing antibody eliminated the protective effects of VEGFB, implying that the benefits of this growth factor are found by binding VEGFR1 (88). In another study, cardiomyocytes were exposed to 48 hours of hypoxia and then 24 hours of reoxygenation with or without VEGFB. The presence of this growth factor decreased the percentage of apoptotic cells and a similar finding was seen with cells treated with the cardiotoxic drug epirubicin (89). VEGFB treatment of cardiomyocytes for 24 hours increased the expression of many genes involved in contractility (αMHC), calcium handling (SERCA2a) and mitochondrial function (PGC1α) in a manner similar to that seen with compensatory hypertrophy induced by the thyroid hormone T3 (Figure 3).

1.7.3.4 VEGFB in diabetes

VEGFB has been indicated to play a role in cell survival and indirectly promote VEGFA induced angiogenesis (44, 69, 74) (Figure 4). Both of these functions are highly desirable, particularly during diabetes, with increased cardiomyocyte demise and poor angiogenesis in the heart being hallmark conditions associated with this disease (90, 91). Currently it is unclear whether this increased cell death or decreased angiogenesis in the heart is an outcome of changes in VEGFB. We injected rats with streptozotocin (STZ), a β-cell-specific toxin to induce diabetes. A single dose of 55 mg/kg (D55) STZ was used to induce moderate diabetes and the animals kept for 6 weeks, a well-established model of diabetic cardiomyopathy (92). Analysis of cardiomyocyte VEGFB protein and mRNA expression revealed a significant decrease in the production of this growth factor (93). Furthermore, there was reduced cell survival signaling as well as a corresponding increase in cell death markers such as cleaved caspase 3 and cleaved PARP. Interestingly, there was a robust increase in VEGFR1 expression in the diabetic animals. However, treatment with recombinant VEGFB did not elicit downstream signaling as seen with control

cardiomyocytes, suggesting a defect in VEGFR1 in the diabetic heart. These results (low VEGFB, increased VEGFR1 and blunted signaling) were also duplicated in animals made severely diabetic with 100 mg/kg STZ (D100) and monitored for 4 days. Interestingly, although insulin treatment of these D100 animals to produce euglycemia restored VEGFB protein expression, there was no change in VEGFR1 expression or its downstream signaling. These data for the first time suggested that the loss of VEGFB and its downstream signaling events is an early event after hyperglycemia, is sustained with disease progression, and could explain diabetic cardiomyopathy. In addition to cardiomyopathy, diabetic retinopathy is also a major consequence of diabetes. In rats made diabetic with 50 mg/kg STZ and injected with multiple intravitreal VEGFB injections 10 weeks later, TUNEL staining of the rat ganglion cell layer revealed a decrease in the number of apoptotic cells in the STZ animals treated with VEGFB (94). During diabetes, the heart can no longer utilize glucose as an energy source and must adapt to use FA to generate ATP (3). While this switch ensures the heart is able to manage its constant energy demands, the increased reliance upon FA leads to a number of consequences. Generating ATP through FA oxidation requires more oxygen than using glucose and in diabetes there is blunted VEGFA mediated angiogenesis leading to a reduced supply of oxygen (95, 96). This lack of oxygen bottlenecks FAO resulting in the diabetic heart having to store the excess FA as triglycerides (20). Furthermore, the accumulation of triglycerides leads to the formation of ceramides and diacylglycerols which can lead to cardiac cell death (2). It is within this paradigm that the efficacy of VEGFB, as a therapy for the diabetic heart, is compelling. VEGFB has the capability of enhancing VEGFA induced angiogenesis (81) which can aid in providing the heart the necessary oxygen to metabolize the increased supply of FA. In addition, through its actions promoting cell survival, VEGFB would be able to limit cardiac cell

death and help delay heart failure. In conclusion, we suggest that using VEGFB as a cardio protective therapy in diabetes is an intriguing concept and should be explored.

1.8 Hypothesis and research objectives

The diabetic heart, compelled to alter its metabolic needs, requires growth factors to protect itself against the damaging effects associated with an overwhelming supply of fatty acids. We hypothesize that there is a role for VEGFB in diabetic cardiomyopathy. The objectives of this thesis were to:

1. Determine the changes in cardiac metabolism following diabetes as a consequence of alterations in VEGFB production.
2. Investigate the mechanisms behind the action of VEGFB in the heart subsequent to diabetes.
3. Identify the potential benefits of VEGFB subsequent to chronic diabetes.

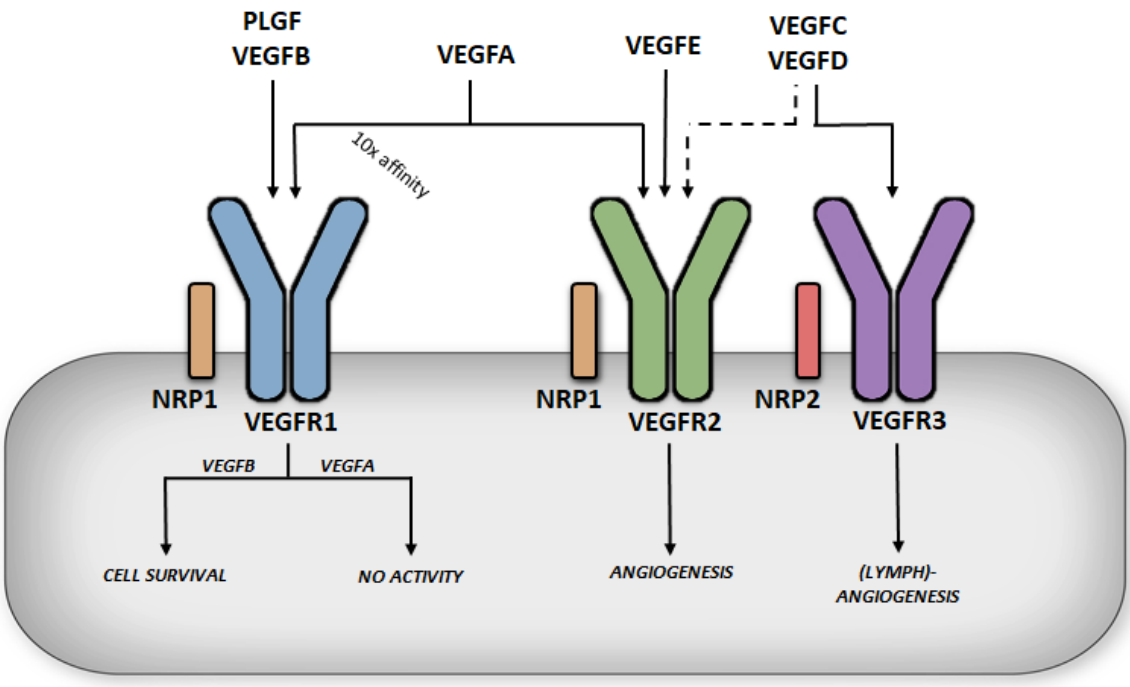

Figure 1. Differential functions of vascular endothelial growth factor receptors. VEGFA binding to VEGFR1 does not produce significant receptor activation (in this case the receptor acts a decoy), whereas VEGFB binding to VEGFR1 has been described to promote cell survival. PLGF can also bind to VEGFR1 but promotes angiogenesis. VEGFA binds to VEGFR2, albeit with a lower affinity, but this is considered a key regulator of angiogenesis, promoting endothelial cell migration and proliferation. Neuropilin-1 (NRP1) and Neuropilin-2 (NRP2) are co-receptors that can bind to VEGFRs to potentiate the latter's action; some VEGFs can also bind independently to NRPs. VEGFC and VEGFD bind to both VEGFR2 and VEGFR3 and play a prominent role in lymphoangiogenesis. VEGFE acts in a similar fashion as VEGFA but only binds VEGFR2.

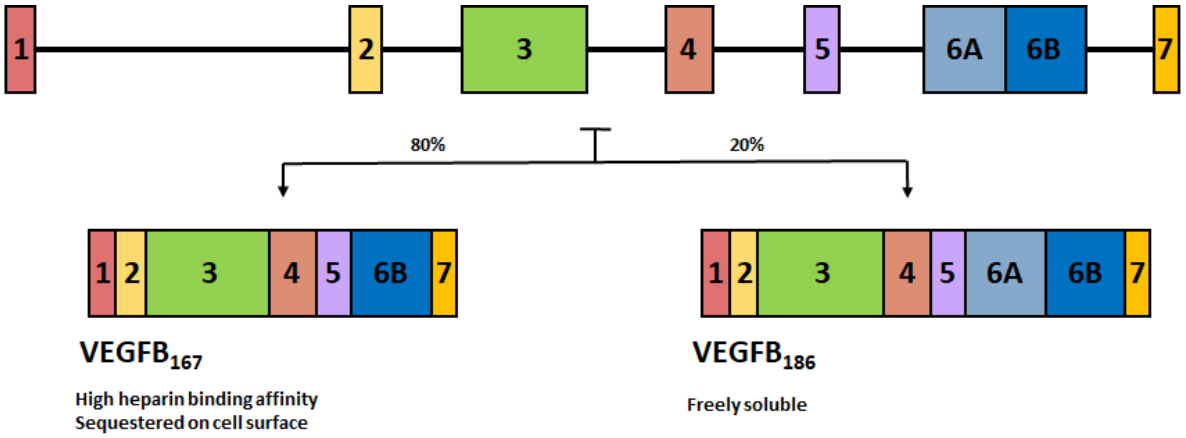

Figure 2. Alternative splicing of VEGFB. Alternative splicing leads to two isoforms. $VEGFB_{167}$ encompasses over 80% of transcripts and contains a highly basic C-terminal heparin binding domain allowing it to be sequestered onto the cell surface. The other isoform, $VEGFB_{186}$ has a hydrophobic C-terminal and no heparin binding domain making it freely soluble.

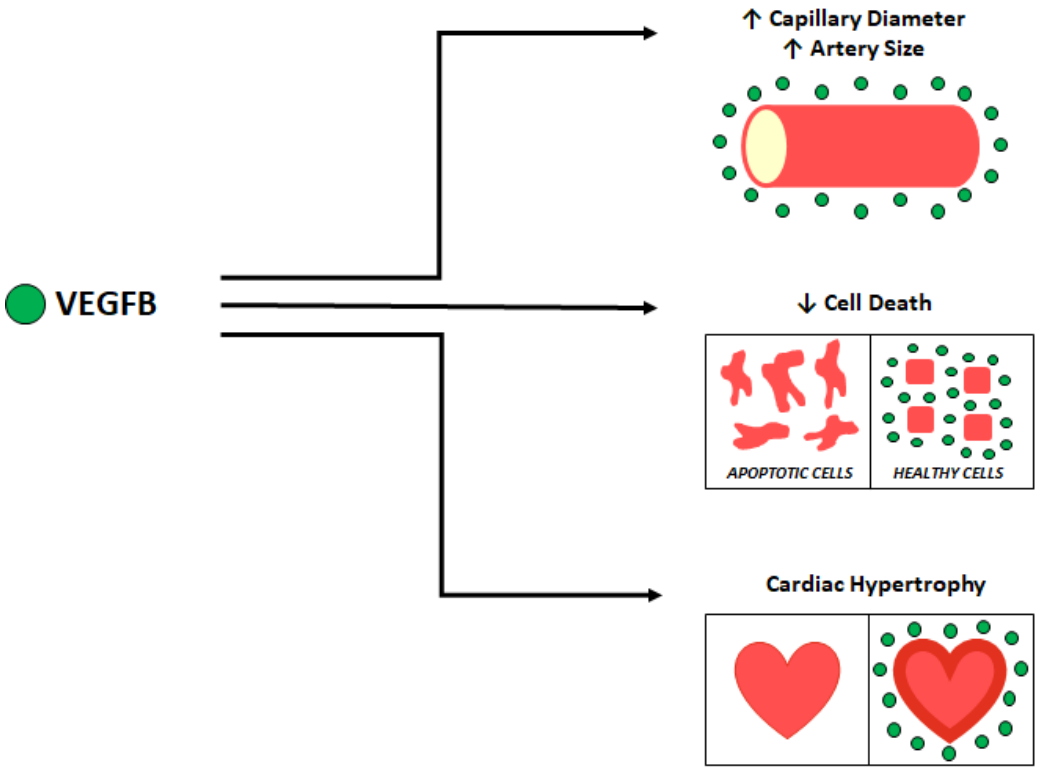

Figure 3. Cardio protective actions of VEGFB. Although it does not play a direct role in angiogenesis, VEGFB has been implicated in increasing capillary diameter and artery size. Additionally, VEGFB has a significant role in protecting against cell death and promoting physiological hypertrophy.

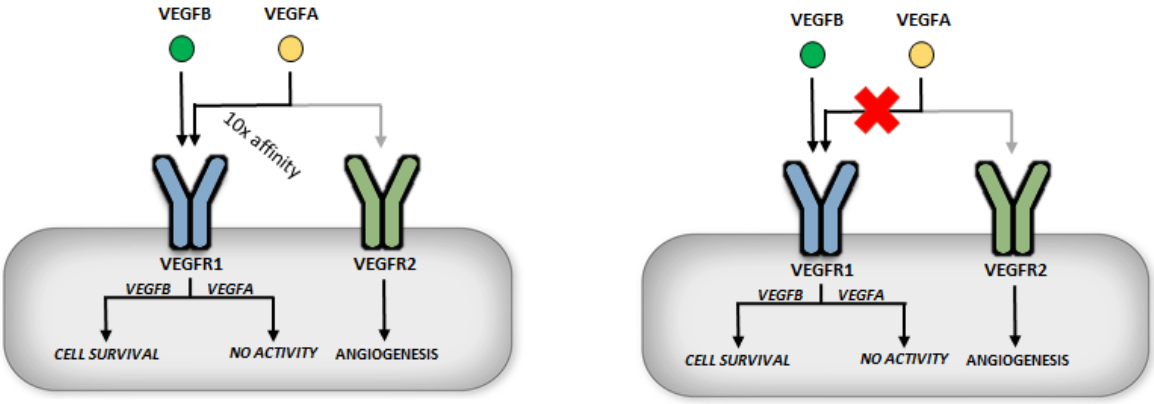

Figure 4. Indirect role of VEGFB in angiogenesis. VEGFR1 has a 10x fold greater affinity for binding VEGFA than VEGFR2 (left panel). Overexpression of VEGFB is suggested to occupy and thus displace VEGFA from VEGFR1. This allows more VEGFA to bind to VEGFR2 and can initiate angiogenesis (right panel).

CHAPTER 2: METHODS

2.1 Materials

Rat heart micro vessel endothelial cells (RHMEC) were obtained from VEC technologies. STZ (S0130) was obtained from Sigma-Aldrich. Anti-VEGFB (sc-1877), anti-phospho PI 3-Kinase p85a (Tyr 508) (sc-12929), anti-PI 3-Kinase p85a (sc-423), anti-insulin receptor β (sc-711), anti-NOS3 (sc-654), anti-PDGFB (sc-7878), anti-PDGFRβ (sc-432) and anti-β-actin (sc-47778) antibodies were purchased from Santa Cruz Biotechnology. Anti-heparanase (ab59787), anti-VEGFR1 (ab32152) antibodies were purchased from Abcam. Anti-vinculin (13901), anti-phospho ERK p42/44 (Thr202/Tyr204) (4370), anti-total ERK (9102), anti-phospho GSK3β (Ser9) (9336), anti-GSK3β (9315), anti-PARP (9542), anti-phospho Akt (S473) (9271), Akt (9272) and anti-caspase 3 (9662) antibodies were obtained from Cell Signaling Technology. Purified Hep-L was prepared as described previously (97), recombinant human active heparanase (7570-GH-005) was bought from R&D Systems, and heparin (Hepalean, 1000U/ml) was purchased from Organon, Canada. For Western blots that detect only Hep-L, we used the heparanase (N-Term) antibody (ABIN786265), which preferentially recognizes the 65 kDa Hep-L, from Aviva Systems Biology. Hydrogen peroxide (H1009) was purchased from Sigma Aldrich. For insulin injection we used Humulin R, 100 U/mL (Eli Lily).

2.2 Experimental animals

Animals were housed under a 12 h light/dark cycle under pathogen-free conditions and with free access to standard chow (LabDiet PicoLab Rodent 20 #5053) and RO water. Adult male Wistar rats (240-260 g) were purchased from Charles River Laboratories. A breeding pair of VEGFB transgenic (TG) rats, with cardiomyocyte specific promoter α-myosin heavy chain (α-

MHC) mediated overexpression of human VEGFB, were a kind gift from Dr. Kari Alitalo (74, 98), wildtype littermates were used as control. Rat had ab libitum access to water and food (Pico Lab Rodent Diet 20). Streptozotocin (STZ) is a β-cell-specific toxin used to induce hypoinsulinemia and diabetes. Under isoflurane anesthesia, animals were injected with a single i.v. dose of 55 (D55) or 100 (D100) mg/kg STZ into the tail vein (38). After 24 h, hyperglycemia (>13 mmol/L) was confirmed in tail-tip blood samples using a glucometer (AccuSoft) and glucose test strips (Accu-Chek Advantage; Roche). Those injected with 100 mg/kg STZ were followed for 4 days (acute severe diabetes; these animals cannot be followed chronically due to near complete destruction of beta cells and mortality beyond 1 week as a consequence of ketoacidosis) before heart isolation. One group of D55 animals was kept acutely for 4 days (STZ-A) whereas another was followed chronically for 6 weeks (Chronic-D or STZ-C), a duration that is necessary for development of DCM (99), with age matched saline injected animals as control.

2.3 Metabolic assessments

At termination, hearts were exsanguinated and blood in the thoracic cavity collected in K2-EDTA tubes and centrifuged immediately for separation of plasma that was used for determination of insulin (rat insulin ELISA; ALPCO), FA (NEFA-HR; Wako Diagnostics) and triglyceride (Stanbio Triglycerides Liquicolor Mono). After acid-ethanol extraction, insulin content in the pancreas was assessed by ELISA (rat insulin ELISA; ALPCO).

2.4 RNA Sequencing and analysis

Total RNA from rat hearts was isolated using TRIzol. Sequencing libraries were prepared from 400 ng total RNA using the TruSeq Stranded mRNA Sample Preparation kit (Illumina, San Diego, CA). Samples were checked for quality using a Bioanalyzer (Agilent, CA, USA) and quantified

using Qubit fluorometer (ThermoFisher, MA, USA). Libraries were multiplexed and sequenced on the NextSeq 500 (Illumina). Following a previously published procedure (100), multiple analysis pipelines were applied and their results combined. The output for each pipeline was a list of genes ranked by the p-value for differential expression after correction for multiple testing. A combined list was obtained by ranking the genes according to their median rank from the various analysis pipelines. Potential outliers within a group were detected when clustering the samples and removed for the differential expression analysis. Network analysis and function categorization were conducted using STRING (set at the highest confidence with evidence from experiments, databases, co-expression, and co-occurrence(101)). GO term enrichment and KEGG pathway analysis (EnrichR software(102)) of differentially expressed genes were also applied to ascertain significantly enriched pathways.

2.5 Separation and characterization of plasma and cardiac lipids

Total plasma and cardiac lipids were extracted and solubilized in degassed chloroform:methanol:acetone:hexane (4:6:1:1v/v/v/v). Separation of triglyceride and FA were achieved using HPLC (Waters 2690 Alliance HPLC, Milford, MA) equipped with an auto-sampler and column heater, as previously described (103). Lipid classes were separated on a YMC DIOL column (4.6 x 250 mm, YMC USA) and the HPLC flow was split with approximately 80% flow going to a Waters FCII fraction collector and the remaining 20% flow going to a Waters evaporative light scattering detector (ELSD). Phospholipid fractions were collected, solvent evaporated under a stream of Nitrogen, then derivatized with boron trifluoride (14%) in methanol. Individual FA methyl esters were then separated using an Agilent 6850 GLC equipped with a flame ionization detector and an SP-2330 capillary column (30 m x 0.25 mm internal diameter) (Supelco, Bellefonte, PA) using hydrogen as a carrier gas. Peak areas were calculated using

Agilent Chemstation software and FA quantified using heptadecaenoic acid (17:0) as the internal standard (Performed by Analytical Core for Metabolomics and Nutrition, BC Children's Hospital Research Institute).

2.6 Isolation of cardiomyocytes

Rats were euthanized using a 100 mg/kg intraperitoneal injection of sodium pentobarbital. Once toe pinch and corneal reflexes were lost, a thoracotomy was performed prior to removal of the heart. After cannulation of the aorta, the heart was secured by tying below the innominate artery, and was retrogradely perfused with Krebs-Henseleit buffer. Ventricular calcium-tolerant myocytes were prepared by a previously described procedure (39). Briefly, myocytes were made calcium tolerant by successive exposure to increasing concentrations of calcium. Cardiomyocytes were plated at a density of 200,000 cells/well on laminin-coated 6-well culture plates. After 6-8 hours of incubation, cells were used for various experimental procedures. Cells were maintained in Medium-199 (M5017, Sigma-Aldrich) and incubated at 37°C in a 5% CO_2 humidified incubator. Unattached cells were washed away prior to different treatment protocols.

2.7 Mitochondrial stress test

Oxygen consumption rate (OCR) was measured using the Seahorse XFe96 extracellular flux analyzer and the Seahorse XF Cell Mito Stress Test kit (Agilent, Santa Clara, CA). Mitochondrial inhibitor concentrations and cell density were optimized, and protocols were based on previously published data (104, 105). Cardiomyocytes were plated at a density of 5,000 cells/well (96 well plate) and incubated overnight in 150 µL of normal culture medium (replicates of 8-12 wells per condition and cell type). The next day, cells were washed twice with warm substrate-limited assay media (XF Base Medium, 2.5 mM glucose, 0.1 mM Sodium pyruvate, 4 mM L-glutamine, 0.5 mM

L-carnitine, 5 mM HEPES, pH7.) and incubated with fresh assay media for 1 h. Immediately prior to assay either BSA, 0.05 mM PA, or 0.1 mM PA were added to the wells (PA:BSA Agilent, Santa Clara, CA). The cartridge was loaded with three metabolic inhibitors, which were sequentially injected into the plate and OCR measured after each addition subsequent to 3 initial baseline readings: oligomycin (2 µM), FCCP (2 µM), followed by the combination of rotenone and antimycin A (2 µM/10 µM). At the end of the assay, OCR was normalized to protein content. All inhibitors were included in the Seahorse XF Cell Mito Stress Test kit (Agilent, Santa Clara, CA).

2.8 Cardiac apoptosis

TdT mediated dUTP nick end labeling (TUNEL) assay on whole heart sections was carried out using a TUNEL kit (Promega) as described previously (103).

2.9 Metabolomic profiling

Untargeted metabolomic analysis was performed using an Agilent 6530 quadrupole-time of flight mass spectrometer (QTOF), Agilent 1290 binary UPLC and MassHunter data acquisition software. The instrument was operated in positive ion, then negative ion mode for reverse phase (RP) and hydrophilic interaction (HILIC) chromatography involving a total of 4 separate runs for each sample. Negative ion tests utilized the same columns but mobile phases were 5 mM ammonium acetate (Fisher Optima LCMS grade) in 98% water 2% acetonitrile, with pH adjusted to 9.2 using ammonium hydroxide. RP chromatography utilized a Waters BEH-C18 column, 2.1 x 100 mm, 1.7 um particle size and similar buffered mobile phases to HILIC with the exception of using methanol rather than acetonitrile. Gradient chromatography was used for both HILIC and RP with starting conditions of 90% organic solvent for HILIC and 90% aqueous for RP and total run times of 35-45 minutes. The 6530 QTOF with Agilent Jet Spray was operated in electrospray

ionization mode and utilized dual ESI nebulizers for simultaneous introduction of sample and reference mass solutions, data was collected at 2 scans/second with a m/z range of 65 to 1050 in all modes of operation. The QTOF was tuned specifically for low masses following the manufacturer's instructions, operated in high resolution mode using 4 GHz data acquisition and used Agilent's standard reference mass solution providing corrected mass accuracy of about 2-3 ppm. Additional runs of pooled heart samples used MS/MS mode and specifically targeted ions of interest with collision energies of 10, 20 or 40 volts to assist in identification of analytes. Data processing used multiple Agilent technologies software packages. Profinder ver10.0 was used for molecular feature extraction then all features were exported to the chemometric software Mass Profiler Professional (MPP). Data imported to MPP was normalized using a 75th percentile shift algorithm, baselined to the median of all samples, then filtered to remove entities that were highly variable within any one sample group. Identification of metabolites utilized a number of resources including Agilent MassHunter ID Browser B.08 software and Metlin accurate mass MS/MS spectral library with matching mass tolerance set at 2mDa +/- 5ppm, online mass spectral libraries from the Human Metabolome Database 26 and MassBank (https://massbank.eu/MassBank/), and a mass spectral/retention time library created from about 200 compounds provided by BC Children's Hospital Newborn Screening program.

2.10 Endothelial cell culture

RHMEC were cultured in MCDB131 (VEC Technologies) growth medium at 37°C in a 5% CO_2 humidified incubator (106). Cells from the fifth to the eighth passages of 3 different starting batches were used.

2.11 Endothelial cell and cardiomyocyte co-culture

For co-culture with cardiomyocytes, ECs were seeded on Transwell inserts (Falcon, 24 mm diameter; 1.0 µm pore size; culture medium MCDB131). Upon reaching 80-90% confluence, MCDB131 was replaced with DMEM (changing the medium did not affect cell morphology or viability within the treatment time used). These inserts were placed in a 6-well plate that had cardiomyocytes attached to the bottom. Cardiomyocytes were plated at a density of 200,000 cells/well.

2.12 Treatments

To promote the secretion of heparanase, EC were incubated in Dulbecco's Modified Eagle Medium (Thermo Fisher Scientific) containing either normal glucose (5.5 mM, NG) or high glucose (25 mM, HG) for 30 minutes. Cell culture media was concentrated with an Amicon centrifuge filter (Millipore) before the detection of heparanase protein. To detect HSPG bound VEGFB, medium was collected from cardiomyocytes incubated with either heparin (10 U/ml) or recombinant latent or active heparanase (2 µg/ml) for 20 minutes. This medium was centrifuged at 500 g for 5 minutes, and VEGFB determined using a rat VEGFB ELISA Kit (LSBio). To examine cell death signals, we used oxidative stress induction with treatments of H_2O_2. RHMEC or cardiomyocytes were pre-treated with VEGFB (100 ng/mL) for 1 hour, followed by treatment with 100 µM H_2O_2 for 4 hours (RHMEC) or 15 minutes (cardiomyocytes). Bax and Bcl2 mRNA expression were also evaluated after VEGFB treatment for 24 hours. In one group of animals made diabetic with 100 mg/kg STZ and kept for 4 days, fast acting insulin (Humulin R; 22 U/kg) was injected via the tail vein, blood glucose monitored at timed intervals, and were euthanized 120 minutes after insulin injection for determination of cardiomyocyte VEGFB.

2.13 Western blotting

Western blot was done as previously described (107). To measure protein expression, 20-40 µg protein was loaded. Membranes were incubated with primary antibodies [1:500 – 1:10,000] diluted in 5% BSA Tris-Buffered Saline, 0.1% Tween-20 (TBST) at 4°C overnight, and subsequently with secondary antibodies (1:2,500-1: 20,000) diluted in TBST at room temperature for 1 hour. Images were visualized using a Li-COR Odyssey digital imaging system. Blots were quantified by Image Studio™ Lite.

2.14 Quantitative real-time PCR

Total RNA was isolated from EC, whole hearts, or cardiomyocytes using TRIzol (Invitrogen). This was followed by extraction using chloroform and isopropanol, washing with ethanol, and dissolving in RNase-free water. 1 µg of RNA was reverse transcribed to cDNA using a mixture of dNTPs, oligo-(dT), and SuperScript II Reverse Transcriptase. cDNA was amplified by TaqMan gene expression assay in triplicate, using a StepOnePlus Real-Time PCR system (Applied Biosystems). Primers for Bax (Rn01480161_g1), Bcl2 (Rn99999125_m1), rat VEGFB (Rn01454585_g1), Angptl4 (Rn01528817_m1) β-actin (Rn00667869_m1) and B2M (Rn03928990_g1) were purchased from Thermo Fisher Scientific. Gene expression was calculated by the comparative cycle threshold (ΔΔCT) method using either β-actin (in Wistar animals) or B2M (in VEFGB TG and littermate controls) as reference genes.

2.15 Lipoprotein Lipase (LPL) activity assay

To measure coronary LPL, hearts were perfused with Krebs buffer containing heparin (5 U/ml), which displaces the vascular enzyme. Perfusion effluent was collected over 30 min and LPL activity determined by measuring in vitro hydrolysis of [^{3}H]triolein substrate (38).

2.16 Statistical analysis

Statistics were performed using Prism 8 (GraphPad Software, San Diego). The Shapiro-Wilk test was performed to determine the normality of the data. Kruskal–Wallis nonparametric test followed by Dunn post hoc comparisons test was applied for non-normal distributions. Wherever appropriate, an unpaired Student's t-test or one-way ANOVA (followed by Bonferonni post hoc comparisons test) were used to determine differences between group mean values. Data are expressed as mean ± SEM with individual data points. The minimum level of statistical significance was set at $p < 0.05$.

CHAPTER 3: RESULTS

3.1 Diabetes severity and a switch from using LPL to adipose-derived fatty acid results in a cardiac metabolic signature that embraces cell death

3.1.1 The severity of STZ diabetes is uncovered by measuring insulin and not glucose.

Using dissimilar doses of STZ, we established models of diabetes of varying intensities. Accordingly, weight gain over 4 days was reduced in D55 animals compared with saline injected controls such that these rats had lower body weights at the time of death. Induction of a more severe diabetes in D100 rats over the same time period resulted in a loss of body weight (as compared to body weight on day zero; Figure 5A). Both D55 and D100 were equally hyperglycemic compared to control over the duration of the study, with no measurable difference between the two diabetic groups (Figure 5B). Intriguingly, the severity of diabetes between D55 and D100 was only uncovered following determination of insulin; D100 animals showed markedly lower plasma and pancreatic insulin compared to D55 (Figure 5C). This dramatic pancreatic β-cell destruction and hypoinsulinemia in D100 was accompanied by robust increases in plasma FA and triglyceride, effects that were essentially absent in D55 animals (Figure 5D). Our data advocates for D55 as a model of moderate T1D with insufficient glycemic management, and an increase in cardiac LPL activity (Figure 5E) to support FA provision to the heart when glucose use is curtailed. Additionally, D100 could be considered as a model of severe T1D with poor glycemic control and dyslipidemia resulting in a loss of LPL activity (Figure 5E).

3.1.2 Plasma FA composition is only altered when insulin reduction by STZ is substantial.

Subsequent to a reduction in circulating insulin, increased AT lipolysis due to lipase (ATGL and HSL) hyperactivity releases FA into the circulating plasma (108). Interestingly, despite the

decline of insulin in D55, these animals exhibited minimal change in average plasma FA concentrations (Figure 6 A-E). However, with increasing severity of diabetes and a further drop in insulin, the predicted increased in FA emerged. Accordingly, D100 animals exhibited close to a 2-3-fold increase in various types of saturated [SFA; palmitic (16:0), stearic (18:0)], monounsaturated [MUFA; oleic (18:1)] and polyunsaturated (PUFA; linoleic (18:2), arachidonic (20:4)] FA that made up approximately 80% of the total plasma pool (Figure 6A-E). It should be noted that despite the absolute increase in plasma SFA, MUFA, and PUFA in D100, the percentage composition of these FAs remained unaltered (Figure 6F). Also, of interest was the observation that circulating very long-chain FAs (VLCFA-with ≥22 carbons; e.g.; docosahexaenoic acid, C22:6n3), that made up a small percentage of the total identified FA and that must undergo initial peroxisomal β-oxidation prior to entering the mitochondria for ATP generation, were also increased in D100 (Table 1). Our data suggests that the D100 heart could use the substantially increased plasma concentrations of these different FA for generation of ATP instead of FA originating from LPL action.

3.1.3 The largest magnitude of change in the ventricular transcriptome of rats with severe diabetes encompasses metabolic pathway genes.

To determine the capacity of the heart to respond to excess LPL or AT-derived FA, we compared the ventricle transcriptome of D55 and D100 animals to control. Figure 7A (lower panel) illustrates that in D55, there were 49 differentially regulated genes (padj < 0.05 and significant in at least 5 out of the 10 analysis pipelines used), and when clustered according to function and ranked based on the false discovery rate (FDR), they were enriched largely for traditional glucose, protein and lipid metabolic processes (Figure 7A & B). Strikingly, in D100, there were dramatic transcriptomic changes with 1574 genes differentially expressed (Figure 7A, upper panel). Like

D55, the majority of genes were annotated as related to metabolic processes [with additional enrichment in genes related to cellular transport, mitochondrial and blood vessel organization, response to oxidative stress, and cell death (Figure 7A and B)]. These results indicate that with the reduced glucose utilization, it is the superimposition of augmented AT-derived FA that likely determines the extent of cardiac gene expression changes following diabetes.

3.1.4 Metabolic gene expression reprogramming following diabetes of varying intensities emphasizes the increase in mitochondrial and peroxisomal β-oxidation.

Glucose and FA are the major sources from which the heart derives most of its energy. However, with the development of diabetes, the ability of this organ to utilize glucose is obstructed (2). Consistent with this finding, we observed a substantial decrease in the expression of genes controlling glucose transport (SLC2A4) and glycolysis (ENO3, HK2, PFKFB2) (Figure 8A). Furthermore, genes that modulate proteins (PDK1 and PDK4) that phosphorylate and inhibit PDH to lower glucose oxidation, increased in expression. All changes related to genes controlling cardiac glucose utilization were more pronounced in the D100 compared to D55 (Figure 8A). Because glucose use is impaired in diabetes, the heart is obliged to primarily metabolize FA and does so by enabling its mitochondrial β-oxidation followed by oxidative phosphorylation, to yield ATP. Related to this requirement, the genes controlling FA transport (CD36, FABP4) and mitochondrial β-oxidation (CPT1A, HADHA, HADHB, ACADL) exhibited increased expression and more so for D100 (Figure 8B). The expression of genes encoding peroxisomal metabolism were also found to be universally elevated in the D100 heart (Figure 8C) and corresponds to the decline in VLCFA (e.g., C22:5n3; C22:6n3) in this organ (Figure 9 and inset). Intriguingly, in D100, cardiac accumulation of the major PUFA (18:2n6) and MUFA (18:1n9) exceeded that of saturated fats like palmitic (16:0) or stearic (18:0) acids (Figure 9). This could indicate that

saturated FA entering the hearts gets preferentially utilized, whereas MUFA and PUFA (which require two additional steps to convert unsaturated to saturated bonds) get stored as triglyceride (109).

3.1.5 Mitochondrial oxidative phosphorylation is actively repressed with increasing severity of diabetes.

Mitochondrial β-oxidation of FA directly produces $FADH_2$ and NADH, as well as Acetyl-CoA (that enters the TCA cycle to also generate NADH and $FADH_2$); which are later consumed by the OXPHOS complexes to produce ATP. We used EnrichR analyses of the transcriptomic data from D100 hearts and determined that of the biological processes that showed the highest enrichment, a disproportionate amount (the top 10 GO terms for biological processes) was those related to mitochondrial functioning (Figure 10A), implicating a significant effect of excess FA on mitochondria. Furthermore, analysis of a protein-protein interaction network in D100 identified functional networks enriched for components of mitochondrial ribosomal protein, respiratory complex 1, and ATP synthase (Figure 10B, pink squares). Closer inspection of the gene expression data revealed that core metabolic genes involved in making enzymes for the mitochondrial TCA cycle (Figure 11A) and oxidative phosphorylation (Figure 11B) were actually universally downregulated in D100 hearts. Unexpectedly, using a substrate limited medium (only low glucose; 2.5 mM), measurement of basal oxygen consumption rates (OCR) as a gauge of cardiomyocyte oxidative capacity indicated that myocytes from D100 hearts had the highest basal respiration (Figure 12A). This was possibly an outcome of metabolism of endogenous triglyceride derived FA as addition of etomoxir (CPT1 inhibitor) lowered OCR in these myocytes (Figure 12A, inset). With addition of increasing concentrations of palmitic acid, although control myocytes responded by increasing their basal respiration, this effect was minimized in D55 and reversed in D100

myocytes (Figure 12A). Similarly, using FCCP to uncouple the proton gradient and maximize oxygen consumption to calculate spare respiratory capacity, control and D55 myocytes under basal conditions had the mitochondrial capacity to respond to this augmented energy demand, an outcome that was lacking in D100 (Figure 12B). FA decreased the response of myocytes from all three groups to FCCP-stimulated OCR. (Figure 12B).

3.1.6 Substantial accumulation of lipid metabolites and triglycerides in heart tissue from D100 animals.

The final products of an abnormal plasma FA profile, together with robust transcriptomic changes in the D100 heart to consume these FA, are metabolites. Using a nontargeted metabolomics approach by LC-MS/MS, we identified a broad set (363) of metabolites that were significantly differentially expressed in the D100 heart compared to control cardiac tissue. We used principle component analysis (PCA, Figure 13A) and an orthogonal partial least squares discriminate analysis (OPLS-DA) scores plot (Figure 13B) to identify the differences in metabolic patterns between control and D100 hearts and found clear separation between data for the two groups. Moreover, the corresponding S-plot of OPLS-DA shows that the metabolite ions (the top 30) with the greatest influence on separation of control from D100 (i.e., located furthest away from the center of the S-plot and with a large VIP value ≥1) included increases in many types of diglycerides (i.e., 18:2/18:1, 16:1/18:0) and phospholipids [i.e., PC(18:2/18:2, 16:0/18:2, 18:0/20:4); PE(18:2/21:0, 19:0/22:6, 22:6/21:0, 18:1/19:0); PS(P-20:0/18:0, P-20:0/16:0, P-20:0/18:1, P-20:0/18:2, P-20:0/22:4, O-20:0/22:4, O-16:0/20:0)], with the highest contribution identified as coming from triacid triglyceride (i.e., 17:1/18:1/19:1, 14:0/20:2/20:2, 17:0/17:1/17:0, 12:0/20:0/22:5, 14:1/18:0/18:0, 16:1/18:0/18:3, 16:1/18:2/22:0, 18:2/19:1/19:1, 16:1/18:2/22:4, 12:0/12:0/12:0, 17:0/17:1/22:1) (Figure 14). These results, when added to the increased expression

of a) genes encoding acyl-CoA thioesterase (ACOT 1, 2 and 4) that contributes to the conversion of acyl-CoAs to FAs and CoA (and thus triglyceride synthesis at the expense of FA oxidation), and b) genes encoding glycerolipid synthesis (GPAM and GPAT3) (Figure 15A) implies that D100 animals with plasma lipid overload and mitochondrial dysfunction results in intracellular triglyceride accumulation (Figure 15B) and likely contributing to an increase in cell death.

3.1.7 Significant apoptotic cell death in D100 hearts.

Electrons from NADH and $FADH_2$ enter the ETC to cause buildup of the proton motive force for OXPHOS and production of ATP. With the availability of excess FA in D100, electrons are donated to molecular oxygen, with electron leakage resulting in abnormally large amounts of ROS generation leading to changes in gene expression related to oxidative stress (Figure 16) and terminally, cell death (lipotoxicity). Indeed, of the genes that were differentially expressed in D100 hearts, a large number were those related to apoptosis, with a dramatic decrease in expression of anti-apoptotic and an increase in pro-apoptotic genes (Figure 17A) together with a significant increase in TUNEL-positive apoptotic cells (Figure 17B). Our data reveal that following severe diabetes, mitochondrial overload, incomplete FA oxidation and oxidative stress pushes the heart towards potentially unrecoverable loss of cardiomyocytes.

3.1.8 Effect of acute and chronic diabetes on cardiac VEGFB.

In animals with chronic diabetes (D55 for 6 weeks), the incidence of a cardiomyopathy is evident 6 weeks after STZ injection (92). Interestingly, measurement of cardiac VEGFB at this time indicated a substantial loss of both protein and gene expression in cardiomyocytes (Figure 18A and inset). These outcomes of a loss in myocyte VEGFB were also noticeable following severe acute diabetes (D100) (Figure 18B and inset). Insulin treatment of these severely diabetic

rats was effective in reducing plasma glucose within 30 minutes of injection and, after 90 minutes, euglycemia was achieved (Figure 18C). Interestingly, insulin reversed the decrease in cardiomyocyte VEGFB within 120 minutes of injection (Figure 18D).

3.2 Loss of VEGFB and its signaling in the diabetic heart is associated with increased cell death signaling.

3.2.1 Differential tissue expression of VEGFB.

Among metabolically active tissues, the heart displayed the highest amount of VEGFB gene (Figure 19A) and protein (Figure 19B) expression. The heart consists of a variety of cell types, including endothelial cells, smooth muscle cells, fibroblasts and cardiomyocytes (110). The majority of VEGFB present in the heart appears to be located in cardiomyocytes (Figure 19C). The heparin binding domain of VEGFB allows it to bind to cell surface HSPG, and hence, to also be displaced by highly negatively charged molecules like heparin. Incubation of isolated cardiomyocytes with heparin resulted in a rapid and robust displacement of VEGFB into the medium (Figure 19D and inset). Our data suggest that, of the VEGFB located in cardiomyocytes, there is a substantial and readily releasable pool localized on the cell surface.

3.2.2 Endothelial cell control of VEGFB release from cardiomyocytes.

Heparanase is an endo-β-D-glucuronidase that is ubiquitously expressed in many organs, with blood and endothelial cells having the highest expression. Heparanase is encoded as a 65-kDa latent precursor (Hep-L) that requires proteolytic cleavage to form the active enzyme (Hep-A) (111). Incubation of RHMEC in HG promoted the release of both forms of heparanase into the incubation medium (Figure 20A). Exposing isolated cardiomyocytes to this HG endothelial cell cultured media (ECCM), for 20 minutes, stimulated the release of VEGFB, likely from the cell

surface pool (Figure 20B). The role of heparanase in VEGFB release was validated using recombinant Hep-A and Hep-L, with the latent form of the enzyme displaying a greater capacity for displacement of the growth factor than the active form (Figure 20C). Moreover, a substantial increase of VEGFB in the medium was only seen when RHMECs were co-cultured with cardiomyocytes in the presence of HG. High glucose per se had no influence on releasing myocyte VEGFB (Figure 20D). These results imply that the immediate response to hyperglycemia and the secretion of endothelial heparanase is the release of cardiomyocyte VEGFB.

3.2.3 The action of VEGFB in RHMEC and cardiomyocytes.

Communication between endothelial cells and underlying cardiomyocytes is an important arrangement to regulate heart function (112). Both RHMEC and isolated cardiomyocytes expressed VEGFB protein, with cardiomyocytes having the higher concentration (Figure 21A). The action of VEGFB is predominately through its binding to VEGFR1 (80). Interestingly, the concentration of VEGFR1 in RHMEC was substantially higher compared to cardiomyocytes (Figure 21B), emphasizing the potential for cardiomyocyte VEGFB to activate VEGFR1 on endothelial cells. A prominent feature in hearts from rats overexpressing VEGFB was activation of ERK (74). In this study, treatment of RHMEC (Figure 22A) or isolated myocytes (Figure 23A) with VEGFB caused a pronounced phosphorylation of ERK, an effect that appeared as early as 5 minutes and dissipated within 1 hour. ERK activation results in inactivation of GSK3β by phosphorylation at the serine 9 residue (113), which can repress cell death (114). In RHMEC and cardiomyocytes treated with VEGFB, the timeline for ERK activation was mirrored by a similar profile of GSK3β inactivation (Figure 22B and Figure 23B). To evaluate the direct effect of VEGFB on cell survival, hydrogen peroxide was utilized as a source of oxidative stress, with cleaved caspase 3 and PARP used as markers of cell death. Pre-treatment of RHMECs and

cardiomyocytes with VEGFB reduced H_2O_2 stimulated caspase 3 (Figure 22C and Figure 23C) and PARP cleavage (Figure 22D and Figure 23D). It should be noted that, in addition to influencing cell survival through signaling, VEGFB also reduced the Bax/Bcl2 gene expression ratio (Figure 22E and Figure 23E), which has been used as an index of cell apoptosis (115). Taken together, our data evoke a role for VEGFB in triggering signaling pathways and gene expression that can influence endothelial cell and cardiomyocyte survival.

3.2.4 Effect of acute and chronic diabetes on cardiac VEGFR1.

Chemical induction of diabetes using different doses of STZ resulted in distinctive changes in body weight. With chronic diabetes, the animals did not gain as much weight compared to control after the six-week study, whereas the severely diabetic animals exhibited an actual loss of body weight after 4 days of diabetes (Figure 24A). Both diabetic groups showed robust hyperglycemia (Figure 24B). Intriguingly, cardiomyocytes from animals with either chronic (Figure 24C) or acute (Figure 24D) diabetes showed a substantial increase in VEGFR1 protein. Our data suggest that, under conditions of hyperglycemia when VEGFB production is impaired, a robust increase in VEGFR1 expression ensues as a possible mechanism to enhance or maintain VEGFB signaling.

3.2.5 Diminished VEGFB signaling in acute and chronic diabetes.

Unexpectedly, despite the enhanced VEGFR1 expression in cardiomyocytes from animals with chronic (Figure 25A and inset) or acute (Figure 25B and inset) diabetes, there was a loss in P-ERK and P-GSK3β. In addition to decreased baseline signaling in diabetic myocytes, the response to VEGFB treatment seen in Figure 23 was also blunted in cardiomyocytes from chronically diabetic animals (Figure 25C and D). Overall our data suggest that, even with an

increase in VEGFR1 following diabetes, cardiomyocytes are unable to respond to VEGFB, which may lead to increased cell death signals.

3.2.6 Increased cell death signals in acute and chronic diabetes.

In addition to the loss of VEGFB production (Figure 18) and signaling (Figure 25), evaluation of latent heparanase, the protein responsible for VEGFB release also showed a significant decline in expression in whole hearts from animals with chronic (Figure 26A) or acute (Figure 26B) diabetes. Defects in these numerous VEGFB pathways were associated with an increased cell death signature in our models of diabetes. With respect to gene expression, there was an increase in the Bax/Bcl2 mRNA ratio in myocytes from animals with chronic diabetes (Figure 27A). Regarding cell death signaling, there was an increase in cleaved caspase 3 (Figure 27BD), which corresponded to an increase in cleaved PARP, in cardiomyocytes from chronically diabetic animals (Figure 27C)—a result also seen in myocytes from animals with acute diabetes (Figure 27D). Altogether, our data indicate that, with the declining influence of VEGFB in the diabetic heart, there is a greater susceptibility to cell death.

3.3 Cardiomyocyte-specific overexpression of VEGFB is linked to an expanded coronary vasculature that amplifies the cardiovascular action of insulin

3.3.1 Cardiomyocyte specific overexpression of human VEGFB enhances coronary vasculature

In TG rats with cardiomyocyte specific promoter α-myosin heavy chain (α-MHC) mediated overexpression of human VEGFB, there was an almost 40-fold increase in gene expression as revealed using RNA Seq (Figure 28A). which was confirmed with PCR amplification of genomic DNA obtained from ear notch genotyping (Figure 28B). Previously characterized as having an

enhanced coronary vasculature and arterial supply (74), we analyzed the ventricle transcriptome of WT and TG animals. There was a striking cardiac transcriptomic change, with over 2100 genes differentially expressed between WT and TG hearts. Of these, 118 genes were altered specifically related to angiogenesis and Figure 29A illustrates the top 15 from a ranked list. These changes in gene expression were confirmed by measuring selective proteins linked to angiogenesis (PDGFB, Nos3, and PDGFRβ which were increased in TG hearts (Figure 29B). These changes in genes and proteins related to angiogenesis translated to an augmented coronary vascular tree as seen in histological sections from VEGFB TG rat hearts (Figure 29C). Our data support previous observations which document cardiac specific VEGFB overexpression to an increased coronary circulatory system and thus myocardial perfusion.

3.3.2 Amplified insulin action in TG Hearts

Determination of blood glucose and plasma insulin, as measures of the overall metabolic status, demonstrated that the levels in WT and TG animals were equivalent (Figure 30A). Nonetheless, measurement of p-AKT(S473) and p-PI3K 85α (Tyr 508), indicators of insulin signalling in the heart revealed that TG animals were more sensitive to basal insulin (Figure 30B). This effect was unlikely a consequence of any change in the amount of the insulin receptor (Figure 30C). Furthermore, expression of several genes linked with insulin regulated pathways that enrich glucose utilization were increased in TG hearts (Figure 30D). A possible molecular mechanism for this increased insulin signalling could be the enhanced delivery of circulating insulin to the heart secondary to greater myocardial perfusion. As such, administration of exogenous insulin i.p. elicited a dramatic increase in insulin signalling in TG hearts that was significantly higher than in WT (Figure 31A). To validate that this increased basal and administered insulin response was specific to the heart, we also evaluated insulin action in skeletal muscle. Unlike the heart, p-AKT

(S473) under basal conditions (Figure 31B) or in response to exogenous insulin (Figure 31C) remained comparable between WT and TG animals. Overall, these results imply that the TG overexpression of VEGFB, displaying enhancement of the coronary vasculature, conceivably allows for greater delivery of insulin and its action in the heart.

3.3.3 Build-up of cardiac diacylglycerol and LysoPC is lower in VEGFB TG hearts

Hydrolysis of circulating lipoproteins by LPL is believed to be an important source of FA for cardiac ATP generation (7). To release LPL from the coronary lumen we used heparin and performed continuous retrograde perfusion in WT and TG hearts. After 30 minutes of recirculation, there was a noticeable decrease in LPL activity in TG hearts (Figure 32A), indicating reduced release of LPL, an outcome that was not a result of lower LPL gene expression (Figure 32B). Interestingly, angiopoetin-like protein 4 (Angptl4) a member of the angiopoietin family, with a suggested role in lowering LPL activity (38), was found to exhibit higher gene expression in TG hearts (Figure 32C). Of even greater interest was the observation that expression of Fabp4/5, two genes encoding proteins with important roles in trans-endothelial transport of FA, were increased. Conceivably, increased Fabp4/5 expression could be responsible for increased purine biosynthesis in EC (Figure 33A and B) for enhanced DNA replication enabling EC proliferation. On the other hand, genes that are key to cardiomyocyte FA uptake, such as CD36 and Fabp3, were lower in TG hearts (Figure 33B). Subsequently there was a drop in perilipin 2 and 5 (Plin2/5), which encode genes responsible for lipid droplet formation (Figure 33C). Additionally, there was reduced diacylglyceride accumulation in TG hearts, lipid metabolites associated with insulin resistance (116) (Figure 34A). Moreover, genes for diacylglycerols kinases, that catalyze the phosphorylation of DAG to produce phosphatidic acid and therefore preventing DAG conversion to triglycerides, were increased (Figure 34B). Furthermore, lysophosphatidylcholines (LysoPC), which can be

formed from DAG and also reduce insulin signaling (117), were lower in TG hearts (Figure 34C). These data suggest that the decreased DAG and LysoPC in TG hearts is an alluring mechanism of enhanced cardiac insulin sensitivity.

3.3.4 Increased cardiac insulin sensitivity in TG animals after chronic STZ diabetes

Utilizing 55 mg/kg STZ, we generated a model of moderate diabetes with low but measurable amounts of insulin. Pronounced hyperglycemia was identified the day after STZ injection and this was maintained throughout the 6-week study (Figure 35A). The level of hyperglycemia between the WT and TG diabetic groups was equal when compared to their respective controls (Figure 35A). Following 6 weeks of diabetes, both diabetic groups displayed decreased plasma insulin (Figure 35B) and weight gains compared to controls (Figure 35C). Even though there was no difference in the level of diabetes between WT and TG rats, myocardial metabolite analysis showed that DAGs and LysoPC lipid metabolites decreased in the TG STZ-C group (Figure 36A and B). Furthermore, S-plot of an OPLS-DA model reveals that the metabolites with the most significant influence in the differences between the WT-STZ-C and TG-STZ-C groups, (metabolites furthest away from the center), contained a number of DAGs and LysoPCs (Figure 37). As DAGs and LysoPCs have been implicated in the development of insulin resistance, basal insulin signaling was analyzed in the two diabetic groups following acute and chronic hyperglycemia. Intriguingly, hearts from TG rats in both acute (Figure 38A) and chronic (Figure 38B) diabetic models exhibited enhanced p-AKT (S473) compared to WT diabetics. Additionally, analysis of RNA Seq data from the two diabetic groups showed that TG-STZ-C rat hearts maintained their angiogenic gene signature (Figure 39A) as well as decreased expression of genes involved in fatty acid utilization (Figure 39B). These results signify that even with hypoinsulinemia and hyperglycemia, strategies that can augment the coronary vasculature and

decrease lipid metabolite accumulation via VEGFB overexpression are able to improve insulin sensitivity in the heart following diabetes.

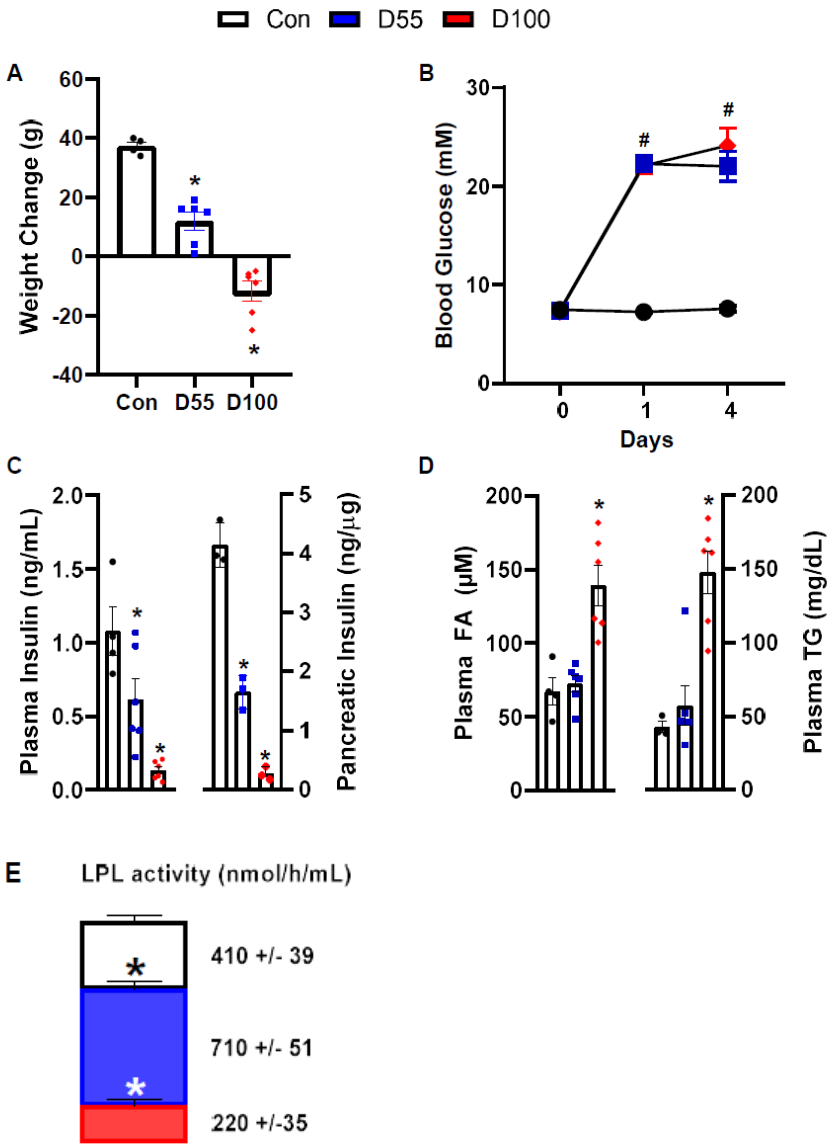

Figure 5. The severity of STZ diabetes is uncovered by measuring insulin and not glucose. Diabetes was induced by injection of two different doses of STZ [55 (D55) or 100 (D100) mg/kg, i.v.] and the animals terminated 4 days later (n=4-6). At termination, weight gain (change in body weight compared to initial value) was assessed (A). Blood glucose was determined throughout the study period from tail tip blood samples using glucose test strips and an Accu-Chek glucose monitor (B). Following heart extraction, blood in the thoracic cavity was collected in tubes containing K2EDTA as anticoagulant. After centrifugation, plasma isolated from this blood was used for determination of insulin (C, left panel) and FA and triglyceride (D). Pancreatic total insulin (ng) was determined following acid-ethanol extraction and measured using a rat ultrasensitive insulin ELISA normalized to total protein (µg; D right panel). LPL activity in the 1.0 mol/L fraction redrawn from original in Wang et. al.(38)] representing dimeric, catalytically active LPL determined in heart homogenates loaded onto a heparin-sepharose column and eluted with increasing concentrations of NaCl. To measure LPL activity, we used in vitro hydrolysis of a [3H] triolein substrate. Data are presented as mean ±SEM. #Significantly different from control; *Significantly different from all other groups; $p<0.05$.

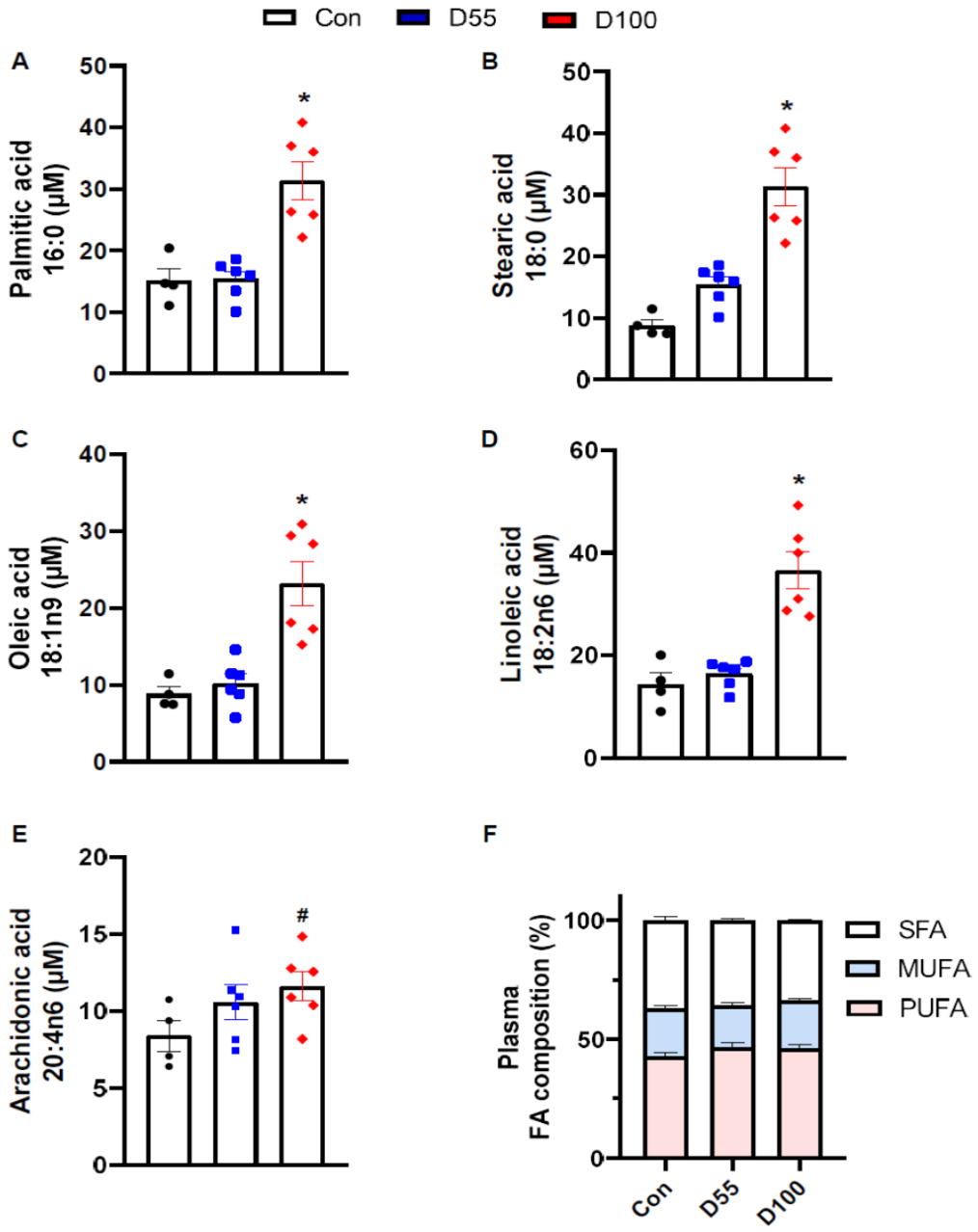

Figure 6. Plasma FA composition is only altered when insulin reduction by STZ is substantial. Four days after injection of STZ, animals were terminated and plasma collected for determination of FA composition (n=4-6). Plasma FA were extracted with chloroform:methanol:acetone:hexane solvent. Separation of FA was achieved using HPLC, followed by conversion to their respective methyl esters, and quantification by GLC. The unadjusted baseline saturated [palmitic acid (A); stearic acid (B)], monosaturated [oleic acid (C)] and polyunsaturated [linoleic acid (D); arachidonic acid (E)] FA composition is shown in control (Con) rats and animals with variable degrees of hypoinsulinemia (D55 and D100). Results are also expressed as the molar percentage of each FA over the total FA measured in the plasma (F). Data are presented as mean ±SEM. #Significantly different from control; *Significantly different from all other groups; $p<0.05$.

	Control		D55		D100	
Fatty Acid	**Mean**	**+/-**	**Mean**	**+/-**	**Mean**	**+/-**
C 12:0	0.09	0.01	0.07	0.02	**0.07***	0.02
C 14:0	0.43	0.1	0.31	0.07	**0.68***	0.17
C 14:1	0.01	0	0.01	0.01	0.01	0
C 16:0 DMA	0.05	0.02	0.06	0.02	0.05	0.01
C 16:1 DMA	0.04	0.01	0.03	0.01	0.06	0.01
C 16:0	15.13	3.79	15.39	2.48	**31.35***	6.03
C 16:1n9	0.28	0.06	0.19	0.05	0.31	0.06
C 16:1n7	0.9	0.4	0.57	0.15	1.2	0.29
C 18:0 DMA	0.1	0.03	0.11	0.03	**0.06***	0.01
C 18:1 DMA	0.64	0.19	0.48	0.12	0.55	0.1
C 18:0	8.82	1.82	9.84	1.67	**13.88***	2.32
C 18:1n9	9.93	3.07	10.22	2.38	**23.21***	5.64
C 18:1n7	1.55	0.43	1.28	0.25	**2.51***	0.5
C 18:2n6	14.32	4.48	16.43	2.16	**36.59***	7.01
C 18:3n6	0.11	0.05	0.11	0.02	0.59	0.83
C 20:0	0.08	0.03	0.09	0.01	**0.24***	0.06
C 18:3n3	0.36	0.13	0.3	0.1	**1.15***	0.32
C 20:1n11	0.17	0.05	0.16	0.03	**0.38***	0.09
C 20:1n9	0.11	0.05	0.07	0.01	**0.31***	0.06
C 18:4n3	0.02	0.01	0.02	0.03	0.08	0.03
C 20:2n6	0.21	0.05	0.17	0.06	0.31	0.07
C 20:3n9	0.1	0.03	0.11	0.06	0.13	0.02
C 20:3n6	0.56	0.19	0.44	0.19	0.55	0.11
C 22:0	0.06	0.02	0.07	0.01	**0.15***	0.03
C 20:4n6	8.39	1.98	10.57	2.23	**11.6#**	1.84
C 20:5n3	0.84	0.31	0.78	0.12	**1.7***	0.38
C 24:0	0.08	0.01	0.08	0.02	**0.16***	0.03
C 22:4n6	0.18	0.06	0.23	0.04	**0.39***	0.08
C 24:1	0.05	0.02	0.04	0.02	0.06	0.01
C 22:5n6	0.06	0.02	0.05	0	**0.18***	0.05
C 22:5n3	0.74	0.27	0.83	0.18	**1.66***	0.37
C 22:6n3	2.9	0.91	3.23	0.33	**9.06***	2.09

Table 1. Micromolar concentration of FA in plasma. Four days after injection of STZ, animals were terminated and plasma collected for determination of FA composition (n=4-6). Plasma FA were extracted with chloroform:methanol:acetone:hexane solvent. Separation of FA was achieved using HPLC, followed by conversion to their respective methyl esters, and quantification by GLC. #Significantly different from control; *Significantly different from all other groups; $p<0.05$.

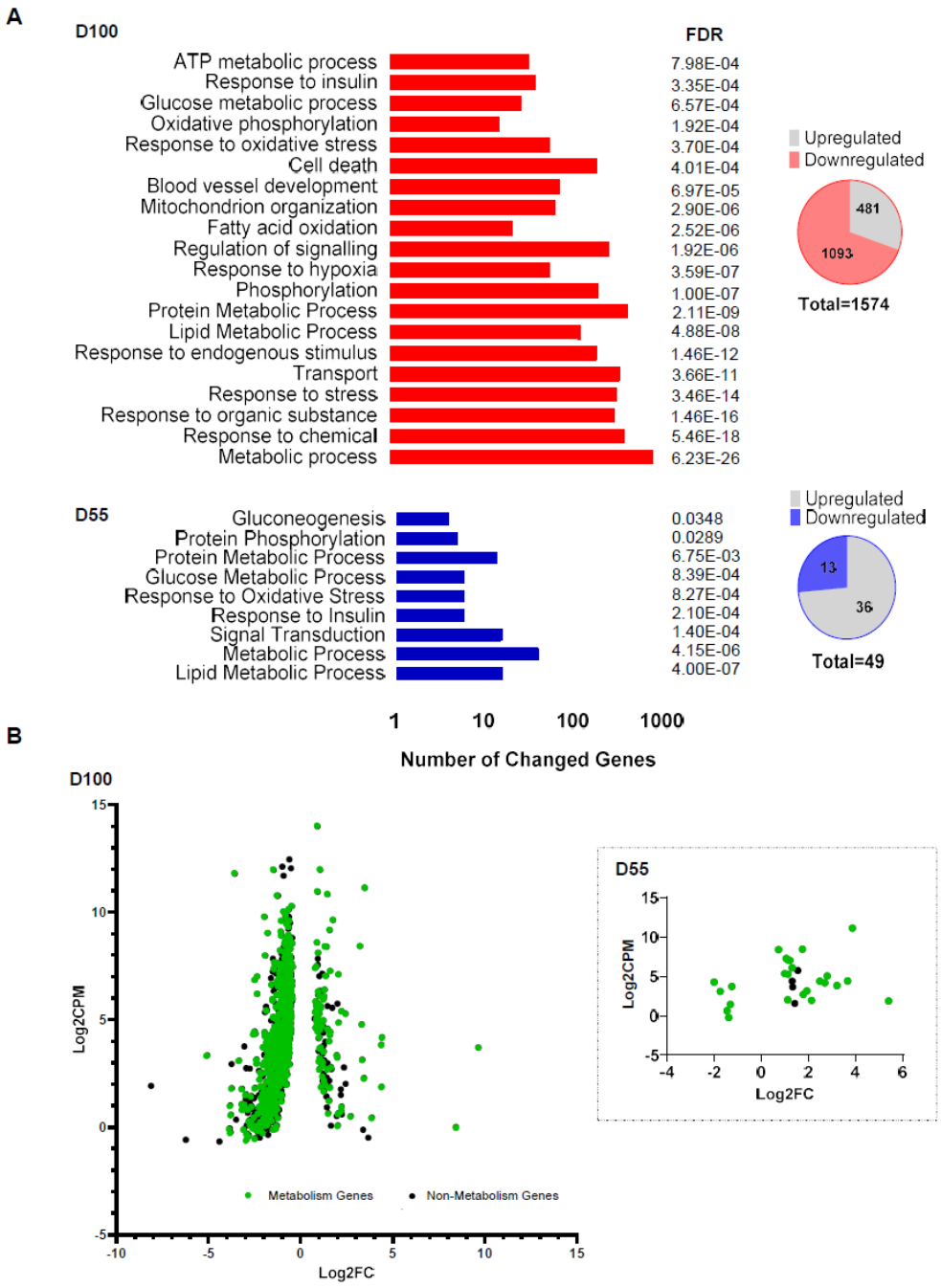

Figure 7. The largest magnitude of change in the ventricular transcriptome of rats with severe diabetes mellitus embraces metabolic pathway genes. Ventricle RNA from the different groups of rats was sequenced (n=4–6), and differentially expressed genes (padj <0.05 and significant in at least 5 of the 10 analysis pipelines used) were clustered according to function and ranked based on false discovery rate (FDR) (A). The insets describe the number of genes whose expression was up- or downregulated. The volcano plot (B) describes the profile of differentially expressed genes in D55 (inset) and D100 rats. The x axis represents Log2FC expression of genes vs Log2CPM on the y axis. Green circles highlight differentially expressed genes related to the metabolic process. CPM indicates counts per million.

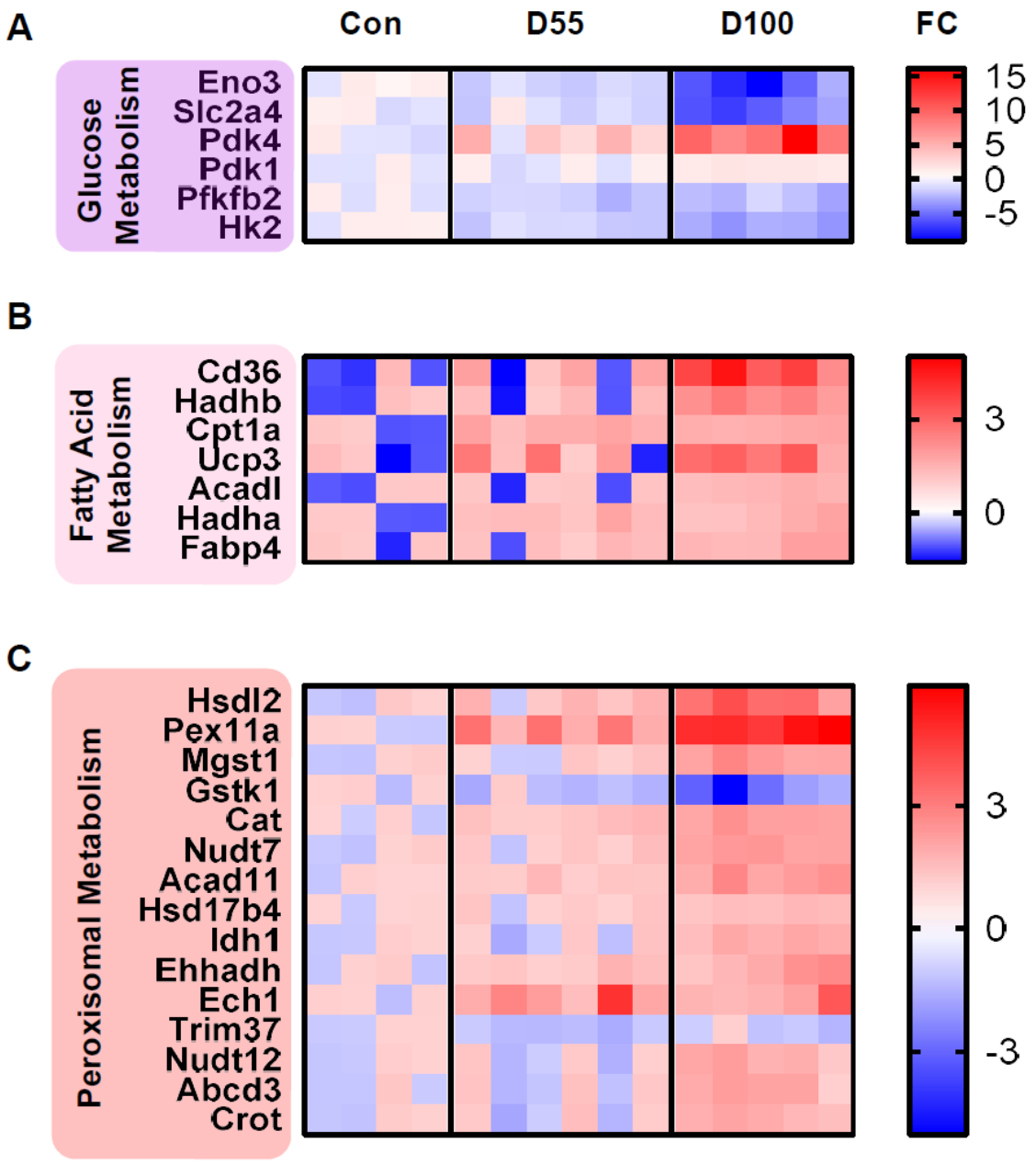

Figure 8. Metabolic gene expression reprogramming following diabetes mellitus of varying intensities emphasizes the increase in mitochondrial and peroxisomal β-oxidation. Heat map of statistically significant genes related to cardiac metabolism of carbohydrates (A) and fatty acid (FA; B). (C) is a heat map pattern showing relative expression values of genes encoding peroxisomal metabolism. The red (high) and blue (low) colors reflect fold change (FC), normalized to CPM (counts per million).

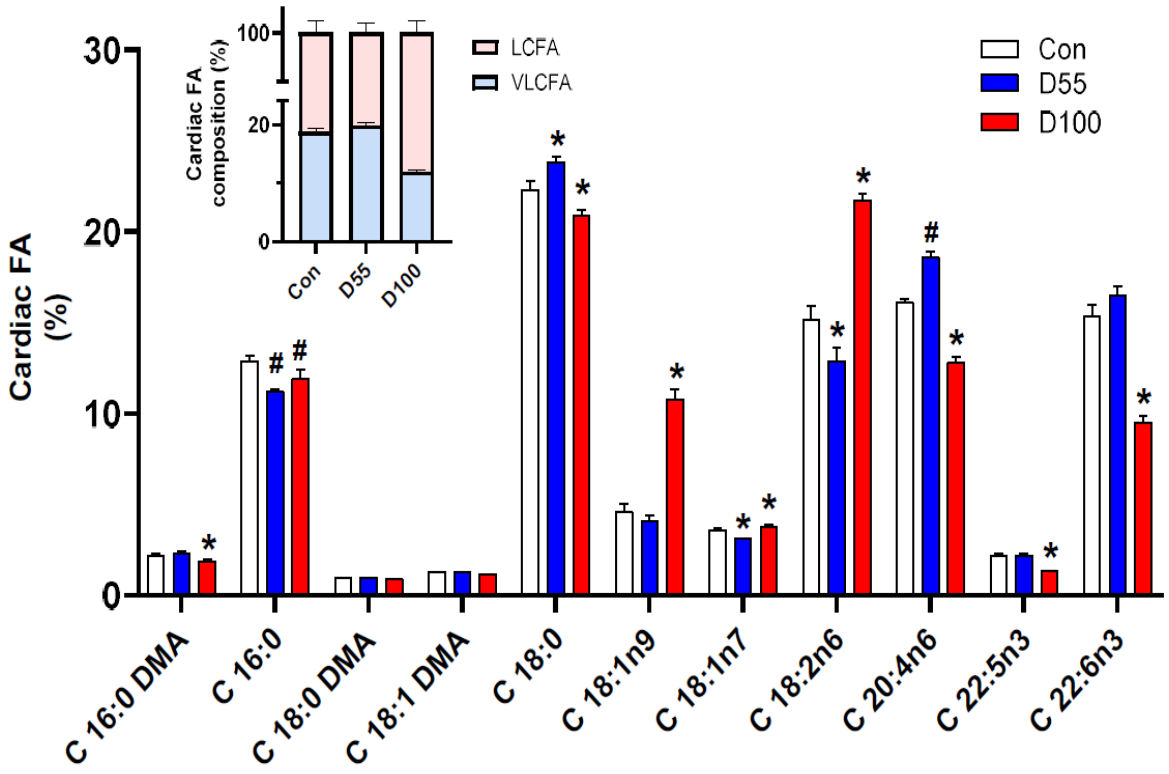

Figure 9. Changes in heart composition following diabetes of varying intensities. Separation of heart FAs was achieved using high-performance liquid chromatography, followed by their conversion to their respective methyl esters and quantification (µg/mg protein) by gas liquid chromatography. The FA depicted made up almost 80% of the eluted peaks and are expressed as a percentage of the total FA extracted. The inset describes the percentage composition of long-chain FA (LCFA) and very-long-chain FA (VLCFA; chain-length with 22 or more carbons) in hearts from the three groups (n=4–6). Data are presented as mean±SEM. #Significantly different from control; *Significantly different from all other groups; $p<0.05$.

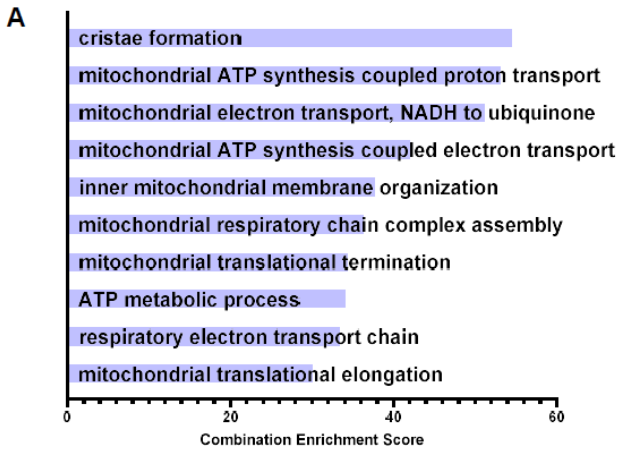
A
cristae formation
mitochondrial ATP synthesis coupled proton transport
mitochondrial electron transport, NADH to ubiquinone
mitochondrial ATP synthesis coupled electron transport
inner mitochondrial membrane organization
mitochondrial respiratory chain complex assembly
mitochondrial translational termination
ATP metabolic process
respiratory electron transport chain
mitochondrial translational elongation
0
20
40
60
Combination Enrichment Score

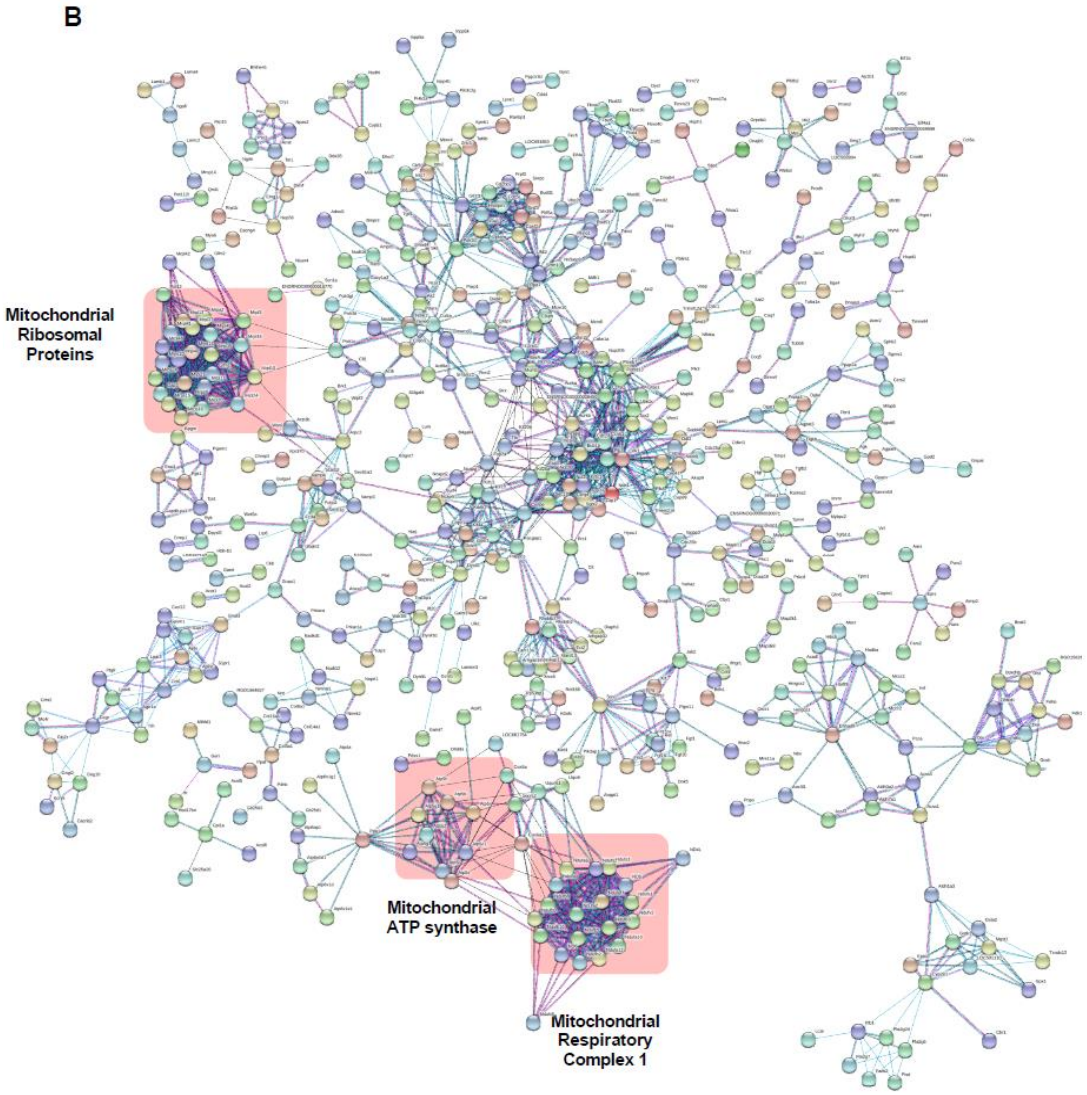
B
Mitochondrial Ribosomal Proteins
Mitochondrial ATP synthase
Mitochondrial Respiratory Complex 1

Figure 10. Mitochondrial dysfunction with increasing severity of diabetes. Gene ontology enrichment analysis of biological processes using the Enrichr analysis tool (A). The gene signature identifying only the top 10 enriched gene ontology (GO) terms is depicted (A). Association network of genes that were significantly different between control (Con) and D100 hearts. The protein-protein interaction network was assembled from RNAseq data. The pink squares illustrate the differentially regulated networks that are related to mitochondrial functioning. Lines represent associations based on differential expression evidence (B).

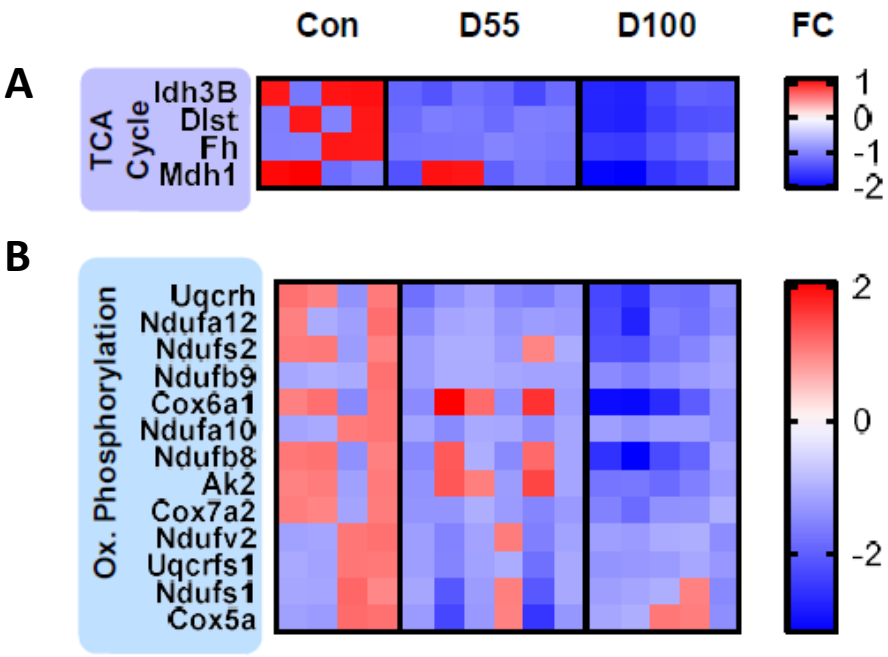

Figure 11. TCA cycle and oxidative phosphorylation genes are decreased with severity of diabetes. Heat map pattern showing relative expression values of genes encoding tricarboxylic acid (TCA) cycle activity (A) and mitochondrial oxidative phosphorylation (B). The red (high) and blue (low) colors reflect fold change (FC).

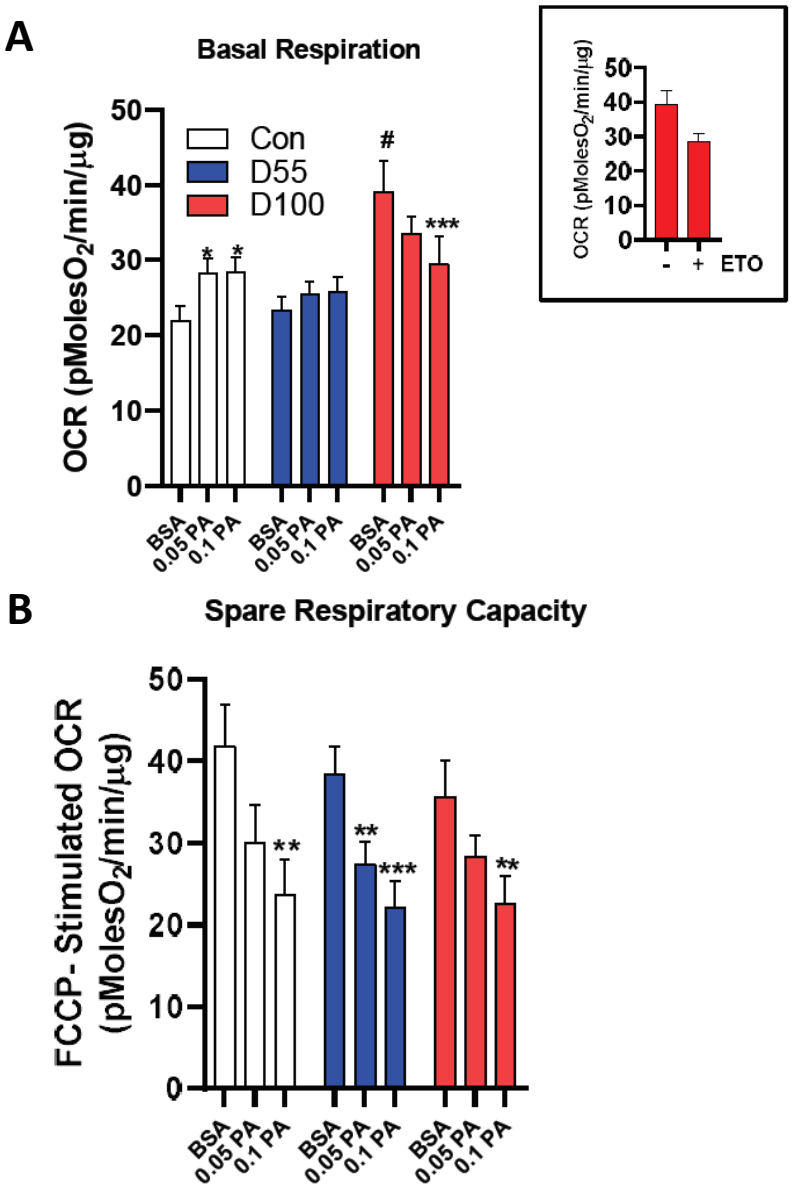

Figure 12. Oxygen consumption rates (OCRs) in cardiomyocytes isolated from Con, D55, and D100 hearts. Immediately before assay, either bovine serum albumin (BSA), 0.05 mmol/L of palmitic acid (PA), or 0.1 mmol/L of PA was added to the wells. Cells were exposed sequentially to the 3 metabolic inhibitors oligomycin, carbonyl cyanide 4-(trifluoromethoxy) phenylhydrazone (FCCP) and rotenone plus antimycin A. OCR is expressed as pmole O2/min per µg protein. Basal respiration (in BSA) was measured in the absence (E) or presence (E, inset) of etomoxir (ETO; 100 µmol/L), an inhibitor of carnitine palmitoyltransferase I (CPT1) (to assess the contribution of fatty acids arising from endogenous triglycerides. Spare respiratory capacity was calculated as OCR following FCCP minus baseline OCR (F). Three separate plates were assayed, each with cardiomyocytes isolated from 3 separate Con, D55, and D100 animals. Data are presented as mean±SEM. *p<0.05, **p<0.01, ***p<0.001 compared to BSA treatment within each group; #p<0.05 compared to BSA-CON.

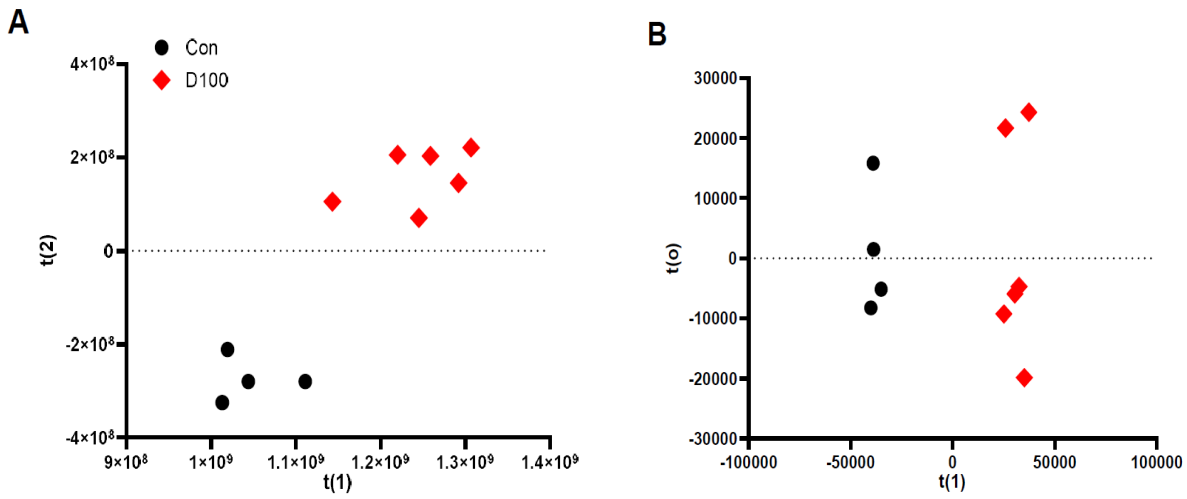

Figure 13. Differences in metabolic patterns between control and D100 hearts. Heart samples (5–10 mg) were powdered, transferred to a 1.7-mL microcentrifuge tube, and 4 volumes of solvent added (acetonitrile for hydrophilic interaction or methanol for reversed phase). Following brief sonication and centrifugation at 20 000g for 10 min, the supernatant was removed to a high-performance liquid chromatography autosampler vial. Hydrophilic interaction chromatography used a Waters BEH-Amide column 2.1×100 mm, 1.7µm particle size, and mobile phases of 5 mmol/L ammonium formate (Fisher Optima LCMS Grade) +0.1% formic acid (Sigma) in 98% water/2% acetonitrile (EMD LCMS Grade) and acetonitrile containing 2% water and 5 mmol/L ammonium formate+ 0.1% formic acid for positive ion tests, both at pH 3.5. T-tests were performed on the filtered data to determine statistical significance of $P<0.05$, and included Benjamini-Hotchberg false discovery rate for multiple hypothesis testing correction. Principal component analysis (R2X=0.992, Q2 (cum)=0.974) (A) and orthogonal partial least squares discriminant analysis (R2X=0.635, R2Y=0.992) (B) score plots acquired by liquid chromatography–tandem mass spectrometry detailing cardiac metabolomics of control and D100 hearts.

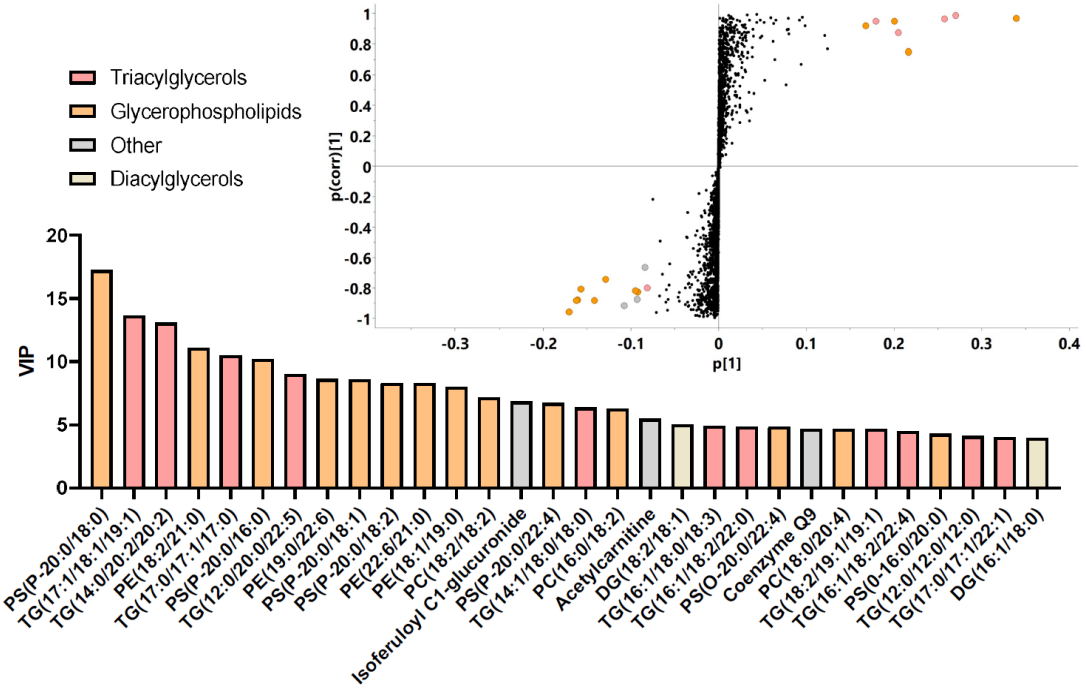

Figure 14. Substantial accumulation of lipid metabolites in heart tissue from D100 animals. The S-plot analysis (inset) and the variable important plot (top 30 metabolites) derived from the metabolite data illustrating the ions that contributed most to the separation of control from D100 hearts.

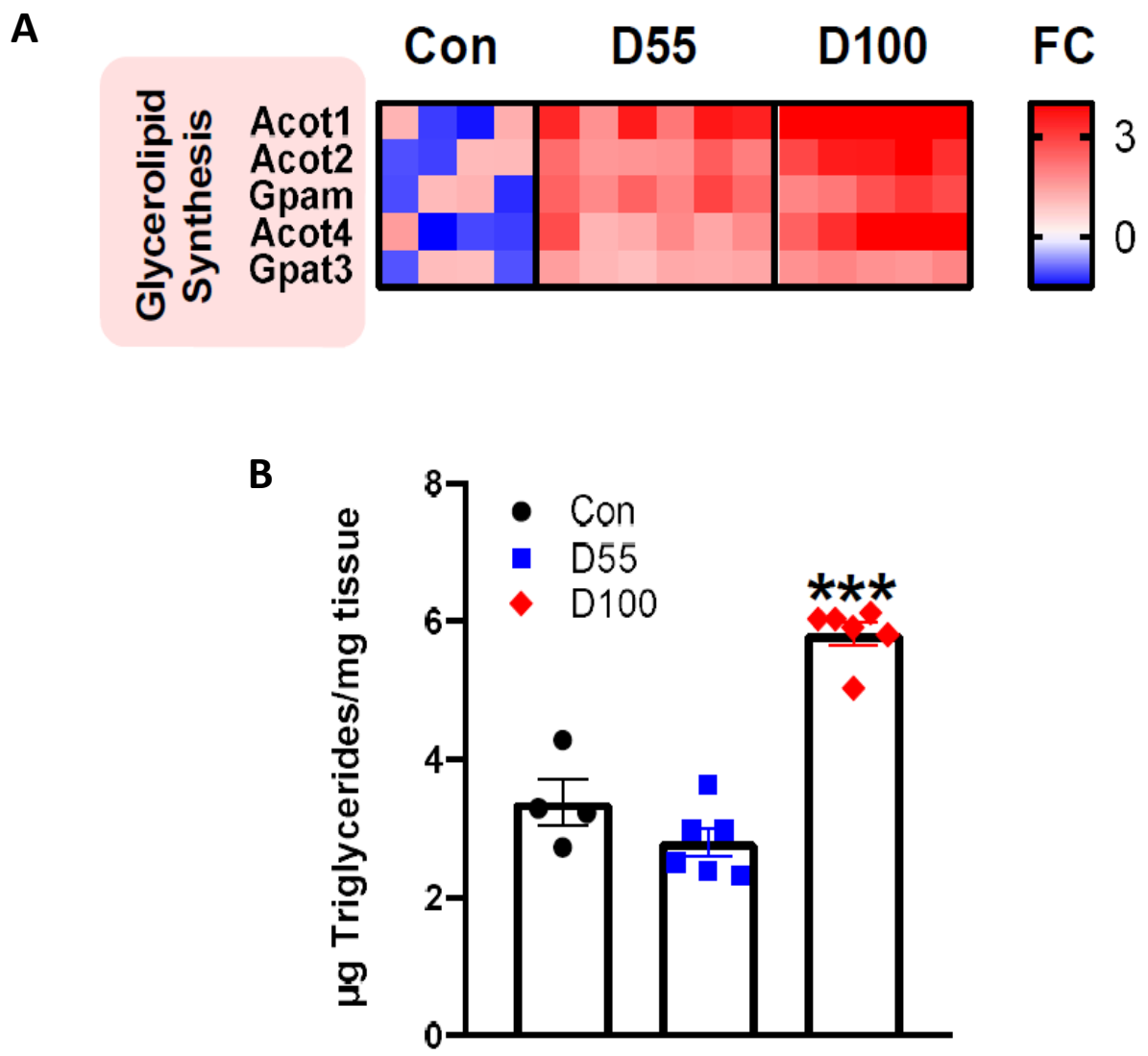

Figure 15. Increased glycerolipid synthesis genes and substantial accumulation of triglycerides in heart tissue from D100 animals. Heat map of genes involved in glycerolipid synthesis in hearts from the different groups of rats (A). The red (high) and blue (low) colors reflect fold change (FC). Total cardiac triglyceride in the different group of animals (B). triglyceride were extracted and solubilized in chloroform:methanol:acetone:hexane (4:6:1:1 v/v/v/v) and measured using high-performance liquid chromatography (n=4–6). Data are presented as mean ±SEM. Significantly different from Con, ***p<0.001.

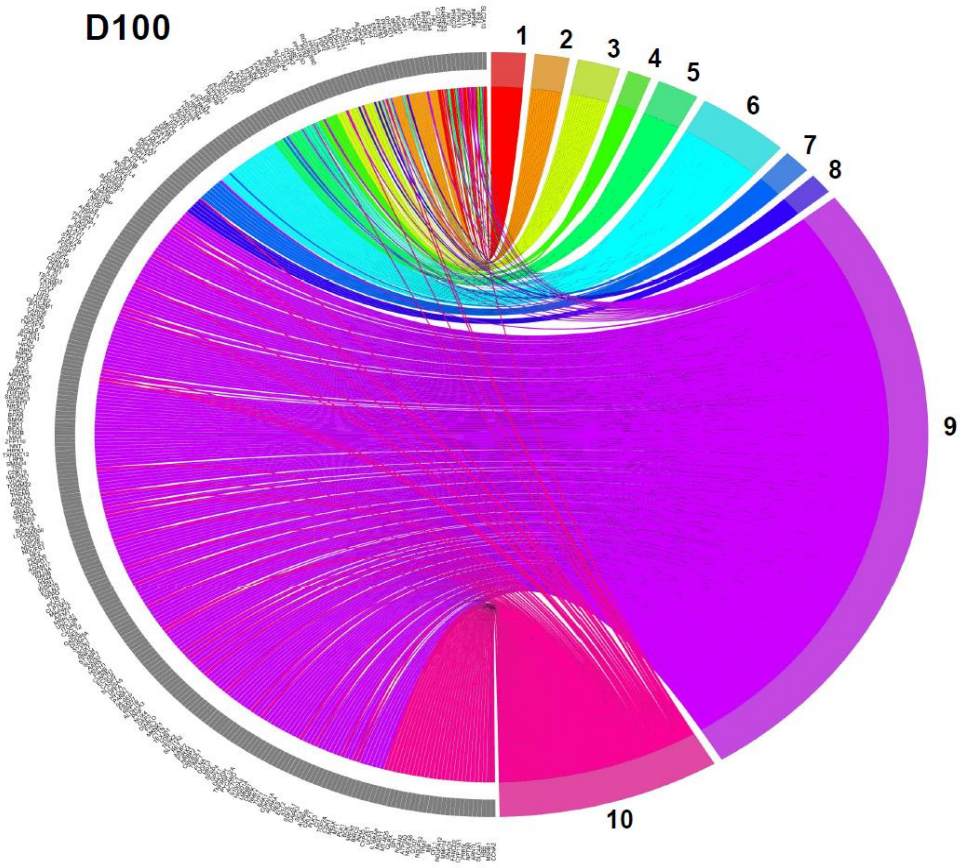

1 - Glucose Transport
2 - Glycolysis
3 - Pyruvate Metabolism
4 - Glycogen Synthesis
5 - Fatty Acid Transport
6 - Fatty Acid Oxidation
7 - Triglyceride Synthesis
8 - Tricarboxylic Acid Cycle
9 - Apoptosis
10 - Response To Oxidative Stress

Figure 16. Association between differentially expressed genes in D100 hearts. A Circos plot was used to display the association between differentially expressed genes in D100 hearts (n=4–6). Expression level of genes involved in the pathways is indicated as a log2 fold change (FC). The vast majority of genes are annotated as being directed towards modulation of metabolism.

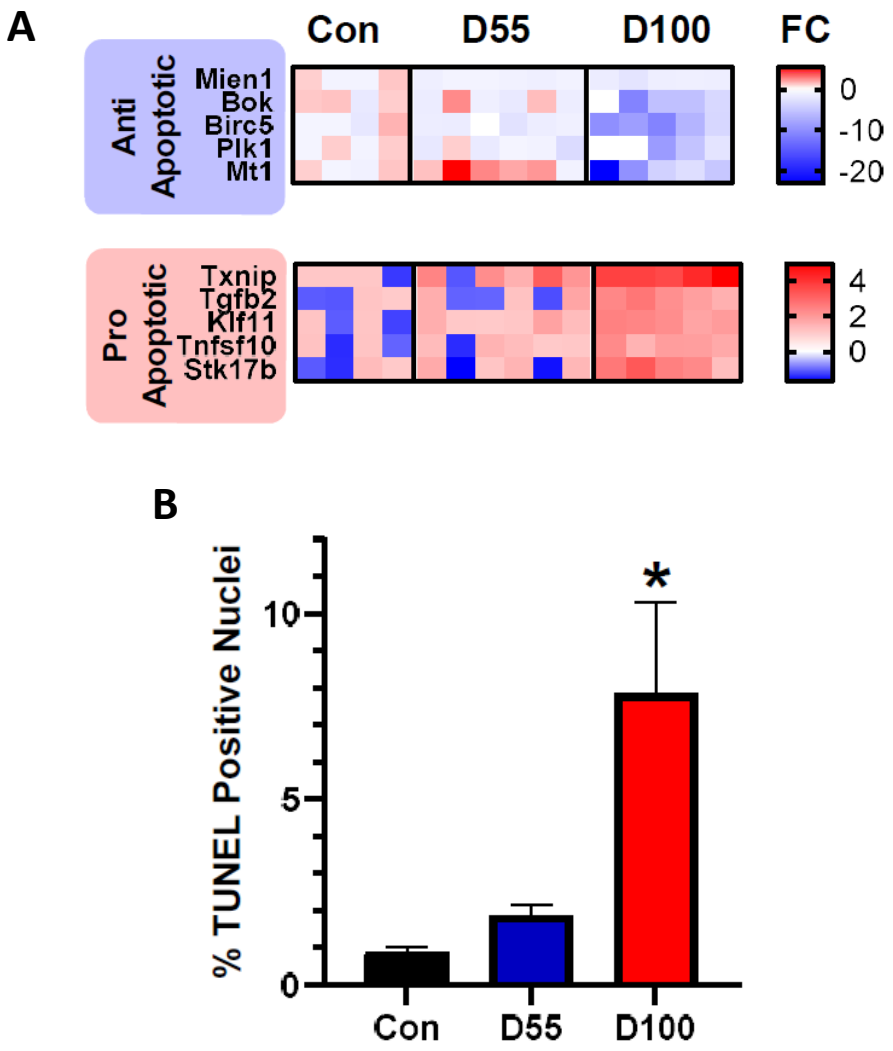

Figure 17. Significant apoptotic cell death in D100 hearts. Heat map of genes involved in anti-apoptosis and pro-apoptosis in hearts from the different groups of rats (A). The red (high) and blue (low) colors reflect fold change (FC). Apoptotic cell death as identified by terminal deoxynucleotidyl transferase dUTP nick-end labeling (TUNEL) assay (B). Isolated rat hearts were retrogradely perfused with phosphate-buffered saline, then 10% formalin, embedded in paraffin, and 5-µm sections prepared. Nuclei were counted from 3 different ventricular sections per animal, from 3 individual animals per group. Data are presented as mean±SEM. Kruskal–Wallis nonparametric test, Dunn post hoc. Significantly different from the control, *P<0.05.

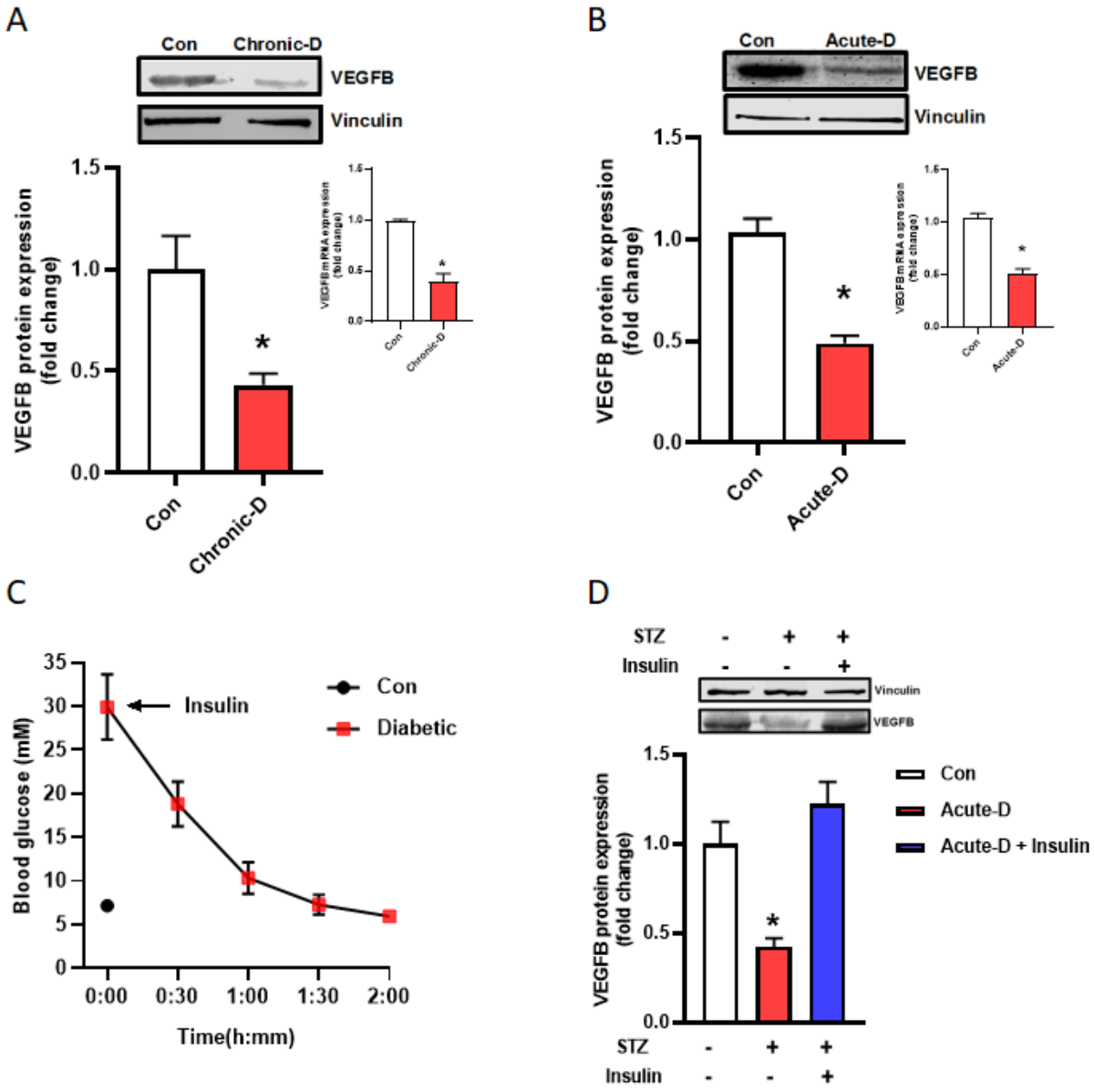

Figure 18. Changes in cardiac VEGFB from rats with acute and chronic diabetes. Male Wistar rats were injected with either saline (control) or streptozotocin to induce diabetes. Rats were monitored for 4 days (Acute-D) or 6 weeks (Chronic-D), at which time animals were euthanized and cardiomyocytes isolated. VEGFB protein and mRNA (insets) were evaluated in isolated cardiomyocytes from chronic (A) and acute (B) diabetic animals using Western blot and qPCR (β-actin used as reference gene), respectively. In animals made diabetic with 100 mg/kg STZ and kept for 4 days, fast acting insulin (Humulin R; 22 U/kg) was injected via the tail vein, blood glucose monitored at timed intervals (C), and were euthanized after 120 minutes of insulin injection for determination of cardiomyocyte VEGFB (D). n=3-6, *p<0.05 vs. all other groups.

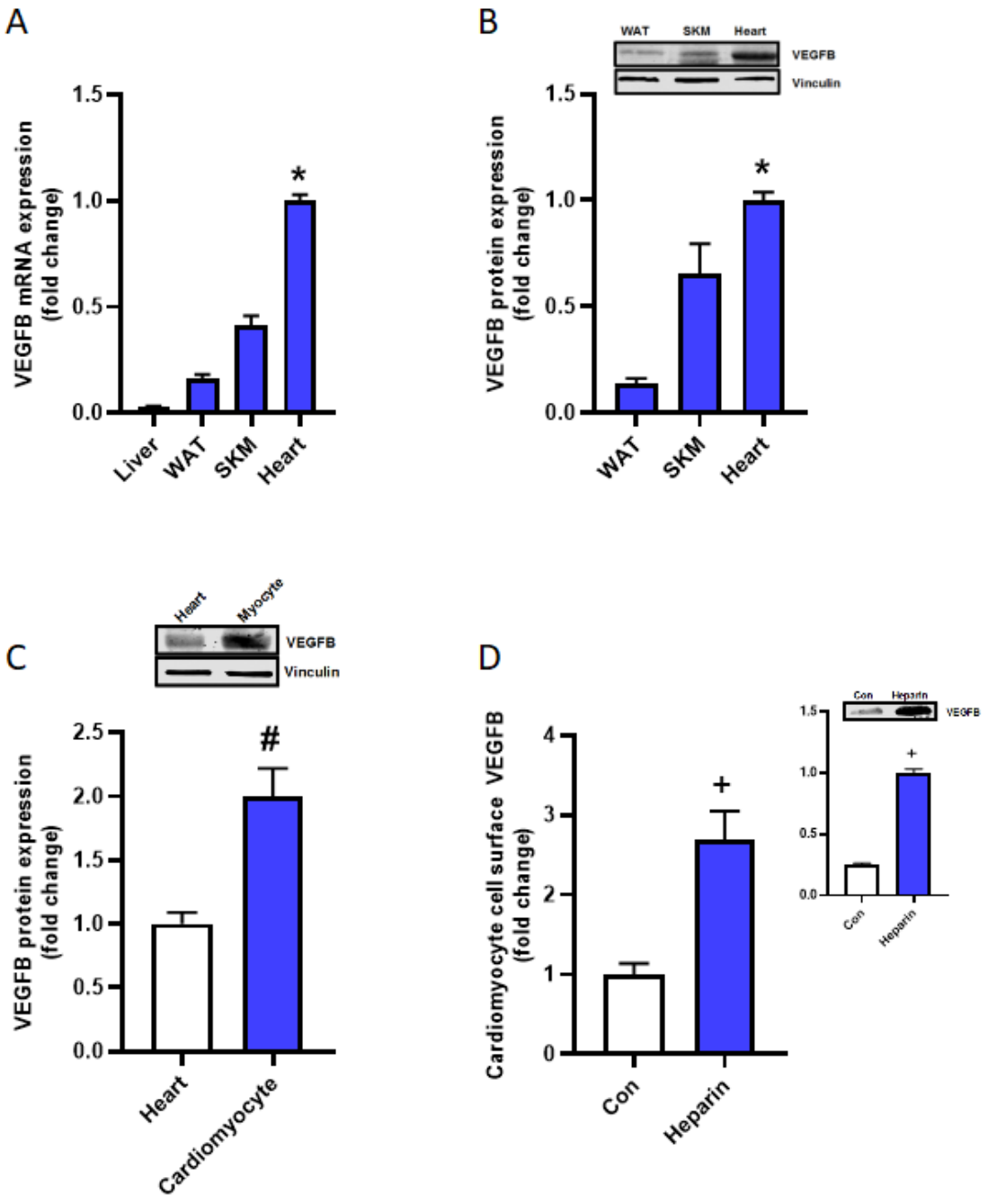

Figure 19. Differential expression of VEGB and its cellular localization in the heart. Selected tissues from male Wistar rats were removed and used for determination of VEGFB mRNA (A) and protein (B). For comparative analysis of VEGFB in cardiac tissue, cardiomyocytes were isolated for determination of VEGFB protein, and the result compared to its expression in the whole heart (C). Cardiomyocyte surface VEGFB was evaluated following incubation of cells with heparin (10 U/mL) for 20 minutes to initiate displacement of the protein and quantification by ELISA (D). The inset depicts VEGFB in the incubation medium following incubation with heparin, concentration of protein using centrifugal filters, and Western blot. n=3-6, *p<0.05 vs. all other tissues; #p<0.05 vs. whole heart; +p<0.05 vs. control (no heparin).

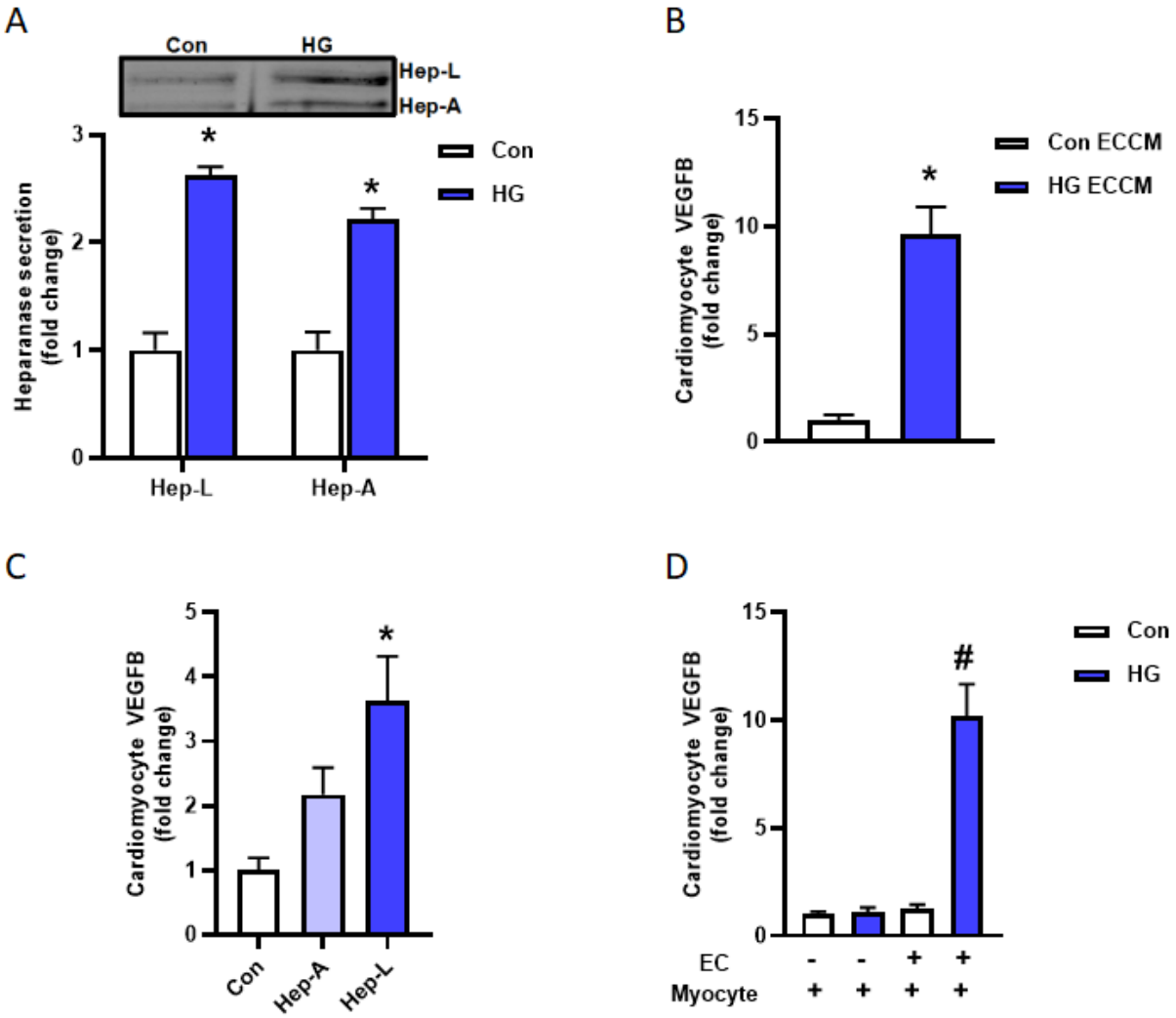

Figure 20. Cardiomyocyte VEGFB is heparanase releasable. Rat heart micro vessel endothelial cells (RHMEC) were incubated in DMEM with either 5.5 mM (control) or 25 mM high glucose (HG) for 30 minutes. The incubation medium was collected, protein concentrated using centrifugal filters, and latent (Hep-L) and active (Hep-A) heparanase quantified by Western blot (A). Isolated cardiomyocytes were treated with endothelial cell culture medium (ECCM) from endothelial cells exposed to either control or HG conditions for 20 minutes. Following this incubation time, medium (containing both Hep-A and Hep-L) was utilized to determine VEGFB release using ELISA (B). Recombinant Hep-A or Hep-L (2 µg/mL) was added to isolated cardiomyocytes for 20 minutes and incubation medium collected. Medium was centrifuged to remove cells and the supernatant evaluated for VEGFB release using ELISA (C). RHMEC were seeded on transwell inserts and cultured until 80% to 90% confluence. The transwell insert was then transferred to a 6-well plate and co-cultured with or without cardiomyocytes, in the presence or absence of HG for 30 minutes. Medium was centrifuged to remove cells and the supernatant evaluated for VEGFB release using ELISA (D). n=3-6, *p<0.05 vs. control, #p<0.05 vs. all other groups.

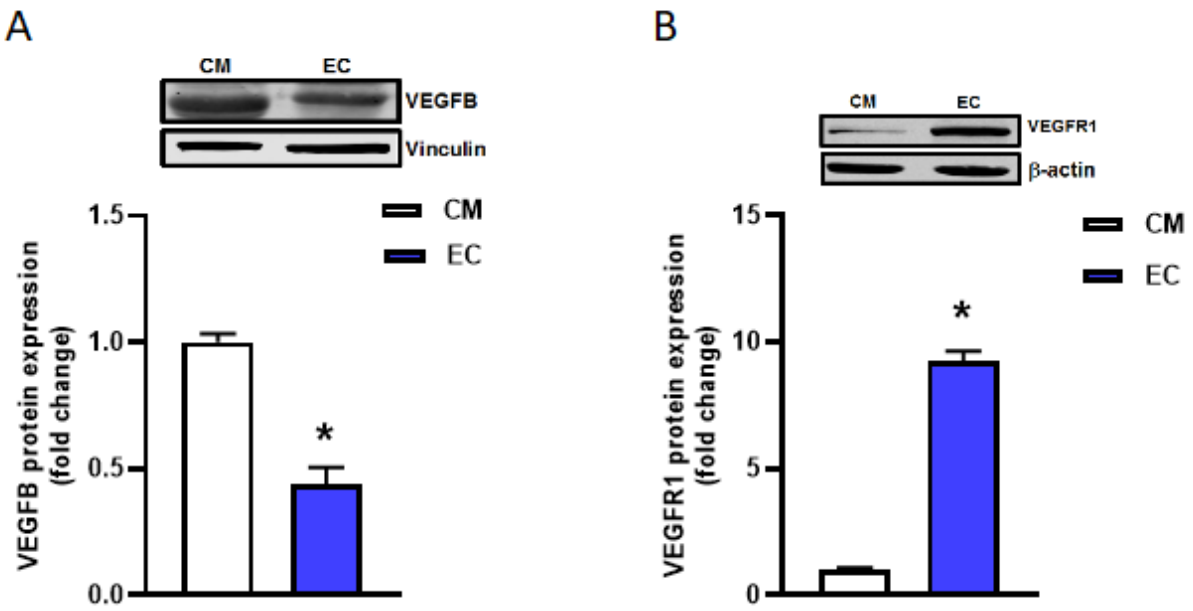

Figure 21. Protein expression of VEGFB and VEGFR1 comparing EC and cardiomyocytes. RHMECs and isolated cardiomyocytes were utilized to evaluate VEGFB (A) and vascular endothelial growth factor receptor 1 (VEGFR1) (B) protein by Western blot. n=3-6, *p<0.05 vs. cardiomyocyte. CM, cardiomyocyte; EC, endothelial cell.

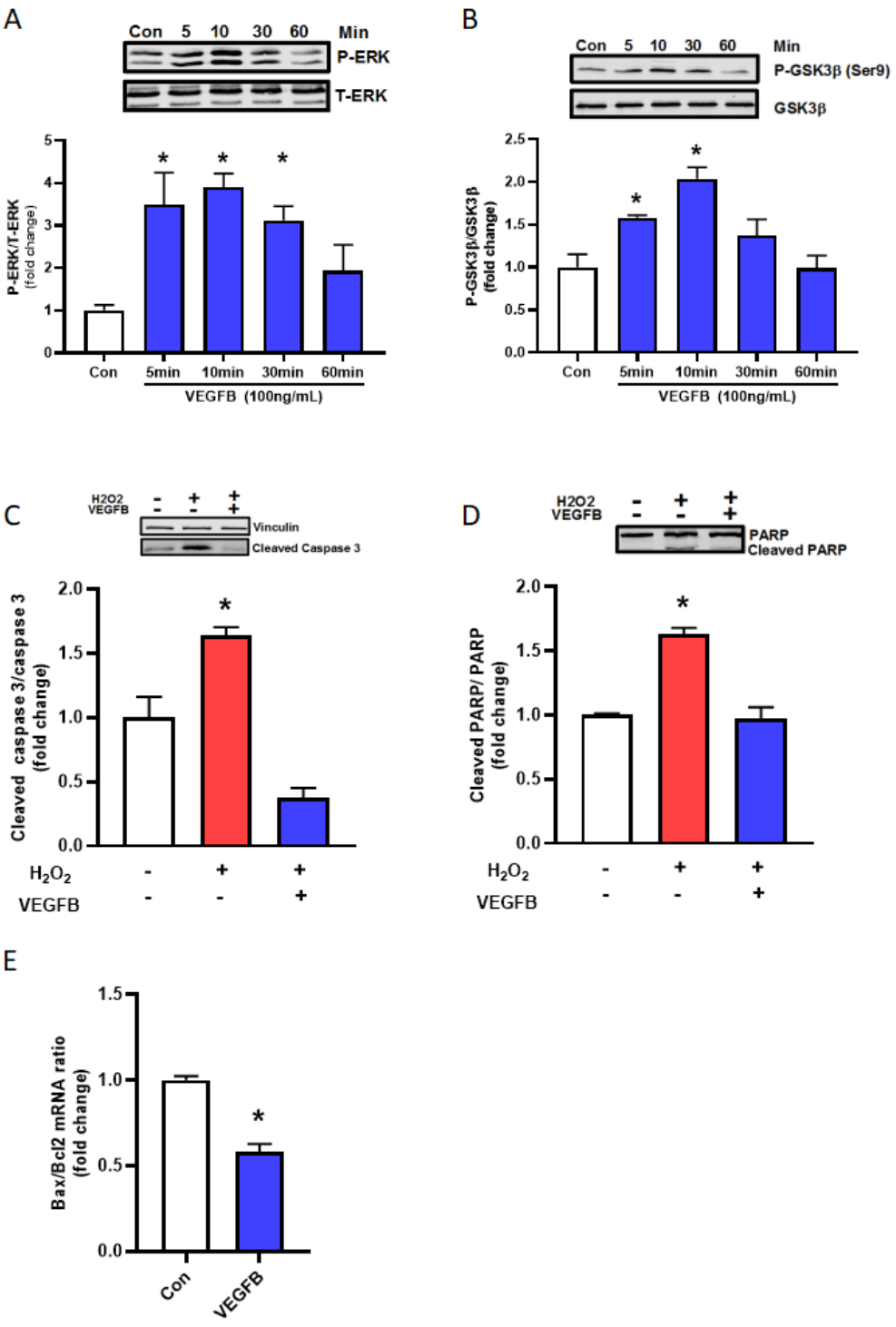

Figure 22. VEGFB action in endothelial cells. RHMECs were incubated with VEGFB (100 ng/mL) for the indicated times, and the ratio of P-ERK/T-ERK (A) and P-GSK3β (Ser9)/GSK3β (B) protein determined. RHMECs were exposed to H_2O_2 (100 μM) for 4 hours with or without pre-treatment of VEGFB for 1 hour, and the ratio of cleaved caspase 3 to vinculin (C), cleaved PARP to PARP analyzed (D). The ratio of Bax/Bcl2 mRNA was examined in RHMECs treated with VEGFB for 24 hours, (β-actin used as reference gene) (E). n=3-6, *p<0.05 vs. control.

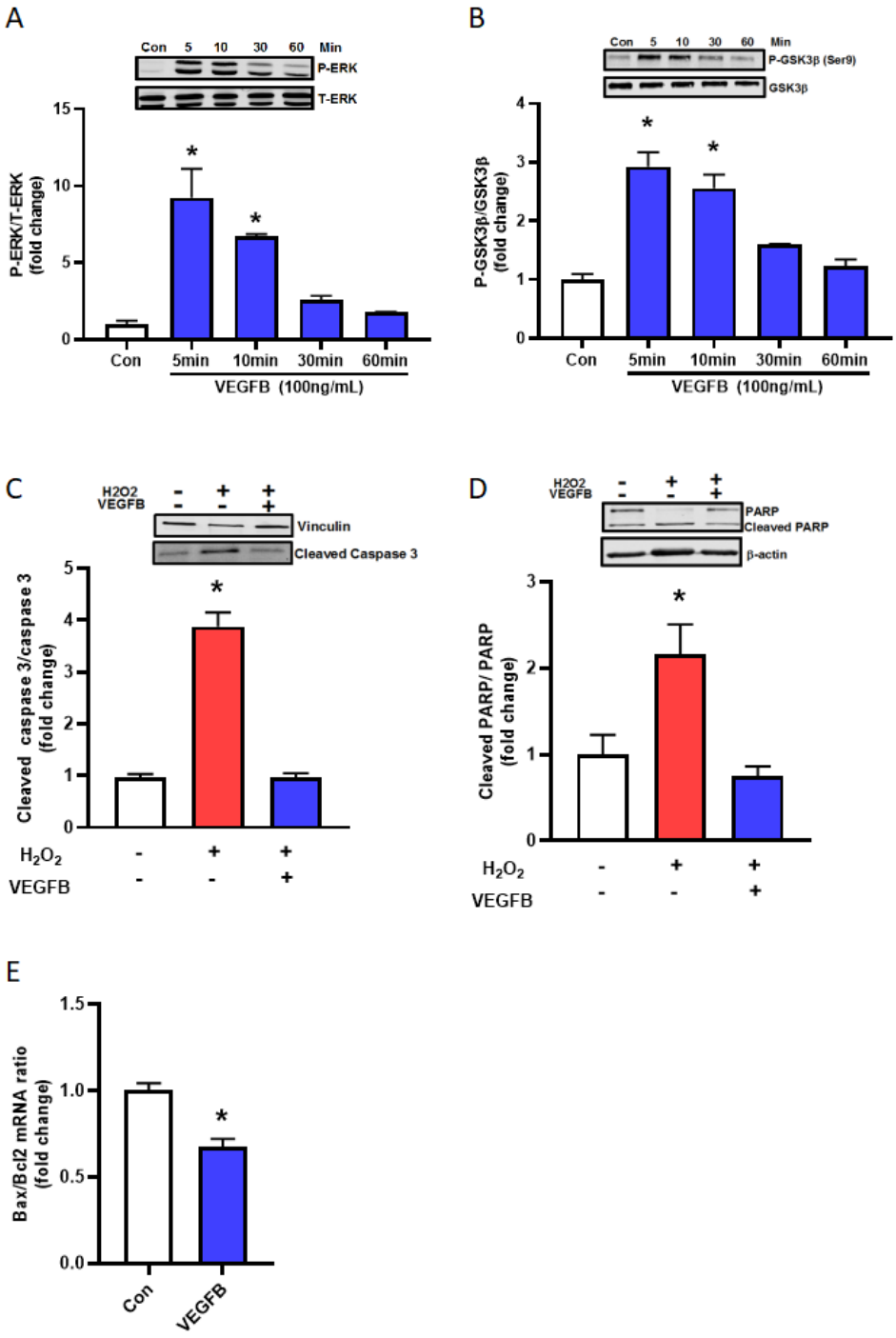

Figure 23. VEGFB action in isolated cardiomyocytes. Cardiomyocytes were incubated with VEGFB (100 ng/mL) for the indicated times, and the ratio of P-ERK/T-ERK (A) and P-GSK3β (Ser9)/GSK3β (B) protein analyzed. Isolated cardiomyocytes were exposed to H_2O_2 (100 µM) for 15 minutes, with or without pre-treatment of VEGFB for 1 hour, and the ratio of cleaved caspase 3 to vinculin (C) cleaved PARP to PARP analyzed (D). The ratio of Bax/Bcl2 mRNA was examined in myocytes treated with VEGFB for 24 hours, (β-actin used as reference gene) (E). n=3-6, *p<0.05 vs. control.

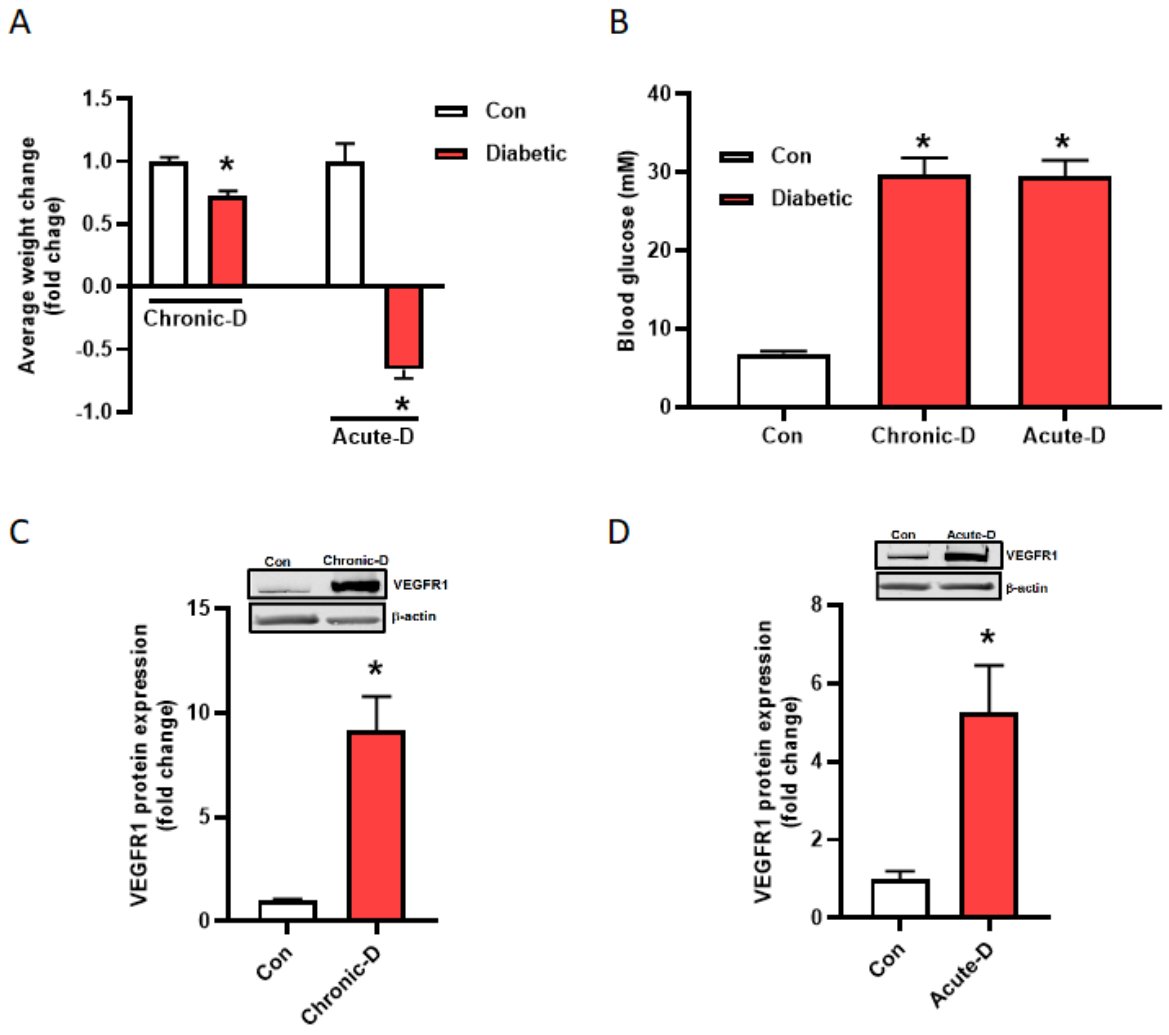

Figure 24. Changes in cardiac VEGFR1 in hearts from rats with acute and chronic diabetes. Male Wistar rats were injected with either saline (control) or streptozotocin to induce diabetes. Rats were monitored for 4 days (Acute-D, 100mg/kg STZ) or 6 weeks (Chronic-D, 55mg/kg STZ), at which time animals were euthanized and cardiomyocytes isolated. Average body weight change (A) and blood glucose (B) in acute and chronic animals with diabetes. VEGFR1 protein was determined in myocytes from animals with chronic (C) or acute (D) diabetes. n=4-8, *p<0.05 vs. control.

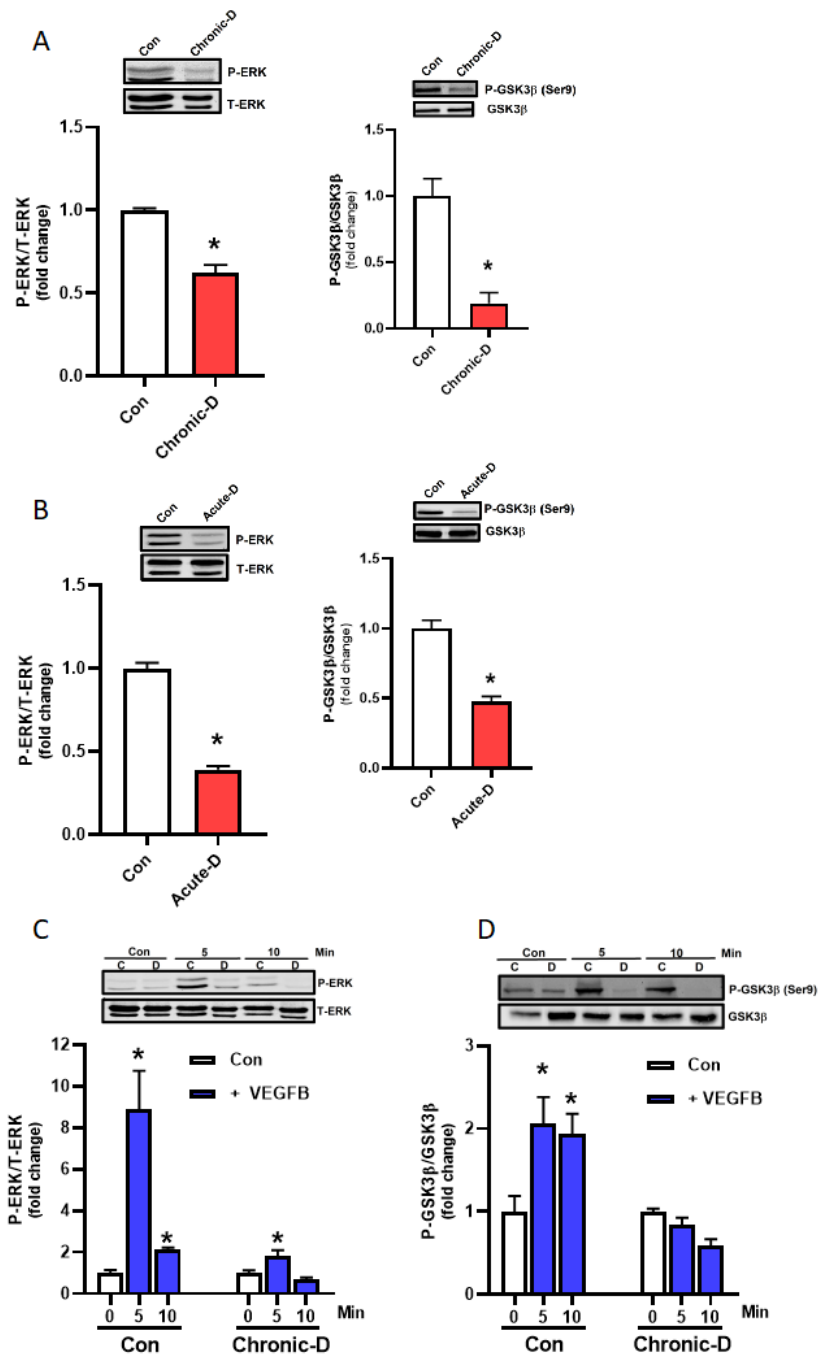

Figure 25. Decreased VEGFB signaling in acute and chronic diabetic rats. Isolated cardiomyocytes were analyzed for the ratio of P-ERK/T-ERK and P-GSK3β (Ser9)/GSK3β protein in a model of chronic (A and inset) and acute (B and inset) diabetes. Cardiomyocytes from animals with chronic diabetes were incubated with VEGFB (100 ng/mL) for the indicated times and the ratio of P-ERK/T-ERK (C) and P-GSK3β (Ser 9)/GSK3β (D) protein analyzed n=4-8, *p<0.05 vs. control.

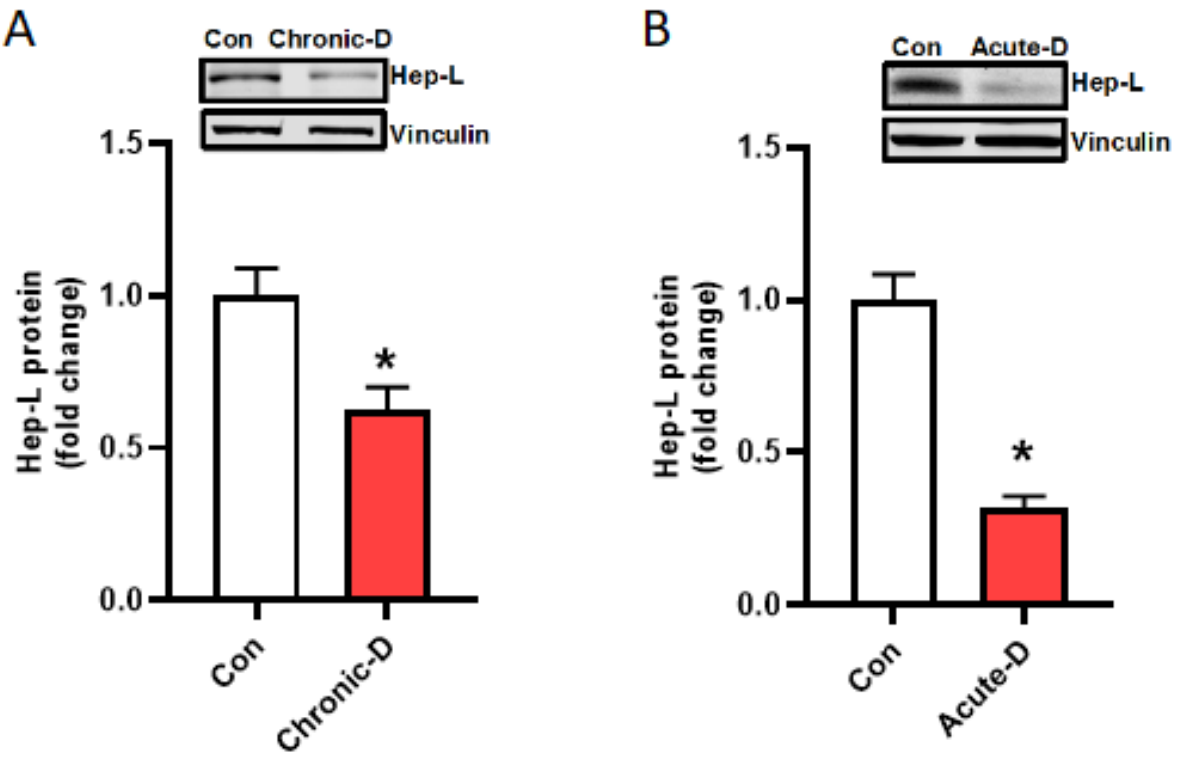

Figure 26. Lower heparanase in hearts from diabetic animals. Whole heart tissue was examined for expression of Hep-L protein in animals with chronic (A) and acute (B) diabetes. n=4-8, *$p<0.05$ vs. control.

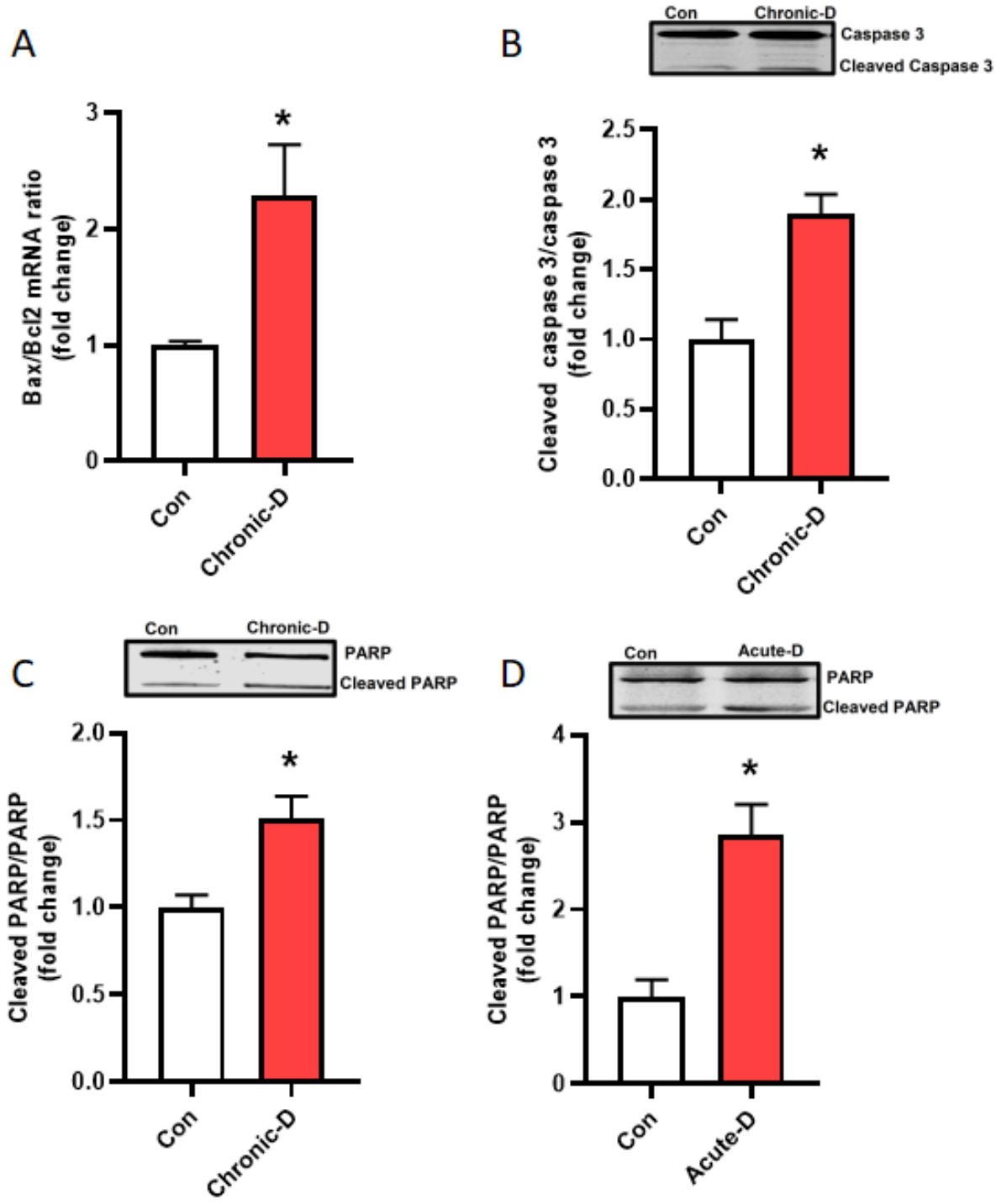

Figure 27. Increased cell death signature in hearts from diabetic animals. The ratio of Bax/Bcl2 mRNA (A) and cleaved caspase 3 to caspase 3 (B) was examined in myocytes from animals with chronic diabetes. The ratio of cleaved PARP/PARP protein was determined in cardiomyocytes from animals with chronic (C) and acute (D) diabetes. n=4-8, *p<0.05 vs. control.

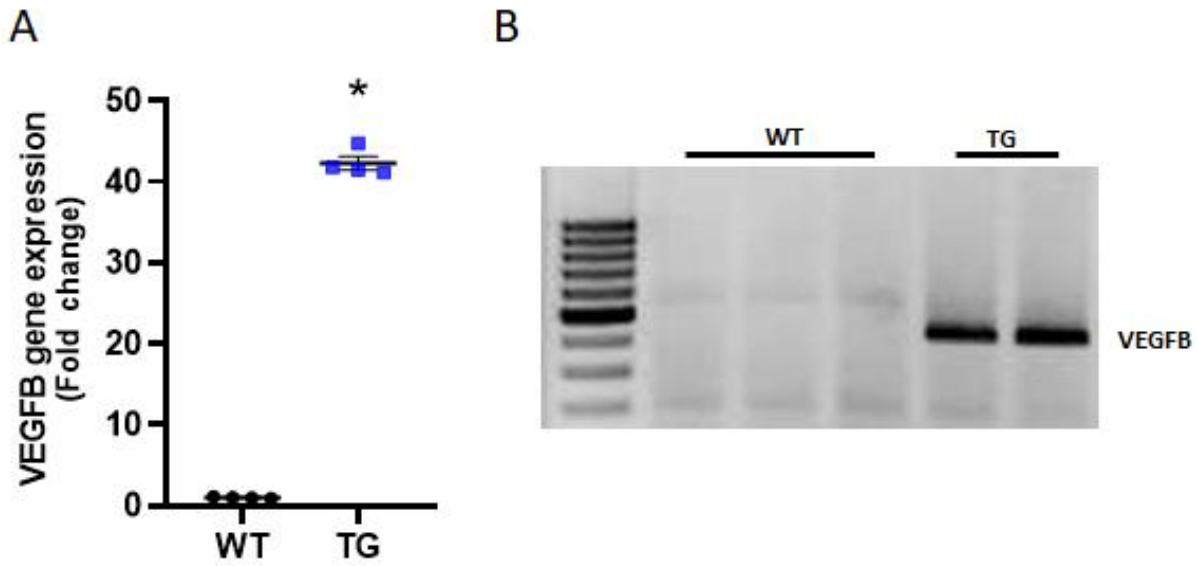

Figure 28. Transgenic hearts overexpressing human VEGFB. (A) Hearts were removed from male wildtype (WT) and transgenic (TG) rats between 8-12 weeks of age and ventricle RNA from the two groups were sequenced and differentially expressed genes (padj < 0.05 and significant in at least 5 out of the 10 analysis pipelines used) analyzed from RNA Seq. (B) In WT and TG rats overexpressing cardiac specific human VEGFB, PCR analysis of gDNA from ear notch samples and human VEGFB primers were used to genotype the animals. (n=4), *p<0.05.

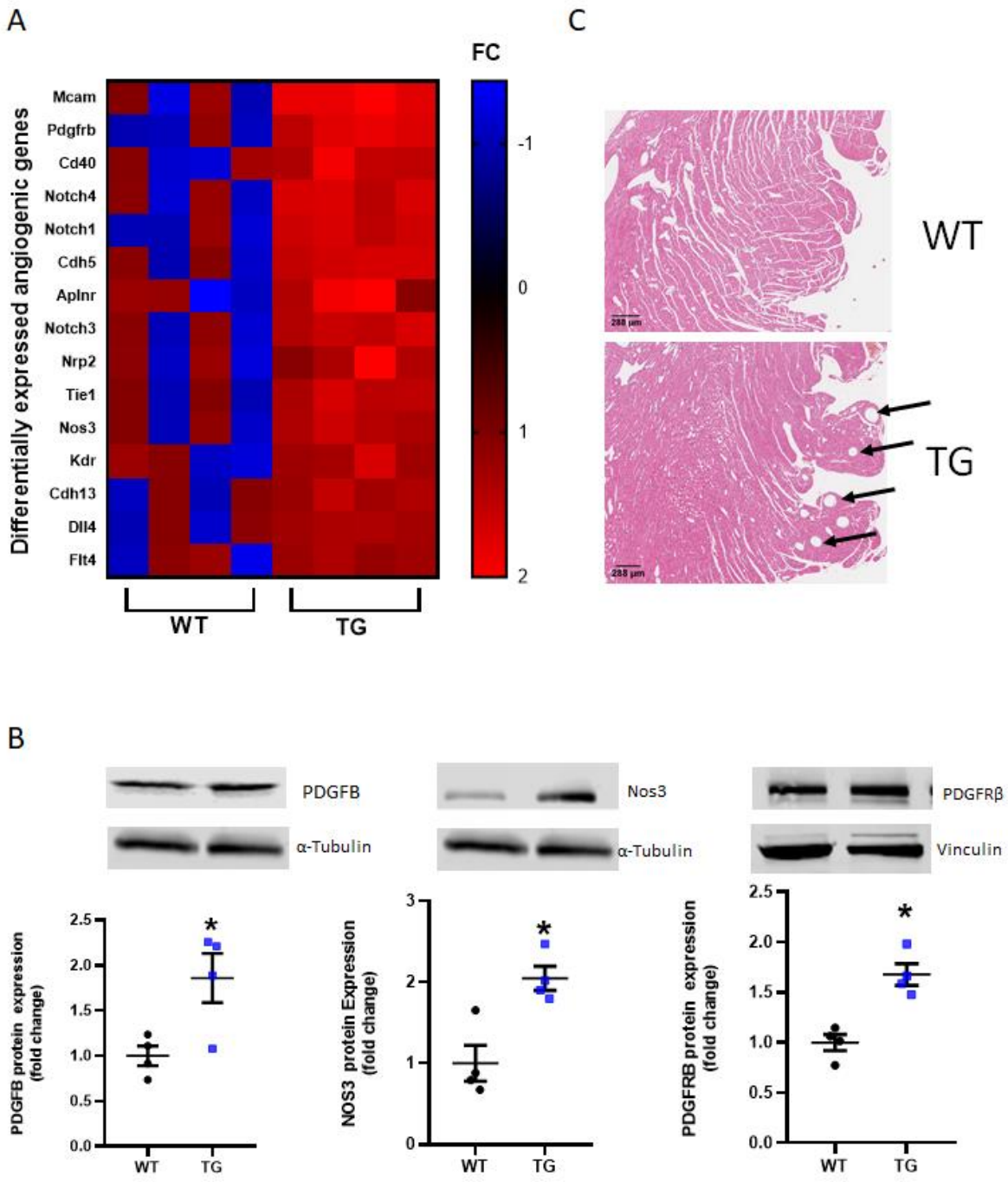

Figure 29. Transgenic hearts exhibit increased vascular growth. (A) Heat map identifying a gene expression profile associated with angiogenesis. The red (high) and blue (low) colors reflect fold change (FC). (B) Western blot of selected proteins associated with angiogenesis in hearts isolated from WT and TG rats. (C) Histological sections from WT and TG rat hearts were fixed, embedded in paraffin and visualized with H and E staining and light microscopy. Arrows identify increased blood vessel diameter in TG hearts. Data are presented as mean ± SEM (Student's t-test). (n=4), *p<0.05.

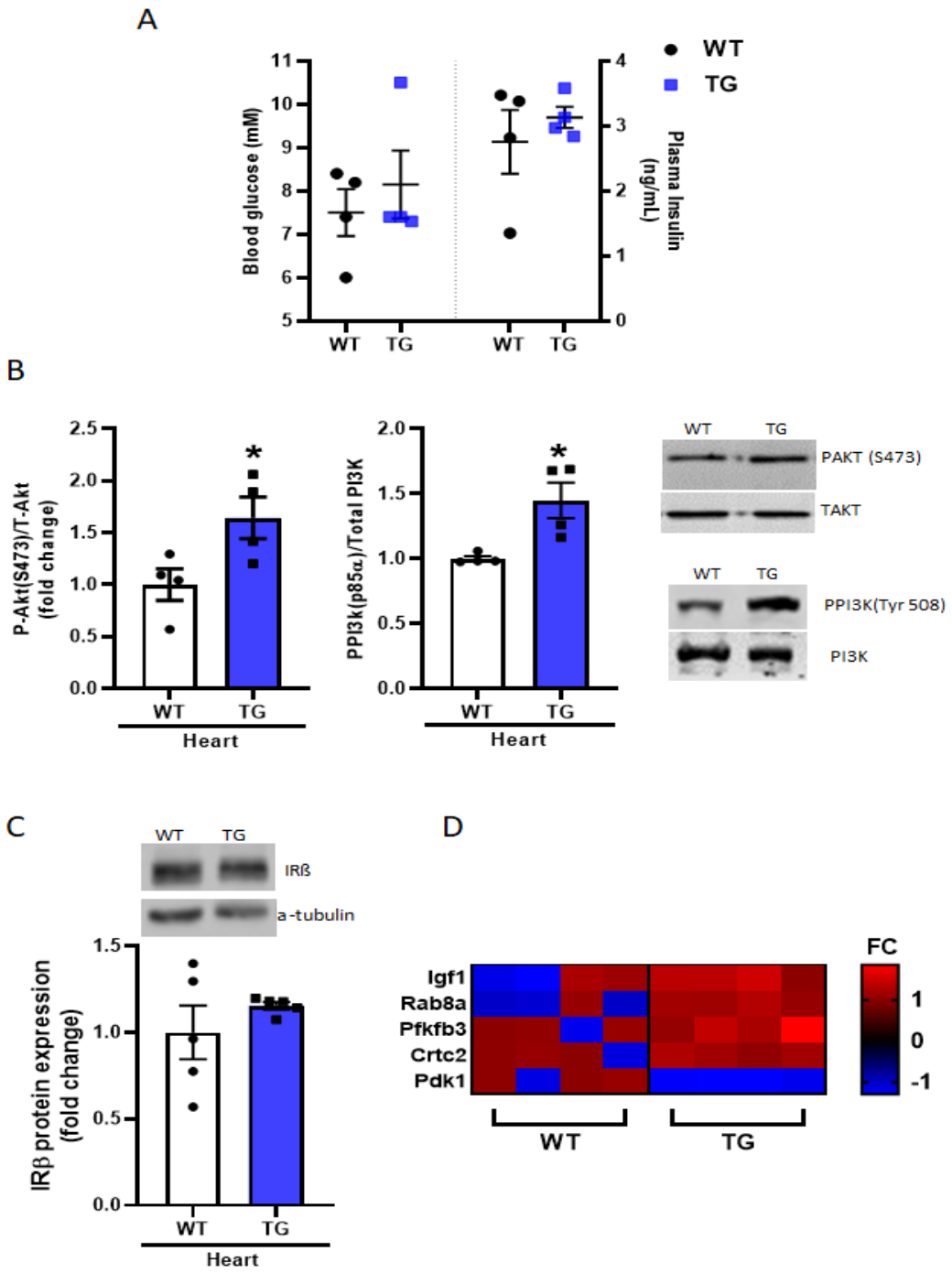

Figure 30. VEGFB TG hearts display enhanced insulin signaling. (A) Tail vein blood was obtained to determine glucose using a glucometer and test strips. Plasma insulin was measured using an ELISA from blood collected from the chest cavity at termination. Animals had ad libitum access to food and water (B) Hearts removed from WT and TG rats were frozen, powdered and lysed to obtain protein used for Western blot of p-AKT (S473) (left panel) and p-PI3K 85α (Tyr 508) (right panel). (C) Western blot of Insulin receptor β. (D) Heat map Identifying a gene expression profile associated with regulation of insulin action. The red (high) and green (low) colors reflect fold change (FC). Data are presented as mean ± SEM, n=3-4, *p<0.05 vs WT.

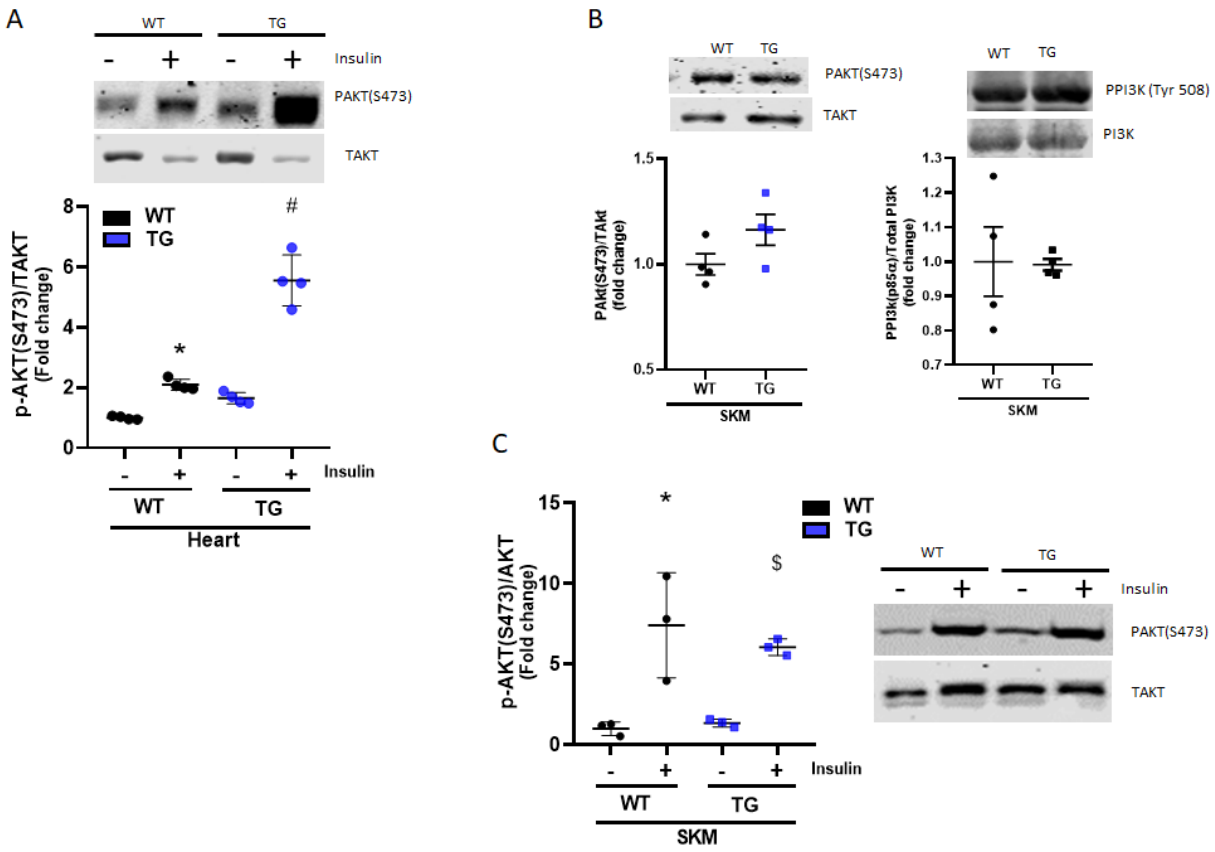

Figure 31. VEGFB TG hearts display enhanced responses to insulin. (A) Fast acting insulin (Humulin R; 5 U/kg), or saline were injected intraperitoneally and animals terminated after 10 minutes. Hearts were immediately removed from WT and TG rats and protein used for Western blot of p-AKT (S473). Animals had ad libitum access to food and water. (B) Skeletal muscle removed from WT and TG rats were frozen, powdered and lysed to obtain protein used for Western blot of p-AKT (S473) (left panel) and p-PI3K 85α (Tyr508) (right panel). (C) In WT and TG rats injected with insulin or saline intraperitoneally, skeletal muscle was immediately removed and protein used for Western blot of p-AKT (S473). Data are presented as mean ± SEM, n=3-4, *p<0.05 vs WT or WT minus insulin, $^{\$}p$<0.05 vs TG minus insulin, $^{\#}p$<0.05 vs all other groups.

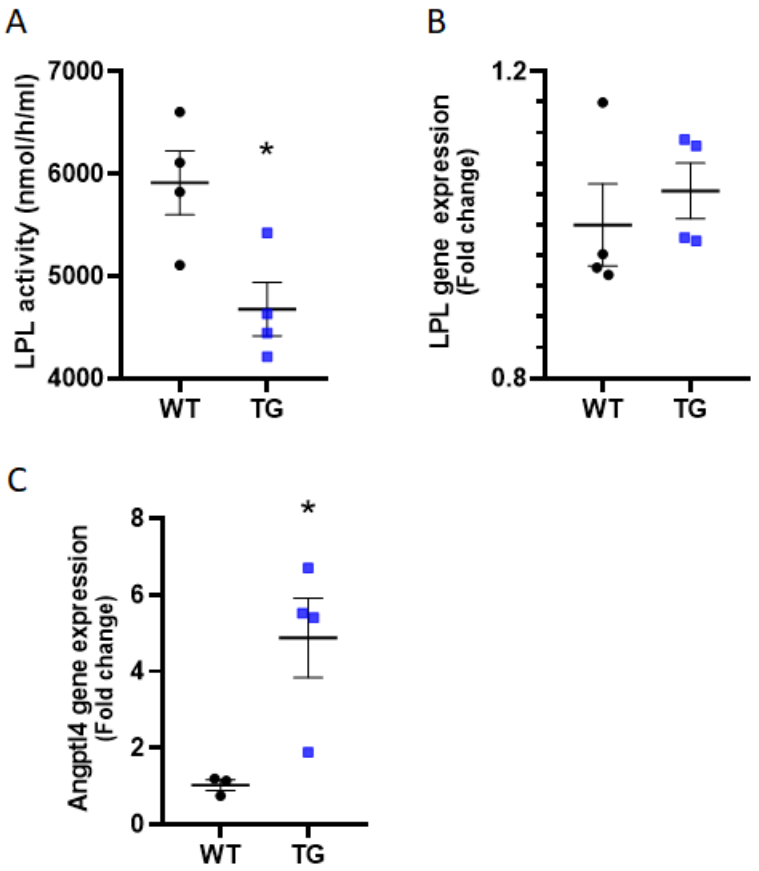

Figure 32. LPL activity is reduced in VEGFB TG hearts. (A) Hearts were perfused with heparin (5 U/ml) using a recirculating Langendorff retrograde perfusion technique. The perfusate over 30 minutes was collected from the buffer reservoir, concentrated and LPL activity determined by measuring the hydrolysis of radiolabeled triolein. (B) mRNA expression LPL in WT and TG hearts as determined using RNA-seq. (C) mRNA expression of Angptl4 in WT and TG hearts as determined using qPCR, (B2M used as reference gene). Data are presented as mean ± SEM, n=3-4, *p<0.05 vs WT.

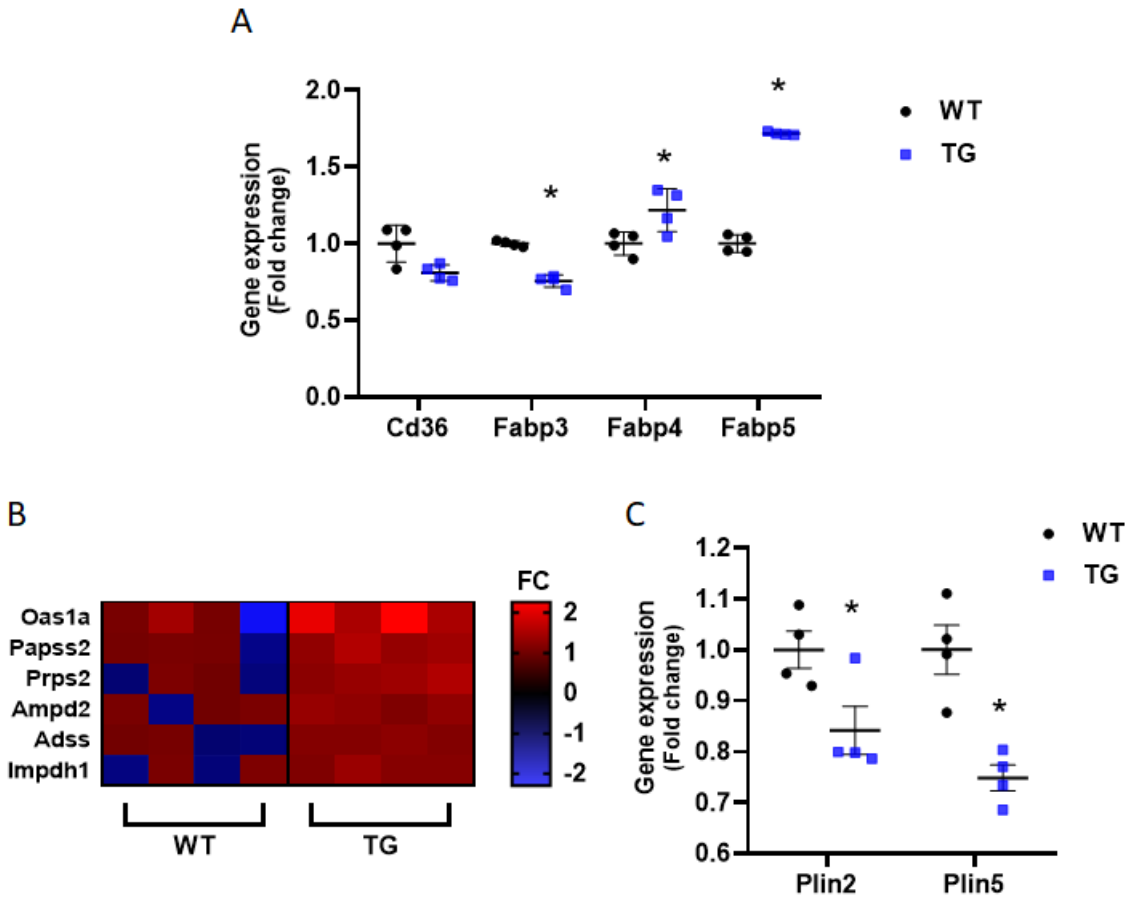

Figure 33. Augmented EC FABP and purine biosynthesis genes with lower gene expression for lipid droplet formation in VEGFB TG hearts. (A) mRNA expression of proteins associated with FA transport in WT and TG hearts as determined using RNA-seq. (B) Heat map Identifying a gene expression profile associated with purine biosynthesis is illustrated. The red (high) and blue (low) colors reflect fold change (FC). (C) Transcriptome analysis of genes related to lipid-droplet synthesis from RNA Seq. Data are presented as mean ± SEM, n=3-6, *p<0.05 vs WT.

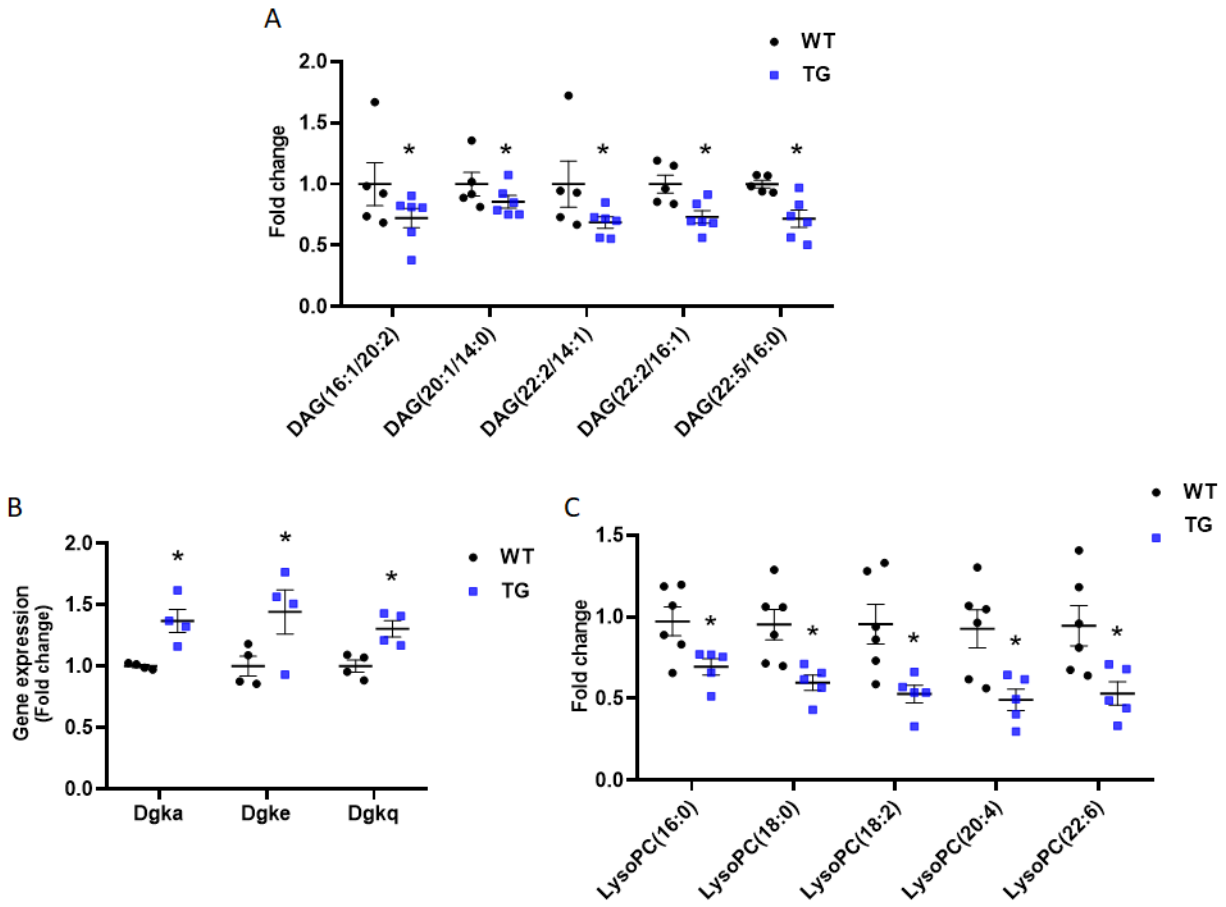

Figure 34. Reduced lipid metabolite accumulation and increased diacylglycerol kinase genes in VEGFB TG hearts. (A) Untargeted metabolomic analysis was performed using an Agilent 6530 quadrupole-time of flight mass spectrometer (QTOF), Agilent 1290 binary UPLC and MassHunter data acquisition software. The accumulation of diacylglycerol (DAG) containing FA are illustrated. (B) Diacylglycerol kinases (Dgk) which catalyze the conversion of DAG to phosphatidic acid was estimated in WT and TG hearts using RNA-seq. (C) Untargeted metabolomic analysis was performed using an Agilent 6530 quadrupole-time of flight mass spectrometer (QTOF), Agilent 1290 binary UPLC and MassHunter data acquisition software. The accumulation LysoPC containing FA are illustrated. Data are presented as mean ± SEM, n=3-6, **p*<0.05 vs WT.

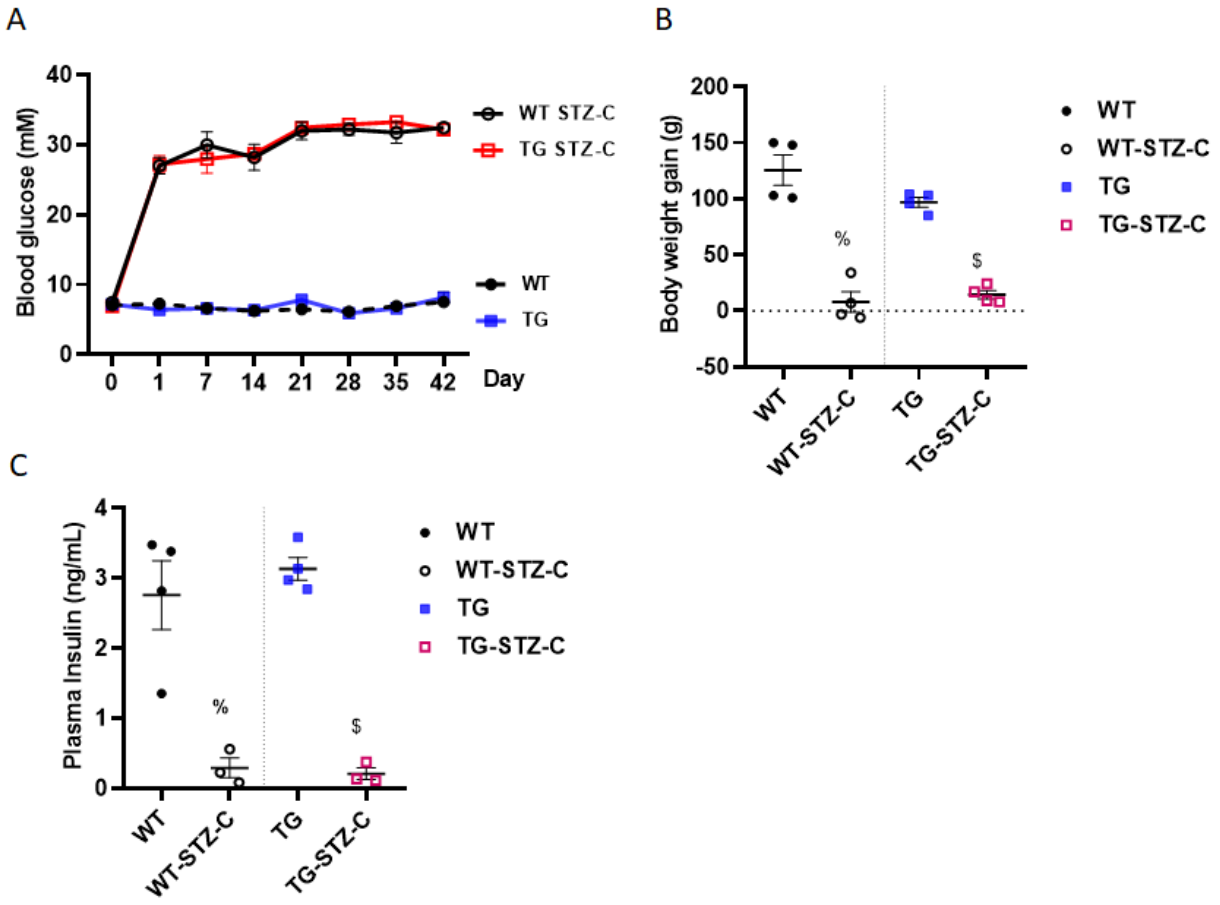

Figure 35. Blood glucose, body weight and plasma insulin in WT and TG rats. (A) To induce Type 1 diabetes, WT and VEGFB-TG rats were administrated STZ and followed chronically for 6 weeks. Blood glucose was measured intermittently over the study period. (B) 6 weeks after STZ injection, body weights of the different groups of animals are indicated. (C) Tail vein blood collected at termination was used for plasma insulin determination. Data are presented as mean ± SEM, n=3-6, $^{\%}p<0.05$ vs WT, $^{\$}p<0.05$ vs TG.

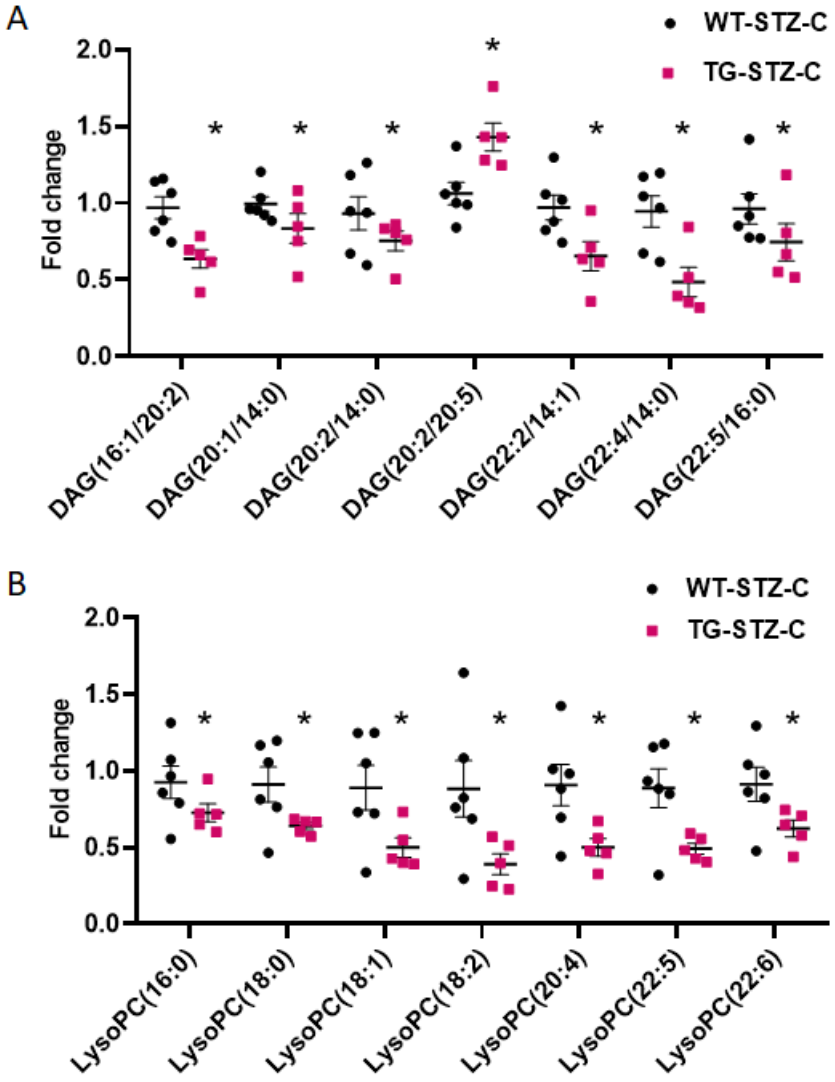

Figure 36. Decreased accumulation of lipid metabolites in TG-STZ-C hearts. WT and VEGFB-TG rats were administrated 55mg/kg STZ and followed chronically for 6 weeks (WT-STZ-C and TG-STZ-C). Untargeted metabolomic analysis was performed using an Agilent 6530 quadrupole-time of flight mass spectrometer (QTOF), Agilent 1290 binary UPLC and MassHunter data acquisition software. The accumulation of (A) DAG and (B) LysoPC (lower panel) containing different FA are illustrated. Data are presented as mean ± SEM, n=3-6, *p<0.05 vs WT-STZ-C.

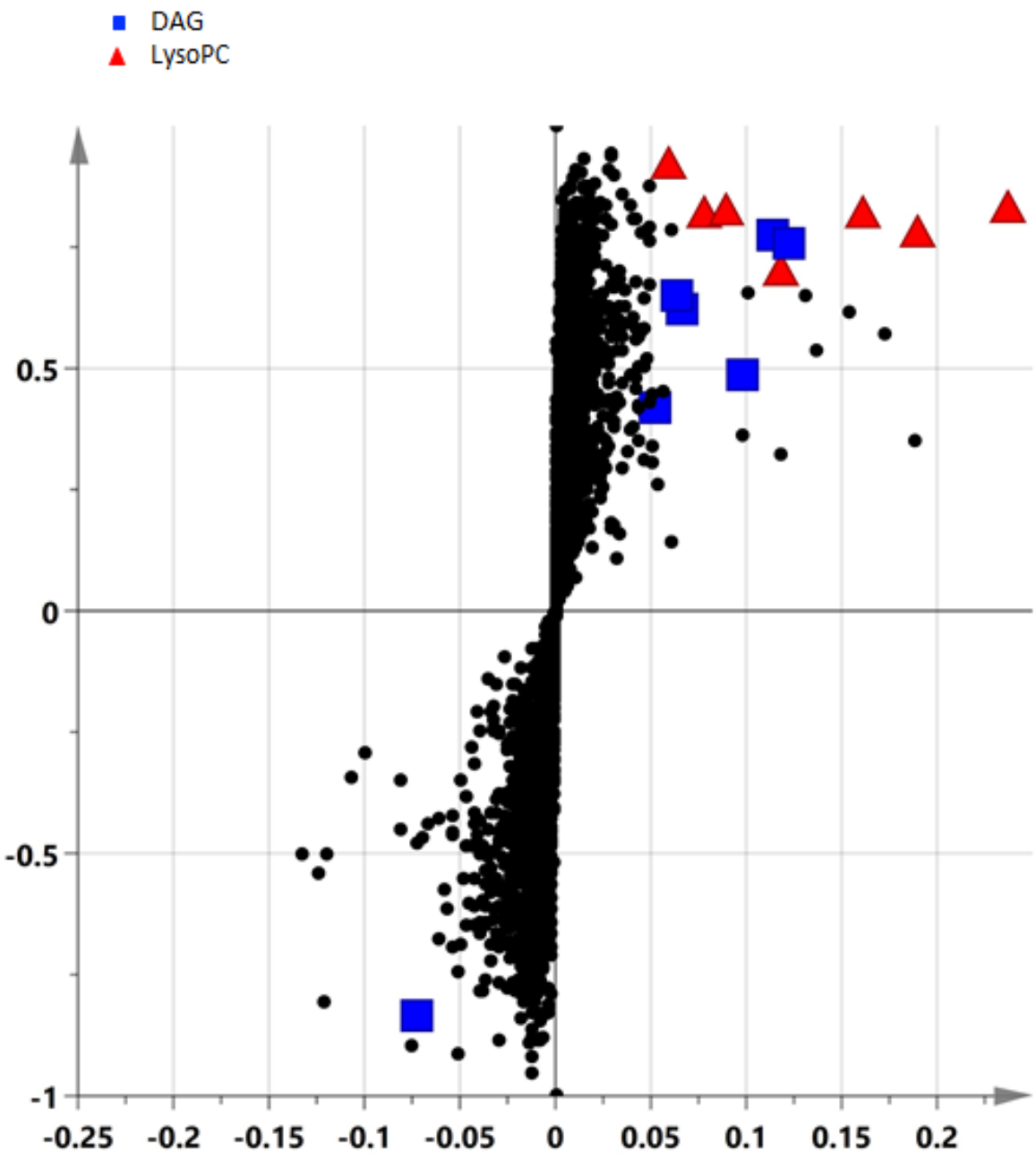

Figure 37. Lipid metabolites differences in WT-STZ-C compared to TG-STZ-C hearts. S-plot analysis illustrating the DAG and LysoPC metabolites that contributed most to the separation of WT-STZC from TG-STZC hearts.

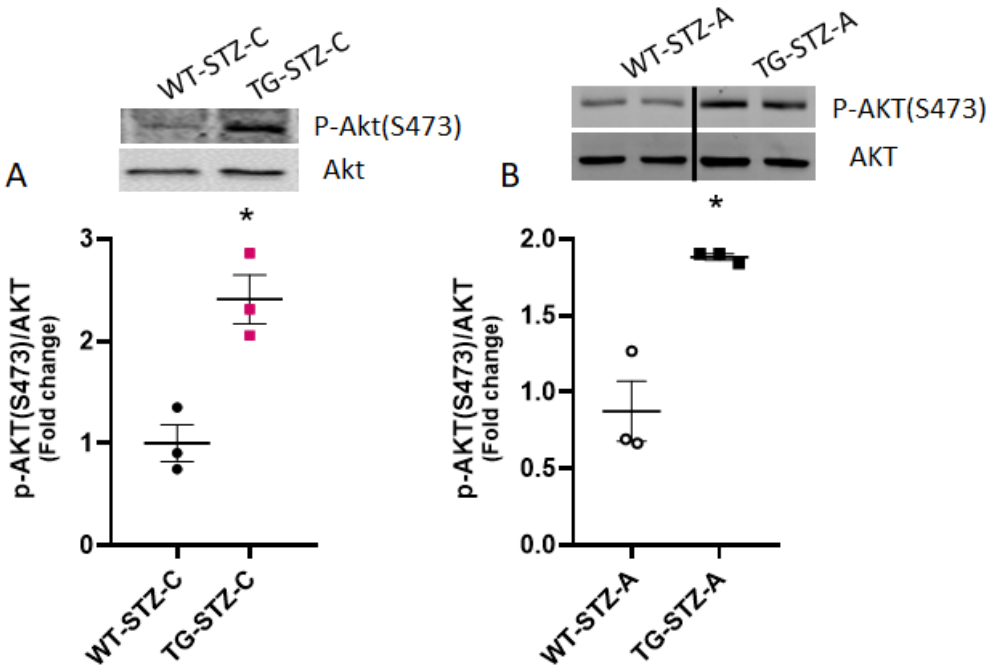

Figure 38. Increased insulin signaling in TG hearts after acute and chronic diabetes. After 6 weeks (STZ-C) or 4 days (STZ-A) of diabetes, hearts were isolated for Western blot to evaluate basal p-AKT (S473). Data are presented as mean ± SEM, n=3-6, **p*<0.05 vs WT-STZ-C.

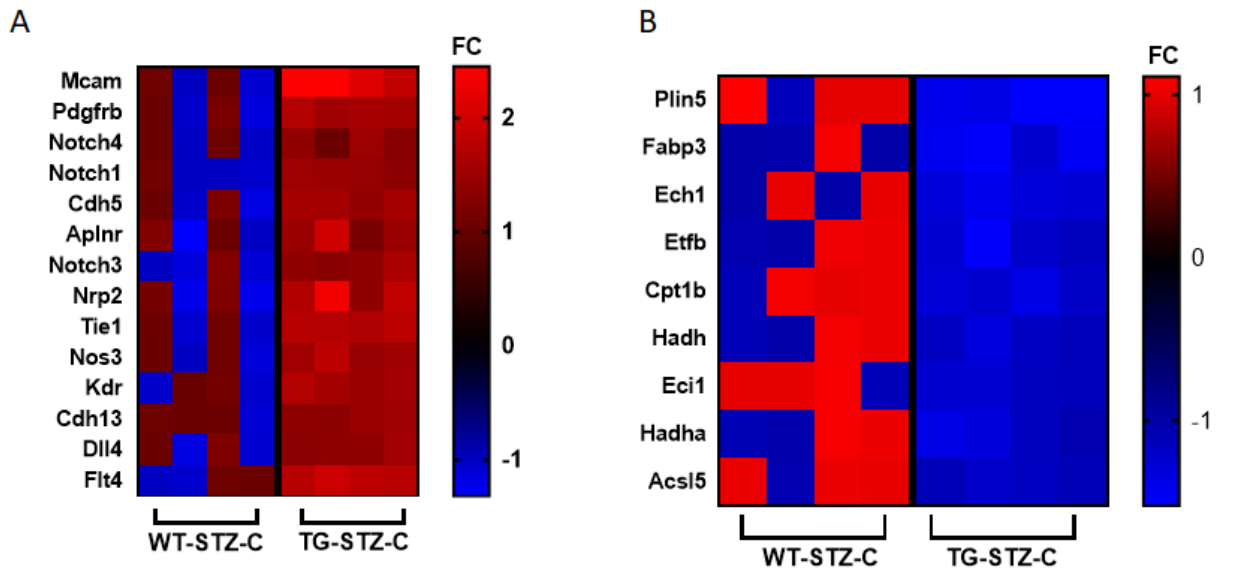

Figure 39. Increased angiogenic genes with decreased expression of fatty acid utilization genes in TG-STZ-C hearts. Heat map Identifying a gene expression profile associated with (A) angiogenesis and (B) fatty acid utilization are illustrated. The red (high) and blue (low) colors reflect fold change (FC).

CHAPTER 4: DISCUSSION

Cardiovascular disease (CVD) is a leading cause of death in individuals with T1D and T2D (118). Although atherosclerosis is considered a primary cause for diabetes-induced CVD, humans and animal models with T1D and T2D have also been diagnosed with cardiomyopathy and eventual heart failure in the absence of vascular disease, with alterations in cardiac metabolism contributing to this pathology (2, 119). Our data suggest that with an increasing severity of diabetes, the heart is unable to control its own FA supply using LPL, and undergoes dramatic reprogramming that is linked to handling of excess FA that likely arise from AT lipolysis. This transition results in a cardiac metabolic signature that embraces mitochondrial FA overload, oxidative stress, triglyceride storage and cell death. Data in this thesis suggests that EC, as the first responders to hyperglycemia, can release heparanase to liberate VEGFB from a myocyte surface pool which can influence EC (paracrine) and cardiomyocyte (autocrine) survival. There is growing recognition of the importance of this growth factor in maintaining cardiac functional equilibrium. Experimentally, VEGFB has demonstrated significant cardio protection against H_2O_2-induced oxidative stress. Unfortunately, the expression of this growth factor is decreased under conditions of hyperglycemic stress, likely playing a role in the cell death observed in our D100 model. Overexpression of VEGFB in the heart, either via adenoviral delivery or transgene introduction in rats, dramatically improved heart function when these animals were exposed to experimental myocardial infarction(74). Surprisingly, even though VEGFB is the only member in the VEGF family not considered a classic angiogenic growth factor, the most compelling effect in rat hearts with cardiomyocyte-specific overexpression of human VEGFB, which is 88% homologous to rat VEGFB, was significantly upregulated genes related to vascular growth and angiogenesis, along with a previously reported enhancement of capillary size and coronary artery density(120). As

microangiopathy (damage to the small arteries and capillaries) is increased in the diabetic heart(121), augmented vascular angiogenesis may be greatly advantageous and potentially protective against DCM.

4.1 Diabetes severity and a switch from using LPL to adipose-derived fatty acid results in a cardiac metabolic signature that embraces cell death

Using a single injection of 55 mg/kg STZ, we produced a model of moderate diabetes that we describe as imitating insufficient glycemic management in T1D subjects where multiple finger pricks and daily insulin injections (3-4/day) may lead to variable compliance and repeated exposure to bouts of hyperglycemia. With this dose of STZ, the insulin reduction was insufficient to increase circulating albumin-bound FA or triglyceride. As a result, production of energy in the diabetic heart is appropriated by LPL; there is augmented processing of this enzyme into an active dimeric form followed by its recruitment to the coronary vascular lumen (122). At the lumen, it breaks down the triglyceride core of circulating lipoproteins to release FA, representing an immediate compensatory response to guarantee FA supply when glucose cannot be used (38, 39). Intriguingly, 100 mg/kg STZ treated animals displayed striking hypoinsulinemia, hyperglycemia, and an augmented pool of circulating plasma FA and triglyceride. We label these animals as being severely diabetic, representing T1D individuals with poor glycemic control. In these animals, the unfettered hydrolysis of AT triglyceride to generate FA results in the diabetic heart using this pool of FA disproportionally. Consequently, to avoid lipid oversupply, there is conversion of LPL to inactive monomers, a reduction of enzyme at the coronary lumen and inhibition of lipoprotein triglyceride hydrolysis (38). Our results imply that the greater the loss of glycemic control in T1D, delivery of FA to the heart shifts from lipoprotein- triglyceride hydrolysis by coronary LPL to AT-derived FA. This is a questionable adaptation as the site of control for FA provision to the heart

changes from a measured regulated delivery by coronary LPL (which is then turned off to avoid further lipid overload) to unrestrained provision of this substrate from AT.

Therapeutic management of blood glucose and its monitoring are the foundational basis of diabetes treatment (123). Regrettably, recommended glycemic goals are infrequently achieved, and this strategy often overlooks other features that are commonly part of this complex disease such as hyperlipidemia. In this respect, insulin deficiency produces activation of lipolysis in AT that results in hydrolysis of stored triglyceride and release of large amounts of FA into the plasma. This is because the primary enzymes responsible for lipolysis in adipocytes, ATGL and HSL, are highly sensitive to inhibition by insulin (124). Unexpectedly, a reduction of plasma insulin by almost 50% was insufficient to stimulate lipolysis. Contrasting with this data, it was only when insulin fell by more than 80% that an increase in plasma FAs was observed. It is important to note that the percentage composition of the main FAs identified in D100 plasma remained unchanged and mirrored the composition of the dietary FA ingested. Following their release, FAs enter into the portal circulation and thus liver (where they induce biogenesis of VLDL), or are delivered to the heart as a complex with albumin (125) and transferred across the plasma membrane to serve as an energy source. Given that the isolated heart exposed to equivalent concentrations of FA oxidize SFA, MUFA, and PUFA at similar rates (1), our results indicate that the augmented FA in D100 would be non-productive as the supply of FA might exceed the capability of the heart to utilize this excess amount of substrate.

With uninterrupted contraction being a feature of the heart, cardiac muscle has a high demand for energy. As such, this organ demonstrates substrate promiscuity, enabling it to utilize multiple sources of energy, including FA, carbohydrates, amino acids and ketones (1). Among these, carbohydrates and FA are the major sources from which the heart derives most of its energy, with

FA producing almost 2.4-fold more ATP than glucose. Accordingly, in a basal setting, glucose and lactate contribute to approximately 30% of ATP generation, with FA oxidation accounting for the remaining 70% (1). Insulin plays an important role in glucose uptake and oxidation and suppression of FA oxidation in the heart (126). It was not surprising then that its reduction in D55 animals was characterized by cardiac gene expression changes that emphasized defects in glucose metabolism and an enrichment in FA utilization. However, in hearts from D100 animals, it was noticeable as to how much more pronounced this change in the metabolism gene profile was, not only related to altered substrate utilization but also to the wide spectrum of associated downstream consequences including mitochondria function, oxidative stress and cell death. Whether this effect is a consequence of the high amounts of plasma FA (127) or the catastrophic loss of insulin in D100, or both, is currently unknown and can only be assessed if these results are compared to animals where plasma FAs are increased without affecting insulin (using lipid and heparin-induced elevation of FA) (127).

The first degradative step in the cardiac utilization of FA involves its β-oxidation in the mitochondria. However, another cytoplasmic organelle, peroxisomes, are also capable of β-oxidation of FA (especially VLCFA), with one key difference. Within peroxisomes, VLCFA only undergo β-oxidation for chain shortening and are incapable of being fully oxidized to CO_2 and H_2O to produce ATP (128); the shorter chain moieties generated in the peroxisomes are transferred to the mitochondria for additional β-oxidation and subsequent ATP generation. When systemic hyperglycemia was superimposed with dyslipidemia, there were more intense gene expression changes in the D100 heart that could direct this organ to use FA by activating both the peroxisomal and mitochondrial β-oxidative pathways. One unappealing outcome of β-oxidation of FA in these organelles is the production of chemically reactive ROS (129, 130) and when combined with the

reduction of antioxidant enzyme genes, causes oxidative stress (131). Another drawback is that it results in the decrease of VLCFA like docosahexaenoic acid (22:6n3) and hence loss of the anti-oxidative and anti-inflammatory effects of this omega-3 FA (132). Thus, in attempting to handle excess FA through stimulation of β-oxidation in peroxisomes and mitochondria, the D100 heart is exposed to oxidative damage and ultimately cellular demise.

The decrease in VLCFA may not be due completely to augmented oxidation, but may also include a pathway to production of eicosanoids involved in an anti-inflammatory response. However, an argument against this view is that D100 hearts had an enrichment of genes annotated as related to a response to oxidative stress, decreased coenzyme Q9, and a higher amount of oxidized lipids (data not shown). Furthermore, linoleic (LA, C18:2n-6) as well as oleic (OA, C18:1n-9) acid are increased in both the heart and plasma FA in D100 rats. The accumulation of LA in metabolic tissues has specifically been proposed to induce oxidative stress through the generation of multiple oxidized LA compounds (133-135). Interestingly, some of them have cardio-specific toxicities which can range from mishandling of calcium to inflammation (136). Such findings are also being increasingly reported in humans (137-139). Additionally, the upregulation of OA in cardiac tissues is known to promote triglyceride accumulation (140, 141) , as we see in our D100 model. While this storage of triglyceride may be adaptive, over time, such accumulation of triglyceride may contribute to cardiomyopathy as has been shown in humans (142-144). We also want to emphasize that both OA and LA require additional steps by isomerases and reductases before they can be completely β-oxidized compared to palmitic acid (PA) (145, 146). Thus, PA without double bonds can undergo β-oxidation in an uninterrupted manner, is a better β-oxidation substrate than LA and OA, and gets utilized faster (its levels are lower in both diabetic groups). Finally, reductases utilize NADPH as the reducing equivalent donor (147). The

preference of the D100 heart to underutilize OA or LA (hence leading to their accumulation) could be an adaptive response to preserve NADPH levels within myocytes to prevent further oxidative stress.

Following β-oxidation, FA catabolism resumes with sequential processing in the mitochondrial TCA cycle and oxidative phosphorylation system to yield ATP (148). Contrary to prediction, the augmented β-oxidation was not matched by elevated TCA cycle activity or enhanced OXPHOS in D100 hearts. In fact, assessment of genes involved in mitochondrial metabolism revealed a critical decline in transcript levels of genes involved in these two pathways. In support of these observations, high fat feeding is also known to increase β-oxidation but reduce TCA cycle intermediates in skeletal muscle of obese rodents (149). As a consequence, in our study, myocytes from D100 hearts were unable to increase their respiration in response to increasing concentrations of FA under both basal conditions or when energy demand is increased. This suggests that when FA supply exceeds the mitochondrial capacity for disposal of this substrate (mitochondrial overload), incomplete oxidation of FA and ATP deficiency are an expected outcomes (149). The subsequent increase of FA intermediates and their diversion to triglyceride, paired with increased ROS formation secondary to excessive β-oxidation can provoke a gene expression program supporting cell death (lipotoxicity). Indeed, a large number of the differentially expressed genes in D100 hearts were those involved in apoptosis. Thus, even though a recent study has suggested that hyperglycemia/hypoinsulinemia alone, without dyslipidemia, is sufficient to impair cardiac function (150), data sets from this study indicate that with the increasing severity of diabetes, the sizeable increase in FA accounts for larger (compared to hyperglycemia alone) transcriptomic, metabolomic and functional consequences and cardiomyocyte cell death (Figure 40). To protect against this cellular demise, intrinsic mechanisms are likely available to maintain heart function.

Based on previous studies indicating vascular endothelial growth factor B (VEGFB) as a regulator of cell survival (69), this growth factor could be one such mechanism. Given the link between cell death and VEGFB, we questioned whether changes in this growth factor could be connected to the cell demise seen in diabetic model of hyperglycemia with hyperlipidemia. These diabetic animals demonstrated a loss in VEGFB production, but insulin treatment of the D100 animals reversed the drop in cardiomyocyte VEGFB protein. Our data suggest that the loss of VEGFB could play a role in cardiomyocyte cell death leading to diabetic cardiomyopathy.

4.2 Loss of VEGFB and its signaling in the diabetic heart is associated with increased cell death signaling

Compared to non-contractile tissues such as white adipose tissue and liver, the heart displayed the highest expression of VEGFB, highlighting the potential of this vascular growth factor in maintaining cardiac function. Of the VEGFB present in the heart, it was the cardiomyocytes that appeared to express this protein the most, further emphasizing its value in the contractile unit. One feature of cardiomyocytes is the presence of HSPG on their cell surface (151). Furthermore, over 80% of VEGFB transcripts have a heparin binding domain (62), allowing for their potential sequestration on the myocyte cell surface through an ionic interaction. This was confirmed using the highly negatively charged molecule, heparin. As this sulfated glycosaminoglycan displaced VEGFB into the medium, our data suggest that the cardiomyocyte surface contains a novel, rapidly releasable pool of this growth factor.

In contrast to heparin that is localized mainly in mast cells, heparanase is an endoglycosidase highly expressed in EC. It is synthesized as a latent (Hep-L) 65 kDa enzyme that undergoes cellular secretion followed by reuptake (11, 12). After undergoing proteolytic cleavage in lysosomes, a 50 kDa polypeptide is formed that is ~100-fold more active (Hep-A) than Hep-L (13, 14). In response

to environmental cues like hyperglycemia, the strategically located EC act as “first-responders” (152, 153) to this metabolic disturbance, and react by secreting heparanase (154, 155). In the current study EC, in the presence HG, elicited the secretion of both Hep-L and Hep-A into the medium. More importantly, this heparanase-containing endothelial cell culture media initiated a robust displacement of VEGFB when given to cardiomyocytes. The utility of EC heparanase in releasing VEGFB was confirmed using recombinant latent and active heparanase, and EC and cardiomyocytes in co-culture in the presence of HG. Intriguingly, Hep-L caused a greater release of VEGFB, a result similar to what we previously reported for VEGFA (17). This suggests that, to release VEGFB, ionic displacement by Hep-L is more efficient than hydrolysis of heparan sulfate by Hep-A, providing an additional function for secretion of Hep-L beyond its simple obligation for reuptake and lysosomal conversion to Hep-A. Released VEGFB from the cardiomyocyte requires binding to VEGFR1 to initiate downstream signaling events (Figure 41). As the EC has a greater preponderance of VEGFR1, we propose that this cell responds to hyperglycemia by secreting heparanase, which initiates release of VEGFB from subjacent cardiomyocytes, as a means to protect itself against impending HG-induced cellular demise.

Of particular interest in this study was the signaling pathway involving the interaction between ERK, GSK3β, and cell death. Phosphorylation and activation of ERK allows for inactivation of GSK3β (156), which can lead to decreased cell apoptosis (157, 158). Additionally, an increase in Bcl2, an important anti-apoptotic protein, is also observed following activation of this signaling pathway (159). Interestingly, in models of heart failure such as dilated cardiomyopathy, overexpression of VEGFB was able to delay progression of heart failure (85, 160), in part through inactivating GSK3β (85). Furthermore, VEGFB treatment of multiple cell lines downregulated expression of a number of apoptotic gene such as Bax (88). Therefore, we investigated whether

there was a role for VEGFB in cell death signaling through ERK, and cell death gene expression via Bax and Bcl2. Indeed, treatment of RHMEC with VEGFB resulted in ERK activation and subsequent GSK3β phosphorylation at its inactivation residue serine 9. Furthermore, pre-treatment of EC with VEGFB reduced cleaved PARP expression, a marker of cell apoptosis, when H_2O_2 was used to induce cell death. Overnight treatment of VEGFB caused a reduction in the Bax/Bcl2 mRNA ratio, further substantiating the influence of VEGFB to act in a paracrine manner and impact EC survival. While cardiomyocytes express less VEGFR1 compared to EC, there is still the potential for VEGFB to act in an autocrine manner and regulate myocyte cell survival. In this regard, similar results were seen in cardiomyocytes given VEGFB, which activated ERK, limiting PARP cleavage and decreasing the Bax/Bcl2 mRNA ratio. Collectively, our data advocate for VEGFB having a cardio-protective role, acting in paracrine and autocrine fashion to promote cellular survival of EC and cardiomyocytes, respectively (Figure 42).

Cardiovascular dysfunction, leading to heart failure, is a hallmark of diabetes. This cardiac dysfunction can be seen in the presence (atherosclerosis) or absence (diabetic cardiomyopathy) of vascular defects (161, 162). Thus, in animals made diabetic with 55 mg/kg STZ, a model of moderate diabetes that resembles poorly controlled T1D, evidence of cardiomyopathy is observed after 6 weeks of hyperglycemia (163). Of the numerous etiological factors involved in the development of diabetic cardiomyopathy, multiple cell death pathways have also been implicated in its pathogenesis (164, 165). Animals with chronic diabetes gained less weight and also displayed robust hyperglycemia. As with our acute D100 model, chronically diabetic animals had a significant drop in VEGFB protein and gene expression. In contrast, both diabetic models had a substantial increase in VEGFR1 protein as a potential compensatory mechanism. Upregulation of VEGFR1 is a phenomenon also observed in cardiomyocytes under conditions of hypoxia,

potentially seeking to maintain VEGFB action for cell survival (89). Intriguingly, the increase in VEGFR1 in this study did not translate into improved VEGFB action. In cardiomyocytes from animals with chronic diabetes, both ERK activation and GSK3β phosphorylation were reduced under basal conditions and in response to VEGFB treatment. These effects, coupled to the drop in Hep-L, an instigator in VEGFB release, resulted in an increase in the cell death signature. Our data suggest that the loss of VEGFB and its downstream signaling events are an early event following hyperglycemia, is sustained with disease progression, and could help explain diabetic cardiomyopathy. More insight into the biology of VEGFB may provide a critical tool to help prevent or delay cardiomyopathy.

4.3 Cardiomyocyte-specific overexpression of VEGFB is linked to an expanded coronary vasculature that amplifies the cardiovascular action of insulin

In VEGFB TG rats, despite VEGFB not being considered a traditional angiogenic growth factor, the most striking change in the transcriptome was identified in genes related to angiogenesis. Correspondingly, proteins for a number of the highest expressed angiogenic genes were upregulated and visualization of TG heart cross sections displayed enlarged blood vessels. These changes build upon the characterization of TG VEGFB animals seen previously (74), which also showed AAV induction of VEGFB into rats was able to replicate this phenotype. This phenomenon could be a result of VEGFB being able to enhance VEGFA mediated angiogenesis. VEGFA can bind to both VEGFR1 and VEGFR2, but only by binding VEGFR2 does VEGFA activate downstream signals that promote EC migration and angiogenesis. Conversely, VEGFB can only bind to VEGFR1 to mediate its functions. Overexpression of VEGFB would likely lead to less VEGFR1 sites available to bind VEGFA allowing more VEGFA (at a physiological level) to activate signals via VEGFR2 (81). In addition to this sensitizing effect, coronary vasculature in

VEGFB overexpressing hearts displayed increased blood vessel diameter (74), an effect likely related to endothelial cell survival.

Plasma glucose and insulin levels between WT and VEGFB TG rats were similar, suggesting that whole body insulin sensitivity was unaffected. Interestingly, key markers of insulin action (p-AKT (S473) and p-PI3K 85α (Tyr 508) were enhanced in TG hearts. Furthermore, analysis of the RNA Seq dataset revealed that a number of genes that play a role in the response to insulin and glucose utilization were also increased, establishing that the TG hearts were more sensitive to insulin. Further validation to this came from the observation of an augmented response to exogenous injection of insulin in the TG heart only with increased p-AKT (S473), an effect not seen in SKM or other tissues. The heart can utilize a variety of substrates for ATP generation, glucose accounts for nearly 30% of its ATP production with FA oxidation contributing most of the remaining 70% (1). Regulated hydrolysis of lipoproteins at the vascular lumen via LPL is considered the preferred source of FA for the heart (4). Measurement of LPL activity at the vascular lumen via heparin release indicated that the TG hearts had lower LPL activity and this difference was not a consequence of changes in LPL gene expression. Post translational modification of LPL by increased Angptl4, which has been shown to inhibit LPL activity (38), as well as play a role in angiogenesis (166), could be a possible outcome. These data indicate that the expanded coronary vasculature in the TG heart, enables increased insulin delivery and enhanced insulin regulated glucose use, thereby reducing the need for FA ATP generation.

In order for FA in the lumen to be delivered to cardiomyocytes, they must first be transported across EC with the aid of FA binding proteins such as Fabp4/5 (167). As the FA transit through the EC, they can be utilized by EC, not for ATP production, but for de novo nucleotide synthesis (168). This study indicates that following CPT1 transport of FA into the mitochondria for β-

oxidation, the resulting carbons are incorporated into amino acids and precursors of dNTPs that are used for EC proliferation. As genes linked to Fabp's and purine biosynthesis had increased expression in the TG heart, we present the exciting idea that EC are using the FA generated at the coronary lumen, although now reduced, to support increased vascular growth. The overall effect would lower the amount of FA transported to the adjacent cardiomyocyte. This is reinforced by the finding that expression of genes involved in FA uptake into myocytes and lipid droplet formation were decreased. Additionally, the amounts of DAG/LysoPC lipid metabolites in the TG heart were reduced. With DAG and LysoPC shown to play a role in insulin resistance (117, 169), our data implies that along with the improved coronary vasculature which can improve insulin delivery to TG hearts, the additional decrease in lipid metabolites likely enhances insulin sensitivity in these hearts.

With reduced glucose consumption the diabetic heart switches to using mostly FA for ATP generation; the surplus of FA will eventually lead to lipotoxicity and cell death (34). This is due to increased FA oxidation which leads to increases in ROS that has been linked to cell demise. Furthermore, there can be an imbalance in the diabetic heart between increased FA delivery and oxidation, resulting in a buildup of toxic lipid metabolites, such as ceramides and DAGs, leading to cell death (3). Using STZ, we observed a comparable diabetic phenotype between WT and TG animals when analyzing blood glucose and plasma insulin levels. Looking beyond these typical markers of diabetes uncovered the significant value of VEGFB overexpression in the heart. TG diabetic hearts exhibited lower levels of lipid metabolites DAG and LysoPCs, suggesting increased insulin sensitivity. Furthermore, the increased angiogenic gene signature in TG-STZ-C hearts indicates enhanced coronary vasculature to aid in insulin delivery. Despite no difference in plasma insulin, measurement of basal p-AKT (S473), a marker of insulin signaling, was correspondingly

enhanced in the TG-STZ-C heart compared to WT-STZ-C. The increase in insulin action would allow the TG diabetic heart to decrease its reliance on FA for ATP generation, which likely results in the decrease seen in FA oxidation genes. In conclusion, we believe that cardiomyocyte-VEGFB overexpression is able to produce coordinated angiogenesis (74), unlike what's seen with VEGFR1 knockout (53) or VEGFA overexpression (46). Under those conditions, VEGFA binds primarily to VEGFR2 promoting uncontrolled angiogenesis. Augmented coronary angiogenesis can improve insulin delivery as well as provide the heart the necessary O_2 to metabolize FA. Metabolically, VEGFB overexpression encompass increasing glucose utilization and decreasing the expression of genes involved in FA metabolism. Lastly, by promoting cell survival (88), VEGFB would also be able to limit cardiac cell death and help delay heart failure.

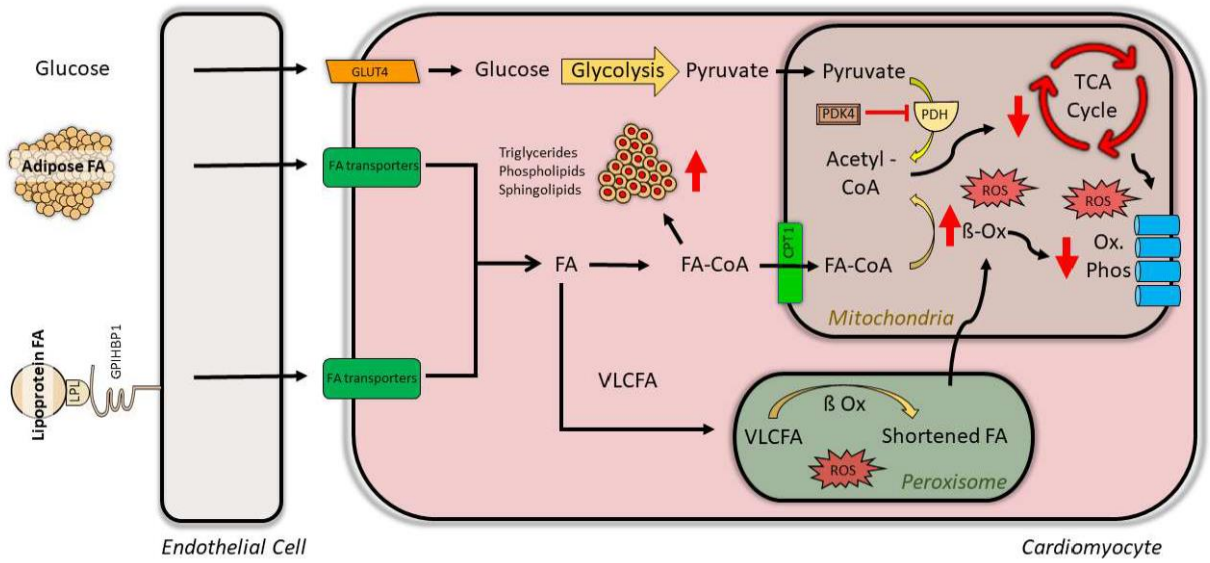

Figure 40. Changes in cardiac metabolism following diabetes of different severities. The summary diagram illustrates that following moderate hypoinsulinemia and hyperglycemia, when plasma fatty acids (FA) have yet to increase, Lipoprotein lipase (LPL) is "switched on", and a robust expansion of coronary LPL follows. In animals with marked hypoinsulinemia and severe diabetes, there is a decline in vascular LPL. As these animals exhibit elevated plasma FA, we concluded that LPL-mediated FA delivery would be redundant in these circumstances and is "turned off". This is a questionable adaptation as the site of control of FA provision to the heart changes from a measured regulated delivery by coronary LPL to the unrestrained and unregulated provision by adipose tissue. Due to this metabolic reprogramming, FA supply exceeds the mitochondrial capacity of cardiomyocytes resulting in incomplete mitochondrial oxidation, accumulation of toxic FA metabolites, flux of excess unoxidized FA to DAGS and triglycerides inducing a gene expression program supporting cell death (lipotoxicity).

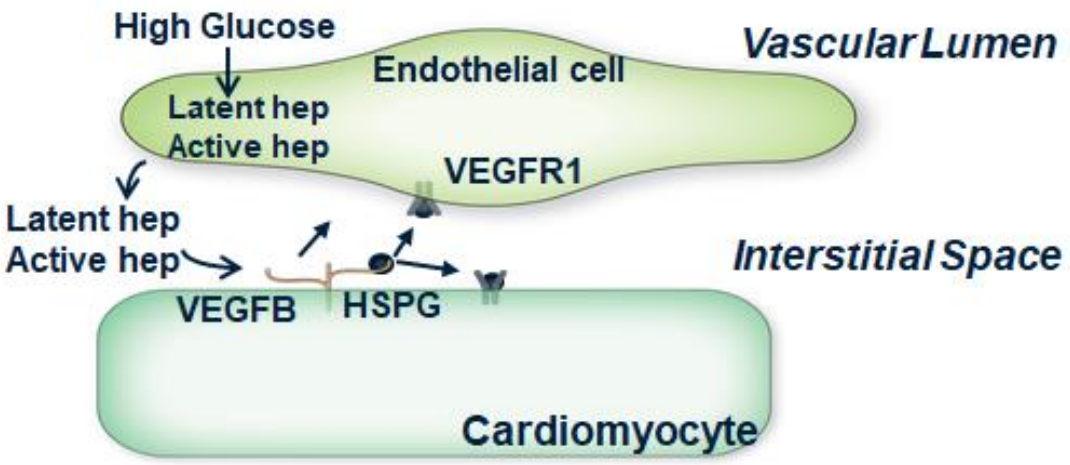

Figure 41. VEGFB is readily releasable. In the presence of high glucose, the EC responds with increased secretion of both Hep-L and Hep-A into the medium. Hep-A through its enzymatic activity, and Hep-L by ionic displacement, releases cardiomyocyte HSPG cell surface bound VEGFB. By binding to VEGFR1 on the endothelial cell (paracrine) or cardiomyocyte (autocrine), VEGFB initiates its action.

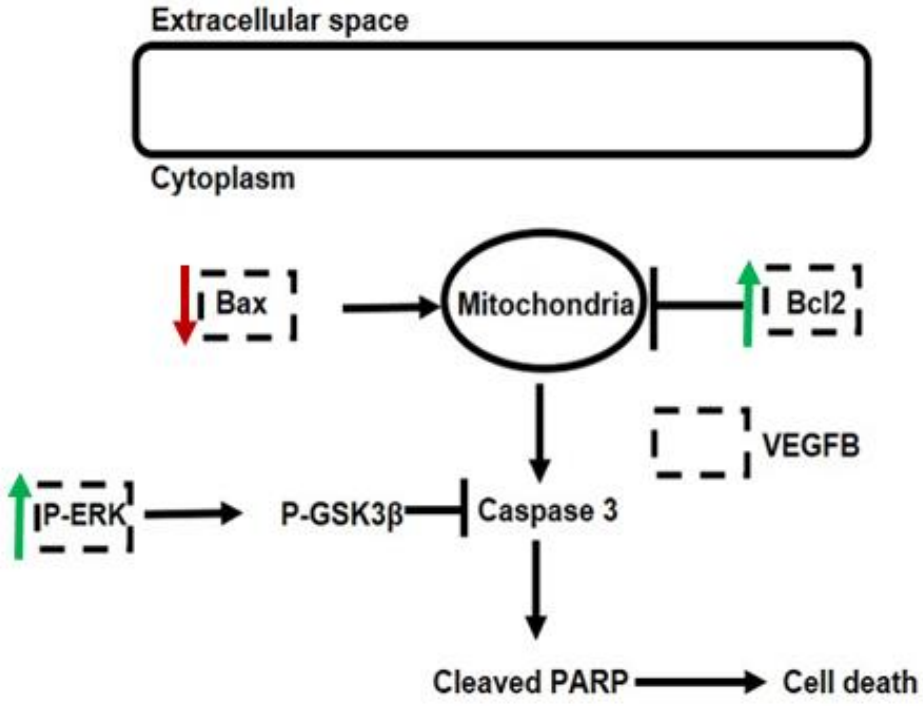

Figure 42. VEGFB action in inhibiting cell death signals. In response to a stressor, like hyperglycemia or H_2O_2, VEGFB, through its signaling effects on activating P-ERK or influencing the Bax/Bcl2 ratio, can protect against cell death. The dotted boxes represent the influence of VEGFB on these molecules.

CHAPTER 5: CONCLUSION AND FUTURE DIRECTIONS

5.1 Conclusion

Following our models of moderate hypoinsulinemia (~50% reduction in plasma insulin) and hyperglycemia (blood glucose >13 mM), when plasma FA have yet to increase, LPL is "switched on", and a robust expansion of coronary LPL follows. In animals with marked hypoinsulinemia and severe diabetes, there is a decline in vascular LPL. As these animals exhibit elevated plasma FA, LPL-mediated FA delivery would be redundant and is "turned off". This is a questionable adaptation as the site of control of FA provision to the heart changes from a measured regulated delivery by coronary LPL to the unrestrained and unregulated provision by adipose tissue. Due to this metabolic reprogramming, FA supply exceeds the mitochondrial capacity of cardiomyocytes resulting in incomplete mitochondrial oxidation, accumulation of toxic FA metabolites, flux of excess unoxidized FA to triglycerides inducing a gene expression program supporting cell death (lipotoxicity). To protect against this cell demise, intrinsic mechanisms must be available to the heart and VEGFB may be one growth factor that plays an important role in protecting against heart failure. Regrettably VEGFB and its downstream signaling are compromised following diabetes. Mechanistically, myocyte bound VEGFB can be released by heparanase, which is secreted from EC in response to high glucose. Through a bi-directional interaction between ECs and cardiomyocytes, this growth factor could provide the diabetic heart protection against cell death. VEGFB has also been shown to decrease gene expression of proteins involved in FAO and increase angiogenesis by potentiating VEGFA signals. This study suggests that insufficient VEGFB production and signaling within the cardiomyocyte, coupled with a loss of the machinery responsible for liberating VEGFB from the myocyte cell surface, could contribute toward the cardiomyopathy seen following diabetes. Cardiomyocyte-specific VEGFB overexpression

induced an angiogenic response that resulted in greater delivery of insulin, amplifying its action in the TG heart. Other mechanisms enabling enhanced insulin sensitivity included less delivery of lipoprotein lipase-derived FA, reduced accumulation of diacylglycerols and LysoPC and lower FA metabolism. These augmented effects of insulin action were conserved following diabetes. In this context, the benefit of VEGFB as a cardio protective therapy against diabetic cardiomyopathy could be a fascinating and thus far unacknowledged approach.

5.2 Future directions

To further investigate if the metabolic changes during diabetes are secondary to changes in VEGFB, the following studies are of potential interest:

1. It should be noted that this study used animals with acute diabetes (4-days). As such, the increase in cardiac LPL in D55 was unable to induce gene expression changes, oxidative stress, triglyceride accumulation and cell death to the same magnitude as D100 hearts exposed to a robust enlargement in circulating plasma FA. This does not imply that augmentation of cardiac LPL, especially chronically, is without health risks (39). As VEGFB production and action is also reduced after chronic diabetes, identifying the metabolic gene signature in chronic D55 animals is important and should be investigated.
2. In this thesis we observed that VEGFB protein and gene expression dropped significantly, while VEGFR1 protein increased substantially as a potential compensatory mechanism. Augmented expression of VEGFR1 has been observed in cardiomyocytes under conditions of hypoxia, possibly seeking to sustain VEGFB action for cell survival (170). Unfortunately, with diabetes, the increase in VEGFR1 in this study did not translate into improved VEGFB action. Understanding the role that hyperglycemia plays in altering

VEGFR1 signaling would be critical to maximize the potential benefit to utilizing VEGFB as an intervention following diabetes.

3. In this thesis, cardiac specific VEGFB overexpression enabled an increase in coronary vasculature which led to increased insulin delivery and a corresponding increase in glucose utilization genes with decreased FA utilization and lipid metabolites. These changes were preserved subsequent to chronic diabetes. Whether the preserved actions of insulin in TG rats helps protect against diabetic heart failure was not determined. Intriguingly, echocardiography of TG animals following experimental MI revealed less severe decrease in ejection fraction, fractional shortening and an increase in left ventricular systolic and diastolic diameters when measured at both 1 and 4 weeks post MI (74). Utilizing our model of chronic diabetes and analyzing heart function using echocardiography would substantiate VEGFB as a cardio protective treatment against diabetic heart disease.

REFERENCES

1. Lopaschuk GD, Ussher JR, Folmes CD, Jaswal JS, Stanley WC. Myocardial fatty acid metabolism in health and disease. Physiological reviews. 2010;90(1):207-58.

2. An D, Rodrigues B. Role of changes in cardiac metabolism in development of diabetic cardiomyopathy. American journal of physiology Heart and circulatory physiology. 2006;291(4):H1489-506.

3. Kim MS, Wang Y, Rodrigues B. Lipoprotein lipase mediated fatty acid delivery and its impact in diabetic cardiomyopathy. Biochimica et biophysica acta. 2012;1821(5):800-8.

4. Voshol PJ, Rensen PC, van Dijk KW, Romijn JA, Havekes LM. Effect of plasma triglyceride metabolism on lipid storage in adipose tissue: studies using genetically engineered mouse models. Biochimica et biophysica acta. 2009;1791(6):479-85.

5. Doolittle MH, Ben-Zeev O, Elovson J, Martin D, Kirchgessner TG. The response of lipoprotein lipase to feeding and fasting. Evidence for posttranslational regulation. The Journal of biological chemistry. 1990;265(8):4570-7.

6. Eckel RH. Lipoprotein lipase. A multifunctional enzyme relevant to common metabolic diseases. The New England journal of medicine. 1989;320(16):1060-8.

7. Kim MS, Wang F, Puthanveetil P, Kewalramani G, Hosseini-Beheshti E, Ng N, et al. Protein kinase D is a key regulator of cardiomyocyte lipoprotein lipase secretion after diabetes. Circulation research. 2008;103(3):252-60.

8. Kim MS, Kewalramani G, Puthanveetil P, Lee V, Kumar U, An D, et al. Acute diabetes moderates trafficking of cardiac lipoprotein lipase through p38 mitogen-activated protein kinase-dependent actin cytoskeleton organization. Diabetes. 2008;57(1):64-76.

9. Iozzo RV, San Antonio JD. Heparan sulfate proteoglycans: heavy hitters in the angiogenesis arena. The Journal of clinical investigation. 2001;108(3):349-55.

10. Iozzo RV. Heparan sulfate proteoglycans: intricate molecules with intriguing functions. The Journal of clinical investigation. 2001;108(2):165-7.

11. Fairbanks MB, Mildner AM, Leone JW, Cavey GS, Mathews WR, Drong RF, et al. Processing of the human heparanase precursor and evidence that the active enzyme is a heterodimer. The Journal of biological chemistry. 1999;274(42):29587-90.

12. Gingis-Velitski S, Zetser A, Kaplan V, Ben-Zaken O, Cohen E, Levy-Adam F, et al. Heparanase uptake is mediated by cell membrane heparan sulfate proteoglycans. The Journal of biological chemistry. 2004;279(42):44084-92.

13. Sambandam N, Abrahani MA, St Pierre E, Al-Atar O, Cam MC, Rodrigues B. Localization of lipoprotein lipase in the diabetic heart: regulation by acute changes in insulin. Arteriosclerosis, thrombosis, and vascular biology. 1999;19(6):1526-34.

14. Otarod JK, Goldberg IJ. Lipoprotein lipase and its role in regulation of plasma lipoproteins and cardiac risk. Current atherosclerosis reports. 2004;6(5):335-42.

15. Zcharia E, Metzger S, Chajek-Shaul T, Aingorn H, Elkin M, Friedmann Y, et al. Transgenic expression of mammalian heparanase uncovers physiological functions of heparan sulfate in tissue morphogenesis, vascularization, and feeding behavior. FASEB journal : official publication of the Federation of American Societies for Experimental Biology. 2004;18(2):252-63.

16. Wang Y, Zhang D, Chiu AP, Wan A, Neumaier K, Vlodavsky I, et al. Endothelial heparanase regulates heart metabolism by stimulating lipoprotein lipase secretion from cardiomyocytes. Arteriosclerosis, thrombosis, and vascular biology. 2013;33(5):894-902.

17. Zhang D, Wan A, Chiu AP, Wang Y, Wang F, Neumaier K, et al. Hyperglycemia-induced secretion of endothelial heparanase stimulates a vascular endothelial growth factor autocrine network in cardiomyocytes that promotes recruitment of lipoprotein lipase. Arteriosclerosis, thrombosis, and vascular biology. 2013;33(12):2830-8.

18. Rodrigues B, Cam MC, McNeill JH. Myocardial substrate metabolism: implications for diabetic cardiomyopathy. Journal of molecular and cellular cardiology. 1995;27(1):169-79.

19. Bugger H, Abel ED. Rodent models of diabetic cardiomyopathy. Disease models & mechanisms. 2009;2(9-10):454-66.

20. Fang ZY, Prins JB, Marwick TH. Diabetic cardiomyopathy: evidence, mechanisms, and therapeutic implications. Endocrine reviews. 2004;25(4):543-67.

21. Pulinilkunnil T, Rodrigues B. Cardiac lipoprotein lipase: metabolic basis for diabetic heart disease. Cardiovascular research. 2006;69(2):329-40.

22. Kraegen EW, Sowden JA, Halstead MB, Clark PW, Rodnick KJ, Chisholm DJ, et al. Glucose transporters and in vivo glucose uptake in skeletal and cardiac muscle: fasting, insulin stimulation and immunoisolation studies of GLUT1 and GLUT4. The Biochemical journal. 1993;295 (Pt 1):287-93.

23. Pessin JE, Bell GI. Mammalian facilitative glucose transporter family: structure and molecular regulation. Annual review of physiology. 1992;54:911-30.

24. Li J, Hu X, Selvakumar P, Russell RR, 3rd, Cushman SW, Holman GD, et al. Role of the nitric oxide pathway in AMPK-mediated glucose uptake and GLUT4 translocation in heart muscle. American journal of physiology Endocrinology and metabolism. 2004;287(5):E834-41.

25. Yang J, Holman GD. Insulin and contraction stimulate exocytosis, but increased AMP-activated protein kinase activity resulting from oxidative metabolism stress slows endocytosis of GLUT4 in cardiomyocytes. The Journal of biological chemistry. 2005;280(6):4070-8.

26. Rask-Madsen C, Kahn CR. Tissue-specific insulin signaling, metabolic syndrome, and cardiovascular disease. Arteriosclerosis, thrombosis, and vascular biology. 2012;32(9):2052-9.

27. Boucher J, Kleinridders A, Kahn CR. Insulin receptor signaling in normal and insulin-resistant states. Cold Spring Harbor perspectives in biology. 2014;6(1).

28. Cong LN, Chen H, Li Y, Zhou L, McGibbon MA, Taylor SI, et al. Physiological role of Akt in insulin-stimulated translocation of GLUT4 in transfected rat adipose cells. Molecular endocrinology. 1997;11(13):1881-90.

29. Olokoba AB, Obateru OA, Olokoba LB. Type 2 diabetes mellitus: a review of current trends. Oman medical journal. 2012;27(4):269-73.

30. Saddik M, Lopaschuk GD. Myocardial triglyceride turnover and contribution to energy substrate utilization in isolated working rat hearts. The Journal of biological chemistry. 1991;266(13):8162-70.

31. Paulson DJ, Crass MF, 3rd. Endogenous triacylglycerol metabolism in diabetic heart. The American journal of physiology. 1982;242(6):H1084-94.

32. Blanchette-Mackie EJ, Masuno H, Dwyer NK, Olivecrona T, Scow RO. Lipoprotein lipase in myocytes and capillary endothelium of heart: immunocytochemical study. The American journal of physiology. 1989;256(6 Pt 1):E818-28.

33. Finck BN, Lehman JJ, Leone TC, Welch MJ, Bennett MJ, Kovacs A, et al. The cardiac phenotype induced by PPARalpha overexpression mimics that caused by diabetes mellitus. The Journal of clinical investigation. 2002;109(1):121-30.

34. Wende AR, Abel ED. Lipotoxicity in the heart. Biochimica et biophysica acta. 2010;1801(3):311-9.

35. Bertoni AG, Tsai A, Kasper EK, Brancati FL. Diabetes and idiopathic cardiomyopathy: a nationwide case-control study. Diabetes care. 2003;26(10):2791-5.

36. Williams SP, Johnson EA. Release of lipoprotein lipase and hepatic triglyceride lipase in rats by heparin and other sulphated polysaccharides. Thrombosis research. 1989;55(3):361-8.

37. Chiu AP, Bierende D, Lal N, Wang F, Wan A, Vlodavsky I, et al. Dual effects of hyperglycemia on endothelial cells and cardiomyocytes to enhance coronary LPL activity. American journal of physiology Heart and circulatory physiology. 2018;314(1):H82-H94.

38. Wang Y, Puthanveetil P, Wang F, Kim MS, Abrahani A, Rodrigues B. Severity of Diabetes Governs Vascular Lipoprotein Lipase by Affecting Enzyme Dimerization and Disassembly. Diabetes. 2011;60(8):2041-50.

39. Rodrigues B, Cam MC, Jian K, Lim F, Sambandam N, Shepherd G. Differential effects of streptozotocin-induced diabetes on cardiac lipoprotein lipase activity. Diabetes. 1997;46(8):1346-53.

40. Niu YG, Evans RD. Metabolism of very-low-density lipoprotein and chylomicrons by streptozotocin-induced diabetic rat heart: effects of diabetes and lipoprotein preference. American journal of physiology Endocrinology and metabolism. 2008;295(5):E1106-16.

41. Holmes DI, Zachary I. The vascular endothelial growth factor (VEGF) family: angiogenic factors in health and disease. Genome biology. 2005;6(2):209.

42. Djordjevic S, Driscoll PC. Targeting VEGF signalling via the neuropilin co-receptor. Drug discovery today. 2013;18(9-10):447-55.

43. Ferrara N. Vascular endothelial growth factor. Arteriosclerosis, thrombosis, and vascular biology. 2009;29(6):789-91.

44. Robinson CJ, Stringer SE. The splice variants of vascular endothelial growth factor (VEGF) and their receptors. Journal of cell science. 2001;114(Pt 5):853-65.

45. Shibuya M. Vascular Endothelial Growth Factor (VEGF) and Its Receptor (VEGFR) Signaling in Angiogenesis: A Crucial Target for Anti- and Pro-Angiogenic Therapies. Genes & cancer. 2011;2(12):1097-105.

46. Hiratsuka S, Kataoka Y, Nakao K, Nakamura K, Morikawa S, Tanaka S, et al. Vascular endothelial growth factor A (VEGF-A) is involved in guidance of VEGF receptor-positive cells to the anterior portion of early embryos. Molecular and cellular biology. 2005;25(1):355-63.

47. Fukumura D, Gohongi T, Kadambi A, Izumi Y, Ang J, Yun CO, et al. Predominant role of endothelial nitric oxide synthase in vascular endothelial growth factor-induced angiogenesis and vascular permeability. Proceedings of the National Academy of Sciences of the United States of America. 2001;98(5):2604-9.

48. Gerber HP, McMurtrey A, Kowalski J, Yan M, Keyt BA, Dixit V, et al. Vascular endothelial growth factor regulates endothelial cell survival through the phosphatidylinositol 3'-kinase/Akt signal transduction pathway. Requirement for Flk-1/KDR activation. The Journal of biological chemistry. 1998;273(46):30336-43.

49. Waltenberger J, Lange J, Kranz A. Vascular endothelial growth factor-A-induced chemotaxis of monocytes is attenuated in patients with diabetes mellitus: A potential predictor for the individual capacity to develop collaterals. Circulation. 2000;102(2):185-90.

50. Dragoni S, Laforenza U, Bonetti E, Lodola F, Bottino C, Berra-Romani R, et al. Vascular endothelial growth factor stimulates endothelial colony forming cells proliferation and tubulogenesis by inducing oscillations in intracellular Ca2+ concentration. Stem cells. 2011;29(11):1898-907.

51. Shibuya M. Structure and dual function of vascular endothelial growth factor receptor-1 (Flt-1). The international journal of biochemistry & cell biology. 2001;33(4):409-20.

52. Boucher JM, Clark RP, Chong DC, Citrin KM, Wylie LA, Bautch VL. Dynamic alterations in decoy VEGF receptor-1 stability regulate angiogenesis. Nature communications. 2017;8:15699.

53. Ho VC, Fong GH. Vasculogenesis and Angiogenesis in VEGF Receptor-1 Deficient Mice. Methods in molecular biology. 2015;1332:161-76.

54. Benest AV, Harper SJ, Herttuala SY, Alitalo K, Bates DO. VEGF-C induced angiogenesis preferentially occurs at a distance from lymphangiogenesis. Cardiovascular research. 2008;78(2):315-23.

55. Bui HM, Enis D, Robciuc MR, Nurmi HJ, Cohen J, Chen M, et al. Proteolytic activation defines distinct lymphangiogenic mechanisms for VEGFC and VEGFD. The Journal of clinical investigation. 2016;126(6):2167-80.

56. Duong T, Koltowska K, Pichol-Thievend C, Le Guen L, Fontaine F, Smith KA, et al. VEGFD regulates blood vascular development by modulating SOX18 activity. Blood. 2014;123(7):1102-12.

57. Karkkainen MJ, Haiko P, Sainio K, Partanen J, Taipale J, Petrova TV, et al. Vascular endothelial growth factor C is required for sprouting of the first lymphatic vessels from embryonic veins. Nature immunology. 2004;5(1):74-80.

58. Lohela M, Helotera H, Haiko P, Dumont DJ, Alitalo K. Transgenic induction of vascular endothelial growth factor-C is strongly angiogenic in mouse embryos but leads to persistent lymphatic hyperplasia in adult tissues. The American journal of pathology. 2008;173(6):1891-901.

59. Ogawa S, Oku A, Sawano A, Yamaguchi S, Yazaki Y, Shibuya M. A novel type of vascular endothelial growth factor, VEGF-E (NZ-7 VEGF), preferentially utilizes KDR/Flk-1 receptor and carries a potent mitotic activity without heparin-binding domain. The Journal of biological chemistry. 1998;273(47):31273-82.

60. De Falco S. The discovery of placenta growth factor and its biological activity. Experimental & molecular medicine. 2012;44(1):1-9.

61. Carmeliet P, Moons L, Luttun A, Vincenti V, Compernolle V, De Mol M, et al. Synergism between vascular endothelial growth factor and placental growth factor contributes to angiogenesis and plasma extravasation in pathological conditions. Nature medicine. 2001;7(5):575-83.

62. Li X, Aase K, Li H, von Euler G, Eriksson U. Isoform-specific expression of VEGF-B in normal tissues and tumors. Growth factors. 2001;19(1):49-59.

63. Li X. VEGF-B: a thing of beauty. Cell research. 2010;20(7):741-4.

64. Olofsson B, Pajusola K, Kaipainen A, von Euler G, Joukov V, Saksela O, et al. Vascular endothelial growth factor B, a novel growth factor for endothelial cells. Proceedings of the National Academy of Sciences of the United States of America. 1996;93(6):2576-81.

65. Enholm B, Paavonen K, Ristimaki A, Kumar V, Gunji Y, Klefstrom J, et al. Comparison of VEGF, VEGF-B, VEGF-C and Ang-1 mRNA regulation by serum, growth factors, oncoproteins and hypoxia. Oncogene. 1997;14(20):2475-83.

66. Aase K, von Euler G, Li X, Ponten A, Thoren P, Cao R, et al. Vascular endothelial growth factor-B-deficient mice display an atrial conduction defect. Circulation. 2001;104(3):358-64.

67. Karpanen T, Bry M, Ollila HM, Seppanen-Laakso T, Liimatta E, Leskinen H, et al. Overexpression of vascular endothelial growth factor-B in mouse heart alters cardiac lipid metabolism and induces myocardial hypertrophy. Circulation research. 2008;103(9):1018-26.

68. Mould AW, Greco SA, Cahill MM, Tonks ID, Bellomo D, Patterson C, et al. Transgenic overexpression of vascular endothelial growth factor-B isoforms by endothelial cells potentiates postnatal vessel growth in vivo and in vitro. Circulation research. 2005;97(6):e60-70.

69. Zhang F, Tang Z, Hou X, Lennartsson J, Li Y, Koch AW, et al. VEGF-B is dispensable for blood vessel growth but critical for their survival, and VEGF-B targeting inhibits pathological angiogenesis. Proceedings of the National Academy of Sciences of the United States of America. 2009;106(15):6152-7.

70. Bry M, Kivela R, Leppanen VM, Alitalo K. Vascular endothelial growth factor-B in physiology and disease. Physiological reviews. 2014;94(3):779-94.

71. Bhardwaj S, Roy H, Gruchala M, Viita H, Kholova I, Kokina I, et al. Angiogenic responses of vascular endothelial growth factors in periadventitial tissue. Human gene therapy. 2003;14(15):1451-62.

72. Tirziu D, Chorianopoulos E, Moodie KL, Palac RT, Zhuang ZW, Tjwa M, et al. Myocardial hypertrophy in the absence of external stimuli is induced by angiogenesis in mice. The Journal of clinical investigation. 2007;117(11):3188-97.

73. Li X, Tjwa M, Van Hove I, Enholm B, Neven E, Paavonen K, et al. Reevaluation of the role of VEGF-B suggests a restricted role in the revascularization of the ischemic myocardium. Arteriosclerosis, thrombosis, and vascular biology. 2008;28(9):1614-20.

74. Kivela R, Bry M, Robciuc MR, Rasanen M, Taavitsainen M, Silvola JM, et al. VEGF-B-induced vascular growth leads to metabolic reprogramming and ischemia resistance in the heart. EMBO molecular medicine. 2014;6(3):307-21.

75. Koch S, Claesson-Welsh L. Signal transduction by vascular endothelial growth factor receptors. Cold Spring Harbor perspectives in medicine. 2012;2(7):a006502.

76. Fong GH, Rossant J, Gertsenstein M, Breitman ML. Role of the Flt-1 receptor tyrosine kinase in regulating the assembly of vascular endothelium. Nature. 1995;376(6535):66-70.

77. Hiratsuka S, Minowa O, Kuno J, Noda T, Shibuya M. Flt-1 lacking the tyrosine kinase domain is sufficient for normal development and angiogenesis in mice. Proceedings of the National Academy of Sciences of the United States of America. 1998;95(16):9349-54.

78. Muhl L, Moessinger C, Adzemovic MZ, Dijkstra MH, Nilsson I, Zeitelhofer M, et al. Expression of vascular endothelial growth factor (VEGF)-B and its receptor (VEGFR1) in murine heart, lung and kidney. Cell and tissue research. 2016;365(1):51-63.

79. Ribatti D. The discovery of the placental growth factor and its role in angiogenesis: a historical review. Angiogenesis. 2008;11(3):215-21.

80. Olofsson B, Korpelainen E, Pepper MS, Mandriota SJ, Aase K, Kumar V, et al. Vascular endothelial growth factor B (VEGF-B) binds to VEGF receptor-1 and regulates plasminogen activator activity in endothelial cells. Proceedings of the National Academy of Sciences of the United States of America. 1998;95(20):11709-14.

81. Robciuc MR, Kivela R, Williams IM, de Boer JF, van Dijk TH, Elamaa H, et al. VEGFB/VEGFR1-Induced Expansion of Adipose Vasculature Counteracts Obesity and Related Metabolic Complications. Cell metabolism. 2016;23(4):712-24.

82. Sun Y, Jin K, Childs JT, Xie L, Mao XO, Greenberg DA. Increased severity of cerebral ischemic injury in vascular endothelial growth factor-B-deficient mice. Journal of cerebral blood flow and metabolism : official journal of the International Society of Cerebral Blood Flow and Metabolism. 2004;24(10):1146-52.

83. Devaux Y, Vausort M, Azuaje F, Vaillant M, Lair ML, Gayat E, et al. Low levels of vascular endothelial growth factor B predict left ventricular remodeling after acute myocardial infarction. Journal of cardiac failure. 2012;18(4):330-7.

84. Huusko J, Lottonen L, Merentie M, Gurzeler E, Anisimov A, Miyanohara A, et al. AAV9-mediated VEGF-B gene transfer improves systolic function in progressive left ventricular hypertrophy. Molecular therapy : the journal of the American Society of Gene Therapy. 2012;20(12):2212-21.

85. Pepe M, Mamdani M, Zentilin L, Csiszar A, Qanud K, Zacchigna S, et al. Intramyocardial VEGF-B167 gene delivery delays the progression towards congestive failure in dogs with pacing-induced dilated cardiomyopathy. Circulation research. 2010;106(12):1893-903.

86. Rasanen M, Degerman J, Nissinen TA, Miinalainen I, Kerkela R, Siltanen A, et al. VEGF-B gene therapy inhibits doxorubicin-induced cardiotoxicity by endothelial protection. Proceedings of the National Academy of Sciences of the United States of America. 2016;113(46):13144-9.

87. Tacar O, Sriamornsak P, Dass CR. Doxorubicin: an update on anticancer molecular action, toxicity and novel drug delivery systems. The Journal of pharmacy and pharmacology. 2013;65(2):157-70.

88. Li Y, Zhang F, Nagai N, Tang Z, Zhang S, Scotney P, et al. VEGF-B inhibits apoptosis via VEGFR-1-mediated suppression of the expression of BH3-only protein genes in mice and rats. The Journal of clinical investigation. 2008;118(3):913-23.

89. Zentilin L, Puligadda U, Lionetti V, Zacchigna S, Collesi C, Pattarini L, et al. Cardiomyocyte VEGFR-1 activation by VEGF-B induces compensatory hypertrophy and preserves cardiac function after myocardial infarction. FASEB journal : official publication of the Federation of American Societies for Experimental Biology. 2010;24(5):1467-78.

90. Boudina S, Abel ED. Diabetic cardiomyopathy, causes and effects. Reviews in endocrine & metabolic disorders. 2010;11(1):31-9.

91. Kolluru GK, Bir SC, Kevil CG. Endothelial dysfunction and diabetes: effects on angiogenesis, vascular remodeling, and wound healing. International journal of vascular medicine. 2012;2012:918267.

92. Spindler M, Saupe KW, Tian R, Ahmed S, Matlib MA, Ingwall JS. Altered creatine kinase enzyme kinetics in diabetic cardiomyopathy. A(31)P NMR magnetization transfer study of the intact beating rat heart. Journal of molecular and cellular cardiology. 1999;31(12):2175-89.

93. Lal N, Chiu AP, Wang F, Zhang D, Jia J, Wan A, et al. Loss of VEGFB and its signaling in the diabetic heart is associated with increased cell death signaling. American journal of physiology Heart and circulatory physiology. 2017;312(6):H1163-H75.

94. Huang D, Zhao C, Ju R, Kumar A, Tian G, Huang L, et al. VEGF-B inhibits hyperglycemia- and Macugen-induced retinal apoptosis. Scientific reports. 2016;6:26059.

95. Chou E, Suzuma I, Way KJ, Opland D, Clermont AC, Naruse K, et al. Decreased cardiac expression of vascular endothelial growth factor and its receptors in insulin-resistant and diabetic States: a possible explanation for impaired collateral formation in cardiac tissue. Circulation. 2002;105(3):373-9.

96. Kessler G, Friedman J. Metabolism of fatty acids and glucose. Circulation. 1998;98(13):1351.

97. Zetser A, Bashenko Y, Miao HQ, Vlodavsky I, Ilan N. Heparanase affects adhesive and tumorigenic potential of human glioma cells. Cancer research. 2003;63(22):7733-41.

98. Kivela R, Hemanthakumar KA, Vaparanta K, Robciuc M, Izumiya Y, Kidoya H, et al. Endothelial Cells Regulate Physiological Cardiomyocyte Growth via VEGFR2-Mediated Paracrine Signaling. Circulation. 2019;139(22):2570-84.

99. Rodrigues B, Xiang H, McNeill JH. Effect of L-carnitine treatment on lipid metabolism and cardiac performance in chronically diabetic rats. Diabetes. 1988;37(10):1358-64.

100. Vuilleumier R, Lian T, Flibotte S, Khan ZN, Fuchs A, Pyrowolakis G, et al. Retrograde BMP signaling activates neuronal gene expression through widespread deployment of a conserved BMP-responsive cis-regulatory activation element. Nucleic Acids Res. 2018.

101. von Mering C, Huynen M, Jaeggi D, Schmidt S, Bork P, Snel B. STRING: a database of predicted functional associations between proteins. Nucleic Acids Res. 2003;31(1):258-61.

102. Chen EY, Tan CM, Kou Y, Duan Q, Wang Z, Meirelles GV, et al. Enrichr: interactive and collaborative HTML5 gene list enrichment analysis tool. BMC Bioinformatics. 2013;14:128.

103. Ghosh S, An D, Pulinilkunnil T, Qi D, Lau HC, Abrahani A, et al. Role of dietary fatty acids and acute hyperglycemia in modulating cardiac cell death. Nutrition. 2004;20(10):916-23.

104. Readnower RD, Brainard RE, Hill BG, Jones SP. Standardized bioenergetic profiling of adult mouse cardiomyocytes. Physiol Genomics. 2012;44(24):1208-13.

105. Mdaki KS, Larsen TD, Weaver LJ, Baack ML. Age Related Bioenergetics Profiles in Isolated Rat Cardiomyocytes Using Extracellular Flux Analyses. PloS one. 2016;11(2):e0149002.

106. Wang F, Kim MS, Puthanveetil P, Kewalramani G, Deppe S, Ghosh S, et al. Endothelial heparanase secretion after acute hypoinsulinemia is regulated by glucose and fatty acid. American journal of physiology Heart and circulatory physiology. 2009;296(4):H1108-16.

107. Pulinilkunnil T, An D, Ghosh S, Qi D, Kewalramani G, Yuen G, et al. Lysophosphatidic acid-mediated augmentation of cardiomyocyte lipoprotein lipase involves actin cytoskeleton reorganization. American journal of physiology Heart and circulatory physiology. 2005;288(6):H2802-10.

108. Schweiger M, Schreiber R, Haemmerle G, Lass A, Fledelius C, Jacobsen P, et al. Adipose triglyceride lipase and hormone-sensitive lipase are the major enzymes in adipose tissue triacylglycerol catabolism. The Journal of biological chemistry. 2006;281(52):40236-41.

109. Cuebas D, Schulz H. Evidence for a modified pathway of linoleate degradation. Metabolism of 2,4-decadienoyl coenzyme A. The Journal of biological chemistry. 1982;257(23):14140-4.

110. Xin M, Olson EN, Bassel-Duby R. Mending broken hearts: cardiac development as a basis for adult heart regeneration and repair. Nature reviews Molecular cell biology. 2013;14(8):529-41.

111. Abboud-Jarrous G, Rangini-Guetta Z, Aingorn H, Atzmon R, Elgavish S, Peretz T, et al. Site-directed mutagenesis, proteolytic cleavage, and activation of human proheparanase. The Journal of biological chemistry. 2005;280(14):13568-75.

112. Tirziu D, Giordano FJ, Simons M. Cell communications in the heart. Circulation. 2010;122(9):928-37.

113. Doble BW, Woodgett JR. GSK-3: tricks of the trade for a multi-tasking kinase. Journal of cell science. 2003;116(Pt 7):1175-86.

114. Vene R, Cardinali B, Arena G, Ferrari N, Benelli R, Minghelli S, et al. Glycogen synthase kinase 3 regulates cell death and survival signaling in tumor cells under redox stress. Neoplasia. 2014;16(9):710-22.

115. Perlman H, Zhang X, Chen MW, Walsh K, Buttyan R. An elevated bax/bcl-2 ratio corresponds with the onset of prostate epithelial cell apoptosis. Cell death and differentiation. 1999;6(1):48-54.

116. Timmers S, Schrauwen P, de Vogel J. Muscular diacylglycerol metabolism and insulin resistance. Physiology & behavior. 2008;94(2):242-51.

117. Han MS, Lim YM, Quan W, Kim JR, Chung KW, Kang M, et al. Lysophosphatidylcholine as an effector of fatty acid-induced insulin resistance. Journal of lipid research. 2011;52(6):1234-46.

118. Forbes JM, Cooper ME. Mechanisms of diabetic complications. Physiological reviews. 2013;93(1):137-88.

119. Jia G, Hill MA, Sowers JR. Diabetic Cardiomyopathy: An Update of Mechanisms Contributing to This Clinical Entity. Circulation research. 2018;122(4):624-38.

120. Bry M, Kivela R, Holopainen T, Anisimov A, Tammela T, Soronen J, et al. Vascular endothelial growth factor-B acts as a coronary growth factor in transgenic rats without inducing angiogenesis, vascular leak, or inflammation. Circulation. 2010;122(17):1725-33.

121. Adameova A, Dhalla NS. Role of microangiopathy in diabetic cardiomyopathy. Heart failure reviews. 2014;19(1):25-33.

122. Wan A, Rodrigues B. Endothelial cell-cardiomyocyte crosstalk in diabetic cardiomyopathy. Cardiovascular research. 2016;111(3):172-83.

123. Armstrong C. ADA Updates Standards of Medical Care for Patients with Diabetes Mellitus. Am Fam Physician. 2017;95(1):40-3.

124. Duncan RE, Ahmadian M, Jaworski K, Sarkadi-Nagy E, Sul HS. Regulation of lipolysis in adipocytes. Annu Rev Nutr. 2007;27:79-101.

125. Stanley WC, Lopaschuk GD, McCormack JG. Regulation of energy substrate metabolism in the diabetic heart. Cardiovascular research. 1997;34(1):25-33.

126. Brownsey RW, Boone AN, Allard MF. Actions of insulin on the mammalian heart: metabolism, pathology and biochemical mechanisms. Cardiovascular research. 1997;34(1):3-24.

127. Garcia-Roves P, Huss JM, Han DH, Hancock CR, Iglesias-Gutierrez E, Chen M, et al. Raising plasma fatty acid concentration induces increased biogenesis of mitochondria in skeletal muscle. Proceedings of the National Academy of Sciences of the United States of America. 2007;104(25):10709-13.

128. Wanders RJ, Waterham HR, Ferdinandusse S. Metabolic Interplay between Peroxisomes and Other Subcellular Organelles Including Mitochondria and the Endoplasmic Reticulum. Front Cell Dev Biol. 2015;3:83.

129. Cortassa S, Sollott SJ, Aon MA. Mitochondrial respiration and ROS emission during beta-oxidation in the heart: An experimental-computational study. PLoS Comput Biol. 2017;13(6):e1005588.

130. Schrader M, Fahimi HD. Peroxisomes and oxidative stress. Biochimica et biophysica acta. 2006;1763(12):1755-66.

131. Li W, Yao M, Wang R, Shi Y, Hou L, Hou Z, et al. Profile of cardiac lipid metabolism in STZ-induced diabetic mice. Lipids Health Dis. 2018;17(1):231.

132. Holub BJ. Docosahexaenoic acid (DHA) and cardiovascular disease risk factors. Prostaglandins Leukot Essent Fatty Acids. 2009;81(2-3):199-204.

133. Ramsden CE, Ringel A, Feldstein AE, Taha AY, MacIntosh BA, Hibbeln JR, et al. Lowering dietary linoleic acid reduces bioactive oxidized linoleic acid metabolites in humans. Prostaglandins Leukot Essent Fatty Acids. 2012;87(4-5):135-41.

134. Schuster S, Johnson CD, Hennebelle M, Holtmann T, Taha AY, Kirpich IA, et al. Oxidized linoleic acid metabolites induce liver mitochondrial dysfunction, apoptosis, and NLRP3 activation in mice. Journal of lipid research. 2018;59(9):1597-609.

135. Goodfriend TL, Ball DL, Egan BM, Campbell WB, Nithipatikom K. Epoxy-keto derivative of linoleic acid stimulates aldosterone secretion. Hypertension. 2004;43(2):358-63.

136. DiNicolantonio JJ, O'Keefe JH. Omega-6 vegetable oils as a driver of coronary heart disease: the oxidized linoleic acid hypothesis. Open Heart. 2018;5(2):e000898.

137. Ramsden CE, Hibbeln JR, Majchrzak SF, Davis JM. n-6 fatty acid-specific and mixed polyunsaturate dietary interventions have different effects on CHD risk: a meta-analysis of randomised controlled trials. Br J Nutr. 2010;104(11):1586-600.

138. Ramsden CE, Zamora D, Majchrzak-Hong S, Faurot KR, Broste SK, Frantz RP, et al. Re-evaluation of the traditional diet-heart hypothesis: analysis of recovered data from Minnesota Coronary Experiment (1968-73). Bmj. 2016;353:i1246.

139. Ramsden CE, Zamora D, Leelarthaepin B, Majchrzak-Hong SF, Faurot KR, Suchindran CM, et al. Use of dietary linoleic acid for secondary prevention of coronary heart disease and death: evaluation of recovered data from the Sydney Diet Heart Study and updated meta-analysis. Bmj. 2013;346:e8707.

140. Listenberger LL, Han X, Lewis SE, Cases S, Farese RV, Jr., Ory DS, et al. Triglyceride accumulation protects against fatty acid-induced lipotoxicity. Proceedings of the National Academy of Sciences of the United States of America. 2003;100(6):3077-82.

141. Listenberger LL, Schaffer JE. Mechanisms of lipoapoptosis: implications for human heart disease. Trends Cardiovasc Med. 2002;12(3):134-8.

142. Szczepaniak LS, Victor RG, Orci L, Unger RH. Forgotten but not gone: the rediscovery of fatty heart, the most common unrecognized disease in America. Circulation research. 2007;101(8):759-67.

143. McGavock JM, Lingvay I, Zib I, Tillery T, Salas N, Unger R, et al. Cardiac steatosis in diabetes mellitus: a 1H-magnetic resonance spectroscopy study. Circulation. 2007;116(10):1170-5.

144. McGavock JM, Victor RG, Unger RH, Szczepaniak LS, American College of P, the American Physiological S. Adiposity of the heart, revisited. Ann Intern Med. 2006;144(7):517-24.

145. Janssen U, Stoffel W. Disruption of mitochondrial beta -oxidation of unsaturated fatty acids in the 3,2-trans-enoyl-CoA isomerase-deficient mouse. The Journal of biological chemistry. 2002;277(22):19579-84.

146. Tserng KY, Jin SJ. NADPH-dependent reductive metabolism of cis-5 unsaturated fatty acids. A revised pathway for the beta-oxidation of oleic acid. The Journal of biological chemistry. 1991;266(18):11614-20.

147. Smeland TE, Nada M, Cuebas D, Schulz H. NADPH-dependent beta-oxidation of unsaturated fatty acids with double bonds extending from odd-numbered carbon atoms. Proceedings of the National Academy of Sciences of the United States of America. 1992;89(15):6673-7.

148. Bugger H, Abel ED. Mitochondria in the diabetic heart. Cardiovascular research. 2010;88(2):229-40.

149. Koves TR, Ussher JR, Noland RC, Slentz D, Mosedale M, Ilkayeva O, et al. Mitochondrial overload and incomplete fatty acid oxidation contribute to skeletal muscle insulin resistance. Cell metabolism. 2008;7(1):45-56.

150. Rohm M, Savic D, Ball V, Curtis MK, Bonham S, Fischer R, et al. Cardiac Dysfunction and Metabolic Inflexibility in a Mouse Model of Diabetes Without Dyslipidemia. Diabetes. 2018;67(6):1057-67.

151. Asundi VK, Keister BF, Stahl RC, Carey DJ. Developmental and cell-type-specific expression of cell surface heparan sulfate proteoglycans in the rat heart. Exp Cell Res. 1997;230(1):145-53.

152. Barrett EJ, Liu Z. The endothelial cell: an "early responder" in the development of insulin resistance. Reviews in endocrine & metabolic disorders. 2013;14(1):21-7.

153. Wang F, Zhang D, Wan A, Rodrigues B. Endothelial cell regulation of cardiac metabolism following diabetes. Cardiovascular & hematological disorders drug targets. 2014;14(2):121-5.

154. Wang Y, Chiu AP, Neumaier K, Wang F, Zhang D, Hussein B, et al. Endothelial cell heparanase taken up by cardiomyocytes regulates lipoprotein lipase transfer to the coronary lumen after diabetes. Diabetes. 2014;63(8):2643-55.

155. Wang F, Wang Y, Kim MS, Puthanveetil P, Ghosh S, Luciani DS, et al. Glucose-induced endothelial heparanase secretion requires cortical and stress actin reorganization. Cardiovascular research. 2010;87(1):127-36.

156. Ding Q, Xia W, Liu JC, Yang JY, Lee DF, Xia J, et al. Erk associates with and primes GSK-3beta for its inactivation resulting in upregulation of beta-catenin. Molecular cell. 2005;19(2):159-70.

157. Cai G, Wang J, Xin X, Ke Z, Luo J. Phosphorylation of glycogen synthase kinase-3 beta at serine 9 confers cisplatin resistance in ovarian cancer cells. International journal of oncology. 2007;31(3):657-62.

158. Das A, Xi L, Kukreja RC. Protein kinase G-dependent cardioprotective mechanism of phosphodiesterase-5 inhibition involves phosphorylation of ERK and GSK3beta. The Journal of biological chemistry. 2008;283(43):29572-85.

159. Yun SI, Yoon HY, Chung YS. Glycogen synthase kinase-3beta regulates etoposide-induced apoptosis via Bcl-2 mediated caspase-3 activation in C3H10T1/2 cells. Apoptosis : an international journal on programmed cell death. 2009;14(6):771-7.

160. Woitek F, Zentilin L, Hoffman NE, Powers JC, Ottiger I, Parikh S, et al. Intracoronary Cytoprotective Gene Therapy: A Study of VEGF-B167 in a Pre-Clinical Animal Model of Dilated Cardiomyopathy. Journal of the American College of Cardiology. 2015;66(2):139-53.

161. Rodrigues B, McNeill JH. The diabetic heart: metabolic causes for the development of a cardiomyopathy. Cardiovascular research. 1992;26(10):913-22.

162. Becher PM, Lindner D, Frohlich M, Savvatis K, Westermann D, Tschope C. Assessment of cardiac inflammation and remodeling during the development of streptozotocin-induced diabetic cardiomyopathy in vivo: a time course analysis. International journal of molecular medicine. 2013;32(1):158-64.

163. Rodrigues B, McNeill JH. Cardiac function in spontaneously hypertensive diabetic rats. The American journal of physiology. 1986;251(3 Pt 2):H571-80.

164. Cai L, Kang YJ. Cell death and diabetic cardiomyopathy. Cardiovascular toxicology. 2003;3(3):219-28.

165. Liu Q, Wang S, Cai L. Diabetic cardiomyopathy and its mechanisms: Role of oxidative stress and damage. Journal of diabetes investigation. 2014;5(6):623-34.

166. Babapoor-Farrokhran S, Jee K, Puchner B, Hassan SJ, Xin X, Rodrigues M, et al. Angiopoietin-like 4 is a potent angiogenic factor and a novel therapeutic target for patients with proliferative diabetic retinopathy. Proceedings of the National Academy of Sciences of the United States of America. 2015;112(23):E3030-9.

167. Iso T, Maeda K, Hanaoka H, Suga T, Goto K, Syamsunarno MR, et al. Capillary endothelial fatty acid binding proteins 4 and 5 play a critical role in fatty acid uptake in heart and skeletal muscle. Arteriosclerosis, thrombosis, and vascular biology. 2013;33(11):2549-57.

168. Schoors S, Bruning U, Missiaen R, Queiroz KC, Borgers G, Elia I, et al. Fatty acid carbon is essential for dNTP synthesis in endothelial cells. Nature. 2015;520(7546):192-7.

169. Erion DM, Shulman GI. Diacylglycerol-mediated insulin resistance. Nature medicine. 2010;16(4):400-2.

170. Ulyatt C, Walker J, Ponnambalam S. Hypoxia differentially regulates VEGFR1 and VEGFR2 levels and alters intracellular signaling and cell migration in endothelial cells. Biochemical and biophysical research communications. 2011;404(3):774-9.